Modelling of Out of plane biaxial flexure of Unreinforced Masonry walls

Manimaran Pari

Master of Science Thesis

TU Delft Delft University of Technology

Civil Engineering and Geo-Sciences

Modelling of Out of plane biaxial flexure of Unreinforced Masonry walls

Master of Science Thesis

For the degree of Master of Science in Civil Engineering, Track - Structural Engineering at Delft University of Technology

Manimaran Pari

June 19, 2015

Faculty of Civil Engineering and Geo-Sciences (CiTG) · Delft University of Technology

Delft University of Technology
Department of
Civil Engineering and Geo-Sciences (CiTG)

The undersigned hereby certify that they have read and recommend to the Faculty of Civil Engineering and Geo-Sciences (CiTG) for acceptance of a thesis titled

Modelling of Out of plane biaxial flexure of Unreinforced Masonry walls

by

Manimaran Pari

in partial fulfillment of the requirements for the degree of

Master of Science Civil Engineering, Track - Structural Engineering

Dated: June 19, 2015

Supervisor(s):

Prof.dr.ir.J.G.Rots

Dr.ir.M.A.N.Hendriks

Ir.G.J.P.Ravenhorst

Dr.V.Mariani

Preface

This report is written as a part of the completion of my Master study in the Faculty of Civil Engineering and Geo-sciences under the Structural Engineering department at TU Delft. The work involves the numerical modelling of two way out of plane bending of unreinforced masonry walls using the finite element software TNO Diana. The validation of the model is done using experimental benchmarks found in literature and the results of different modelling approaches are presented in a comprehensive manner.

I would like to thank my graduation Committee; Jan, Max, Geert and Valentina for their invaluable guidance during the course of this thesis and also my family, friends and colleagues of the Masonry research group at the structural mechanics division.

Delft, University of Technology
June 19, 2015

Manimaran Pari

Table of Contents

List of Figures

List of Tables

Summary

Masonry as a construction material has been widely used around the world for a very long time now. They have good resistance to all kinds of gravity loads but the quasi-brittle response to lateral loads like earthquakes is a matter of concern.

When an unreinforced masonry (URM) building is subjected to shaking during a seismic activity, the walls experience a combination of in plane and out of plane response. Past research work into seismic behaviour of URM buildings has been dominated by in-plane studies as it provides the primary load path for the transfer of seismic forces to the foundation. Out of plane walls, although not a part of the primary load path, requires sufficient capacity to resist local out of plane failures which is also dangerous sometimes. In situations where out of plane walls are load bearing, their local failure could affect the global lateral in-plane and the gravity load paths causing partial or global failures.

The context of this thesis work is based on the induced seismic activity at Groningen due to exploration of natural gas over the years. NAM has commissioned a research program involving ARUP, EUCENTRE and TU Delft, to get insight on the strength and stability aspects of existing URM buildings in the area. The objective of the thesis is to create a numerical model to simulate the two way out of plane bending of unreinforced masonry walls. Subsequently, they are validated using experimental benchmarks available in literature, although very sparse work has happened in this direction.

Van der Pluijm's work on "Tests on Laterally Loaded Clay Brick Panels, Nov 2000" [12] and "Cyclic testing of unreinforced masonry walls in two-way bending, 2006" by *Griffith et al.* [13] are chosen as benchmarks to validate the computational model developed to simulate the behavior of walls in out of plane flexure. The tests results present isotropic properties of the URM wall in the tension and compression regimes.

The modelling work done during the thesis can be broadly articulated in the following manner:

1. **Preprocessing and Analysis**: Based on knowledge from literature, the macro modelling approach of Total strain based cracking models is deployed as a start using an isotropic approach considering the computational constraints and the accuracy level. The discretization of the walls are carried out in different ways and the shell elements and solid elements are used to create finite element models. The constitutive relation in tension is exponential softening as is the case with quasi brittle materials and in compression an assumption of elastic or ideal behaviour is made and checked later for reliability.

2. **Results**: The response of these models to non linear static analysis do not simulate the strength and stiffness degradation of URM walls typical to the two way bending case in the pre-peak regime. The degradation is caused by the creation of horizontal cracks and the subsequent diagonal cracks aiding the redistribution of moment capacity in the wall. Furthermore, the post peak behaviour is highly unstable which led to the use of a different analysis procedure termed Quasi-dynamic analysis in this report. This procedure gives us an insight into the post peak behaviour and the crack patterns at later stages which are not obtained in the non linear static analysis. This is then used as a precursor to the variation of the shell element model called the localized model to obtain a pre-peak response very close to the experimental benchmarks. Solid element model is analysed with isotropic properties as a variation study and yields stable post peak response with quasi-dynamic analysis but a pre peak response similar to the shell element model.

3. **Conclusions**: Some of the main conclusions drawn from the study are as follows:

   - Use of 11 integration points along the thickness direction of the URM wall is essential in obtaining accurate results.
   - Necessity of orthotropy to accurately simulate the two way out of plane bending. The localized model, a variation of the shell element model, indirectly simulates the orthotropy to a considerably good accuracy.
   - Quasi-dynamic approach is an improvement over the non-linear static analysis to obtain the post peak behaviour

4. **Recommendations**: The recommendations which would help modelling the behaviour in a better manner are as follows:

   - Tests to otain accurate results with regards to tension and compression regimes, i.e fracture energy and strength parameters.
   - Results are required in orthogonal directions to simulate the two way out of plane bending response. In other words, Orthotropy is a must.
   - Use of sequential linear analysis to increase the levels of accuracy in obtaining a stable post peak response as against the quasi-dynamic analysis
   - Attempts to use other different discretization methods like the discrete crack approach using predefined interface elements

"To Amma, Appa, Panda and Tuhina ...."

Chapter 1

Introduction

1-1 Masonry as a Building Material

Masonry is the building of structures from individual units laid in and bound together by mortar; the term masonry can also refer to the units themselves. The common materials of masonry construction are brick, stone, marble, granite etc. Brick masonry is the most commonly used form. It is a form of construction which ensures fire protection since it's a non-combustible product; reduced life cycle costs as painting can be avoided and is in general a good construction material.

Masonry has high compressive strength under vertical loads but has low tensile strength (against twisting or stretching) unless reinforced. Failure of masonry is thus generally governed in tension, instances where it's subjected to bending. The tensile strength of masonry walls can be increased by thickening the wall, or by building masonry piers (vertical columns or ribs) at intervals. In practical situations, steel reinforcements such as windposts or CFRP (Carbon Fiber Reinforced Polymers) can be added and thus masonry could be broadly classified as Unreinforced and Reinforced Masonry.

1-2 Context of Present study

Masonry has been used widely in The Netherlands in residential, commercial, religious buildings among others since a long time. The durability of masonry has helped it withstand the test of time and has also had to face the wrath of nature over centuries now.

During the late 1950s, a giant natural gas field was discovered in the Groningen countryside. But extensive gas explorations have led to subsidence and subsequent induced earthquakes. This has become a cause of concern in recent times with magnitudes of earthquakes just starting to touch 3 on the richter scale [14]. This jeopardizes the state of residential and other

buildings in Groningen and the people living there. It calls for preventive action and in this regard Arup, EU Centre and TU Delft have been commissioned by the NAM as a part of a broader research program to analyze the state of masonry structures for their load capacity and instability. There is need to perform nonlinear finite element analyses on Groningen unreinforced masonry buildings subject to earthquake loading, both nonlinear static push over analyses and nonlinear dynamic analyses. The goal is to cross validate computational methods, to validate them against existing and upcoming lab structural tests, to reveal possible conservativeness in current approaches and then to predict the capacity of the Groningen building stock under seismic action, in the current state and after strengthening.

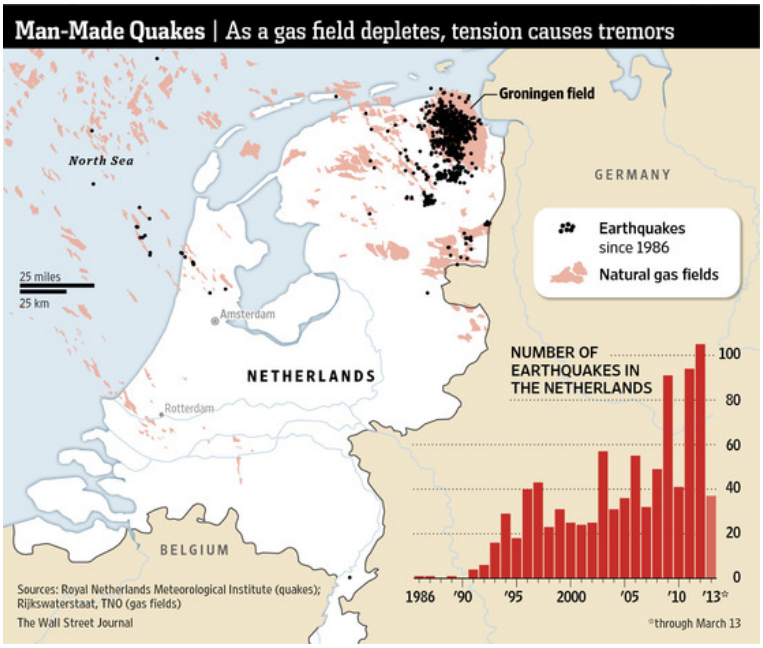

Figure 1-1: History of earthquakes in The Netherlands in recent times [1]

1-3 Objective of study and approach

Out of plane bending of masonry walls is more complex and critical. It's one of the major governing modes leading to failure mechanisms when subjected to seismic loads and hence the numerical modelling of this complex behaviour becomes essential. The objective of the thesis is to model the behaviour as accurately as possible using existing experimental work in this topic as benchmarks. It's decided to restrict the scope of the study to subjecting the finite element model to only non-linear static analysis and treat Quasistatic/transient dynamic analysis as a possibility and further cross validation using the benchmarks.

This report examines the effects of finite element modeling parameters on the nonlinear strength and deformation response of Unreinforced Masonry walls due to cracking when subjected to Out of plane loads. Convergence properties of the macroscopic measures of response, including load-deflection curves and general cracking patterns, are of primary interest. Globally convergent finite element models are generated to obtain load-deflection curves

and compared with the benchmarks. Nonlinearity is limited to masonry employing a Total strain crack model where a "smeared" representation is used to incorporate cracks in the finite element mesh. The crack formation is governed by the limiting tensile bond strength of the Masonry and the fracture energy involved in the process.

Van der Pluijm's work on *"Tests on Laterally Loaded Clay Brick Panels, Nov* 2000*"* [12] and *"Cyclic testing of unreinforced masonry walls in two-way bending,* 2006*"* by *Griffith et al.* [13] are chosen as benchmarks to validate the computational model developed to simulate the behavior of walls in out of plane flexure.

It's hoped that this thesis contributes to the superior goal of computationally estimating the capacity of the Groningen masonry buildings under seismic loads in the current state.

1-4 Synopsis

This MSc. thesis is divided into five chapters with the following subjects:

Chapter 2: This chapter investigates the past experimental work in the area of out of plane bending of unreinforced masonry walls and presents the subsequent choice of benchmarks for the validation of the computational model to be used in this study. It also describes the unreinforced masonry behaviour in detail and also the material modelling, load characteristics and computational strategies available to deduce the best option for an efficient and reliable model to simulate the response to seismic loading.

Chapter 3 This chapter deals with the Van der Pluijm benchmark and the modelling approach for the study including constitutive models and other finite element options associated. It also elaborates on the results of the different models used to model the behaviour in terms of the load displacement curves and the cracking patterns. Also, the study on effect of mesh objectivity, control procedures, integration schemes among other variation studies is presented.

Chapter 4 This chapter elaborates the implementation of the model on the Griffith benchmark chosen for this study and the types of models used. It also involves elaborate description on the macroscopic measure of the response namely, the load displacement curves and the cracking patterns.

Chapter 5 This chapter presents the overall conclusions of this thesis. It also includes some recommendations for future work.

Chapter 2

Literature Study

The goal of this part of the thesis is to provide detailed information on the subject of out of plane bending of Masonry. Firstly, the general use of masonry in buildings and some general terminology regarding masonry and its components have been described. Then the out of plane behaviour of masonry and the experimental investigation done in this regard is discussed. This leads us to the choice of benchmarks which would provide the experimental data to validate the realistic numerical model to be developed with high accuracy, efficiency and good convergence properties. Furthermore, the background material regarding the numerical model like the load characteristics, material model, types of elements used etc. is presented.

2-1 Unreinforced Masonry

Masonry is one of the oldest building materials being used to-date. The concept of placing units (bricks or stones) on top of one another and adjacent to each other is used to create structures all over the globe including The Netherlands. The type of units used (stones, clay bricks, calcium silicate bricks etc.); types of mortar joints used to connect the units and the pattern of stacking determine the type of masonry. Masonry, as discussed in the Introduction chapter, has appreciable behaviour in compression and is good in bearing gravity loads but when subjected to lateral loads like wind or seismic loads, the resistance is comparatively lower which can be primarily attributed to the low tensile strength of Masonry and it's quasi brittle nature which leads to sudden collapse. This is critical particularly in the case of seismic loads. This led to the advent of the use of steel reinforcements and other fibre-reinforced polymers to improve the tensile strength of Masonry and in-turn the mechanical behaviour of masonry in response to lateral loads.

However, the aim of the thesis is to contribute to the research program that focuses on the brick masonry buildings in Groningen which are primarily unreinforced and thus the study is restricted to unreinforced brick masonry, which is referred to as "Masonry" from here on.
Masonry exhibits composite behaviour because of the differences in properties of the constituent parts:

- Bricks
- Joints
  - Head joints (vertical joints)
  - Bed joints (horizontal joints)
- Brick-mortar interface

The stacking of bricks is done in different patterns and the most commonly used ones are the English bond, Stack bond, Flemish bond, Stretcher (running) bond, and American (common) bond which are shown in Figure 2-1. The head joints are vertical and separate adjacent bricks in the longitudinal direction while the bed joints run throughout the length of the wall acting as discontinuities in the vertical direction. The result is the variation of effective properties in the vertical and horizontal directions of a Masonry wall which in principle is referred to as "Orthotropy".

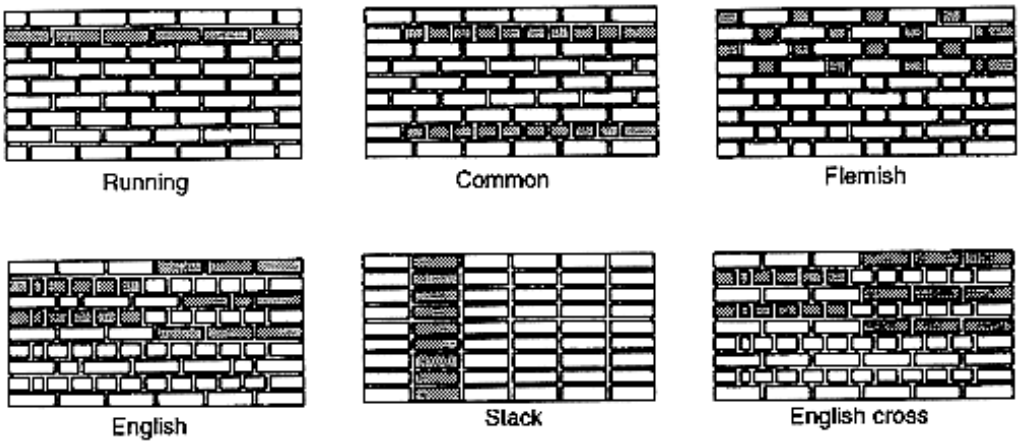

Figure 2-1: Types of Bond in Masonry

2-2 Material properties & Models

There are three major modes of fracture involving crack propagation in brittle and quasi brittle material. These are Mode-I (opening/tension), Mode-II (in-plane shear) and Mode-III (out of plane shear) and are shown in Figure 2-2. The out of plane flexure of masonry leads to tensile failure which is characterised by the tensile strength and the fracture energy involved in the process of crack formation, referred to as Mode-I fracture energy.

This section describes the behaviour of masonry in tension. The behaviour of units and mortar-joints under tension is very similar to that of other softening materials like concrete. Experience in describing the non-linear behaviour of concrete under tension could be applied

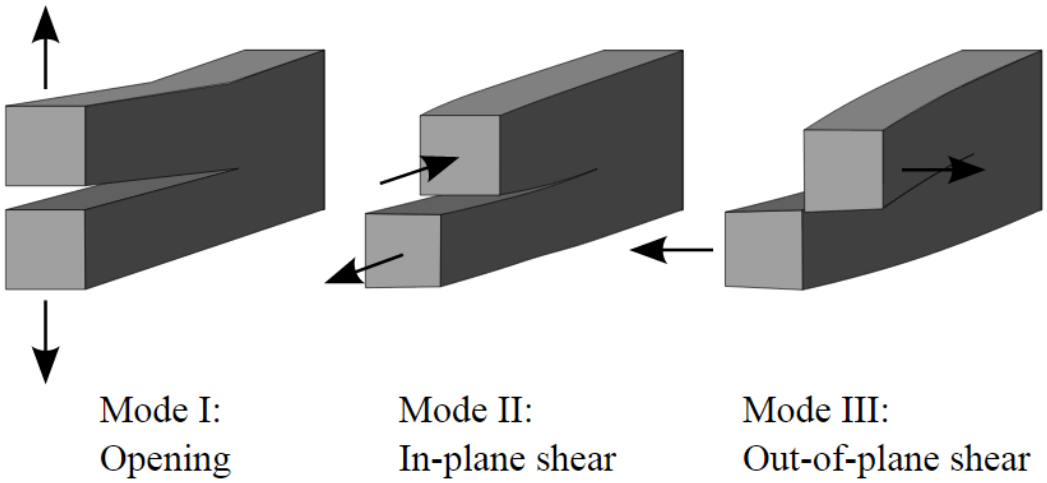

Figure 2-2: The three fracture modes

to the masonry components. The mode I fracture energy of masonry specimens tested was of the same magnitude as that of concrete, as is described by Van der Pluijm [15]. In compression, hardening behaviour is found after initial crushing after which a parabolic softening relation is used depending upon the availability of parameters for behaviour in compression. In the absence of adequate parameters, an elastic or Ideal behaviour (with only the compressive strength) can be used safely. The material models for compression are shown in Figure 2-3. The parameters G_c, h and f_c refer to the fracture energy in compression, the crack bandwidth and the compressive strength of the material respectively. The mortar-brick interface is usually not as strong as the bricks which causes a typical stepped diagonal cracking pattern as described in 2-3. The constitutive relation for both tension and compression can be applied to the model in different ways according to the method of Structural analysis used.

The investigation of the behaviour of the masonry components under tension enables the modelling of masonry in tension/flexure. In a tensile test of a quasi-brittle material like

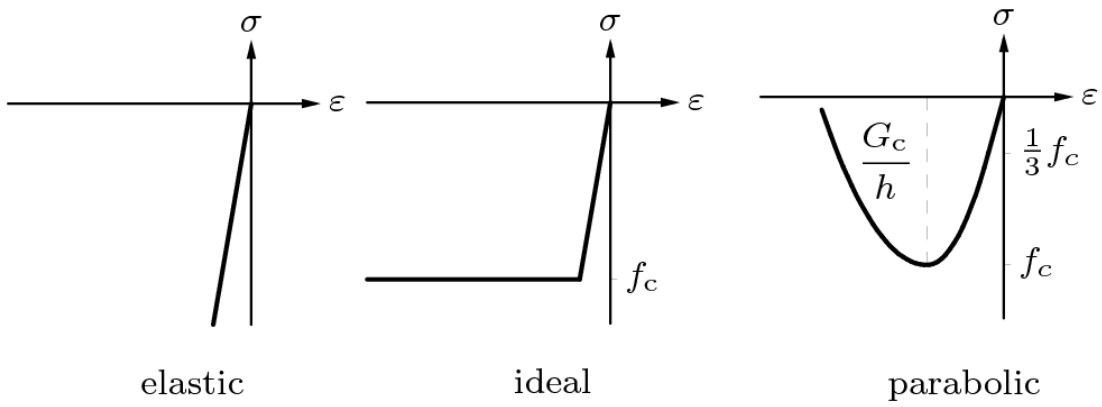

Figure 2-3: Material models in Compression

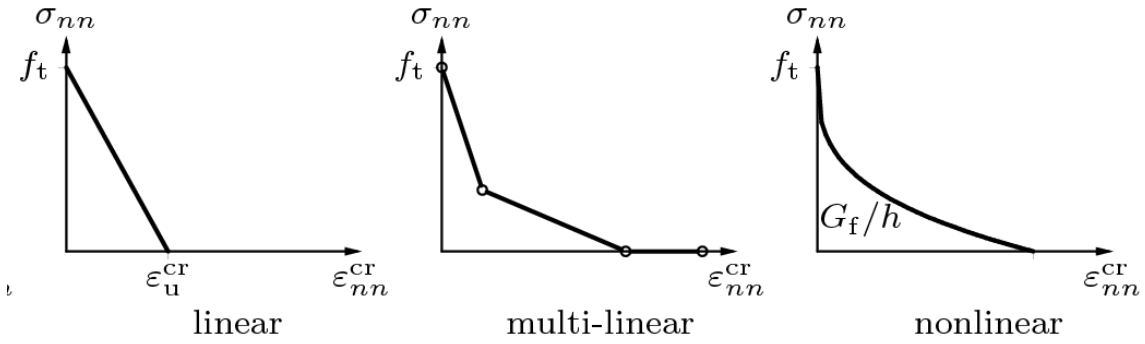

Figure 2-4: Material models in Tension - Post peak behaviour

concrete, masonry-units or mortar-joints is controlled beyond the maximum load and the constitutive relation is obtained. With the term "quasi-brittle", it is referred to a situation where the transferred force does not immediately drop back to zero, but gradually decreases. This kind of behaviour is often described by the term "softening". The behaviour prior to the maximum load is predominantly linear behaviour. The post peak behaviour must be described in one or another way. There are several approaches to describe the constitutive relation / softening behaviour like linear, multi-linear and non-linear softening as shown in Figure 2-4. The parameters G_f, h, σ_{nn}, ϵ_{nn}^{cr} and f_t refer to the fracture energy in tension, the crack bandwidth, the stress sigma, the ultimate crack strain and the tensile strength of the material.

An approach that has been proven to be successful for plain concrete is shown in Figure 2-5 which is actually the fictitious crack model developed by Hillerborg et al. [2]. This model assumes that in front of a visual crack, a process zone is present in which fictitious cracking occurs. In this zone stresses are still being transferred and this model forms the basis for most of the constitutive relations that exist for the mechanical behaviour of materials like masonry, concrete et al. On the micro level, cracks are growing in this zone making the material weaker i.e the material softens.

2-3 Masonry failure modes

Masonry structures have to be designed for lateral forces like wind and seismic actions apart from the general vertical loading due to overburden, dead and live loads. Masonry is very good in compression and tension generally governs the failure as has been mentioned in previous sections. It's an anisotropic material and for practical modelling purposes considering constraints, it's treated as orthotropic or isotropic material. In masonry buildings, the walls are the main structural elements and are subjected to in-plane loads and out-of-plane loads. The cyclic random nature of these actions on any wall in a building is as shown in Figure 2-6.

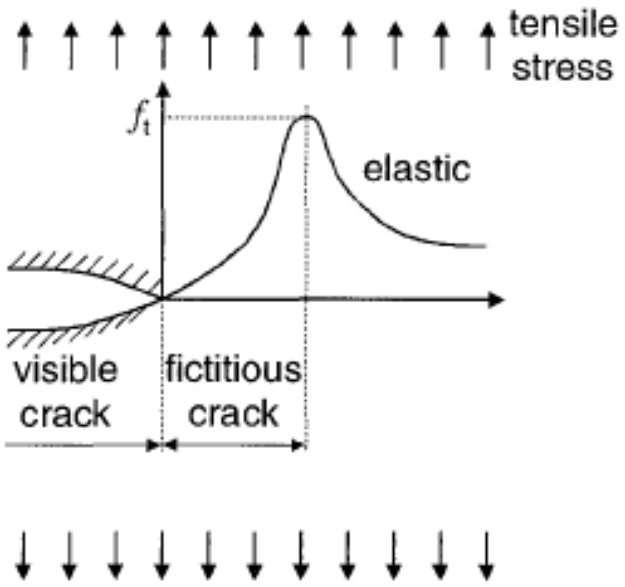

Figure 2-5: Fictitious crack model with the assumed stress distribution ahead of a visible crack according to Hillerborg et al.[2].

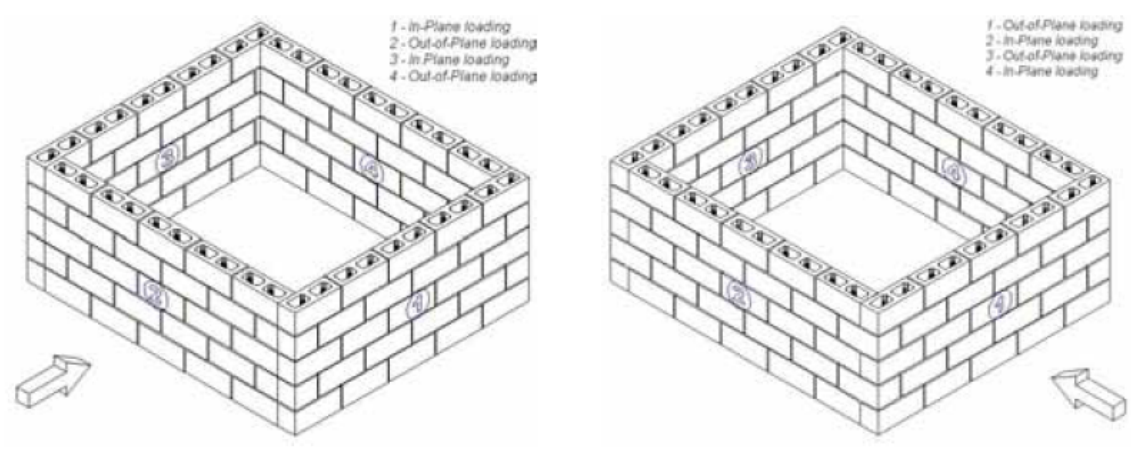

Figure 2-6: Behaviour of the walls due to cyclic random nature of the loading

2-3-1 In-Plane behavior - Shear walls

Factors like applied loads, wall geometry, properties of the materials, bond as suggested by Vasconcelos [16], influence the failure modes of a masonry wall subjected to in-plane loads which are commonly known as Shear Walls. They have been studied extensively in the past by several researchers like Anthoine and Magonette, [17]; Kikuchi et al., [18] for the effect of aspect ratio of the wall on the behavior.

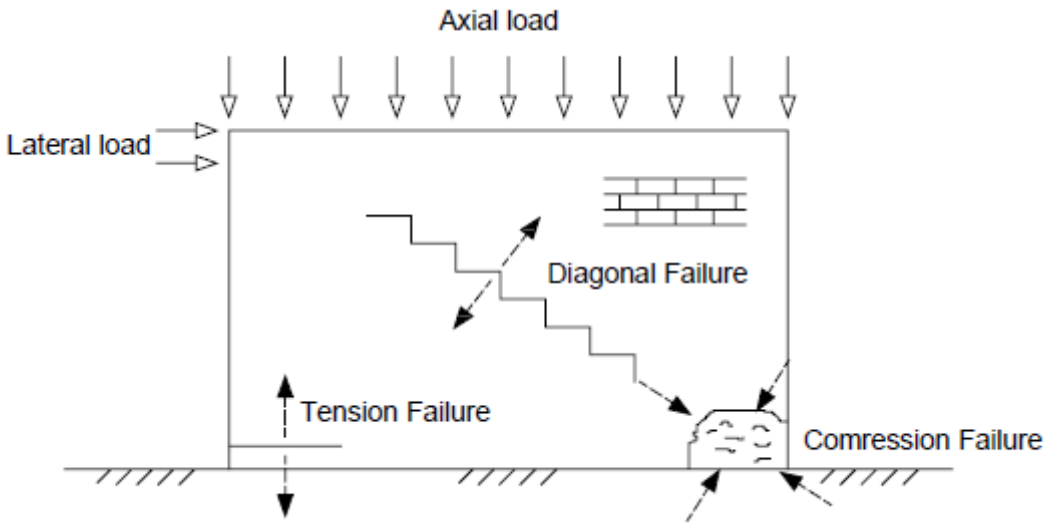

Figure 2-7: General modes of failure in shear walls.

The general modes of failure, also shown in Figure 2-7 are:

- Diagonal failure: Also known as shear failure caused by sliding of joints. This is associated with low aspect ratios and lower axial loads. Cracks go through unit-mortar interface and the unit itself or through the former as it's a case of biaxial tension compression state.
- Flexure failure: This is the combination of tension and compression failure in masonry walls. The first stage is the breaching of the tensile bond strength leading to a tensile crack in the mortar-brick interface, shown as tension failure, followed by the loss of the resisting section resulting in compressive crushing called the toe crushing, shown as the compression failure.

Besides, in reinforced masonry walls, the details of the reinforcement also influence its in-plane behaviour.

2-3-2 Out of Plane behavior - Flexure walls

The past research in the field of masonry behaviour has been dominated by the in-plane shear behaviour studies due to the fact that it provides the primary load path for transfer of seismic loads to the foundation. The out-of-plane behaviour is considerably more complex than in-plane behaviour of walls but doesn't contribute much to the load path. However, the out of plane failure of Masonry walls is critical as it can lead to partial collapse or global collapse if it is a load bearing wall. It has been experimentally studied by various researchers with keen interest in the past like Paulay and Priestley (1992) [19] who were one of the first to appreciate the out of plane behaviour as a critical one. The presence of flexible diaphragms and the lack of proper connections between walls and diaphragms and between perpendicular walls are common causes of seismic vulnerability in existing masonry buildings, which tend to

exhibit local out-of-plane responses rather than a global behaviour governed by the in-plane wall capacity. These walls are commonly called flexure walls. The tensile strength of masonry is key in the flexural behaviour of walls just like the case of in-plane bending.

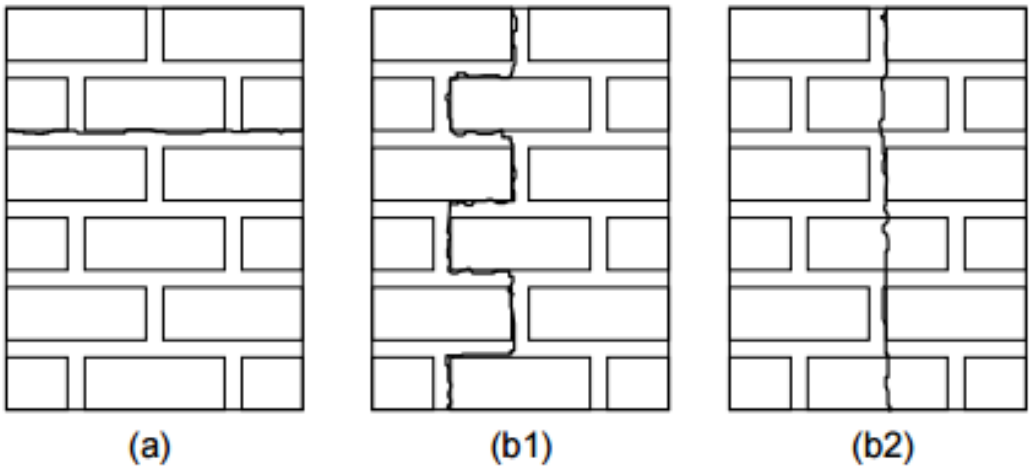

Figure 2-8: General modes of failure in flexure walls. a) debonding (vertical bending, failure parallel to bed joints) b1) toothed and b2) splitting (horizontal bending, failure perpendicular to bed joints).

Two kinds of failure modes, also shown in Figure 2-8, exist:

- Vertical bending failure:
  - Debonding : For bending leading to failure in a plane parallel to the bed joints ("vertical bending"), failure is generally caused by the relatively low tensile bond strength between the bed joints and the unit, see Figure 2-8 (a). When the tensile bond strength is higher, the unit tensile strength becomes governing.
- Horizontal bending failure:
  - Splitting : For bending leading to failure in a plane parallel to the bed joints ("horizontal bending"), cracks zigzag through head and bed joints.
  - Toothed: Depending upon the relative strength of joints and units in horizontal bending, cracks could also run vertically through the units and head joints.

2-4 Experimental work - Out of plane behaviour and Benchmarks

Since the scope of the study is restricted to static and quasistatic out-of-plane bending cases, the case on dynamic testing of out of plane walls is mentioned sparsely. Performing out-of-plane tests in masonry walls was a difficult task since it required special care. The stability conditions of the wall under was always a critical issue upon the onset of cracking. And for this reason, prior to 2000, the out-of-plane tests were predominantly conducted on horizontal specimens and had been preferred in relation to the vertical specimens as shown in Figure 2-9 (Heeringa and McLean, 1990) [3]. The most common specimens tested under out-of-plane loading have the top and bottom edges free to rotate and the displacements out of the plane are constrained. The base of the wall is restrained for axial displacements and the top is free for axial load application (Bhende and Ovadia, 1994 [4]), as shown in Figure 2-10. The load is applied in two lines by using two steel sections but this kind of loading doesn't help realise the two way bending of walls. This led to the concept of Air mattress loading to create a distributed uniform loading which was used in many studies ranging from RILEM (1994) [5], Van der Pluijm (2000) [12], Griffith et al. (2007) [13] to the recent Airbag testing of multi-leaf unreinforced masonry walls subjected to one-way bending by Griffith, Derakshan et al. (2013) [20]. The RILEM set up is shown in Figure 2-11.

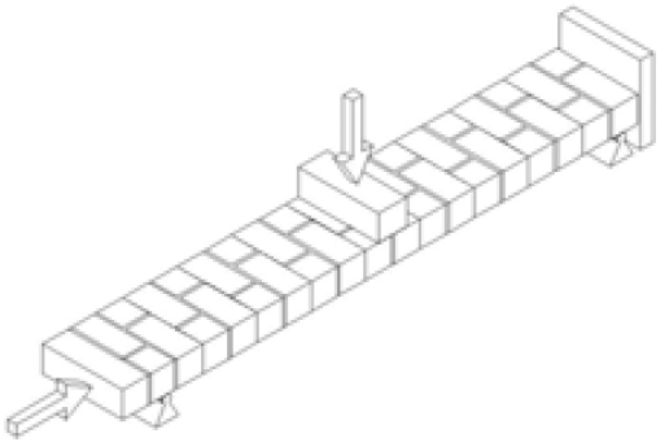

Figure 2-9: Test setup used by Heeringa and McLean (1990) [3]

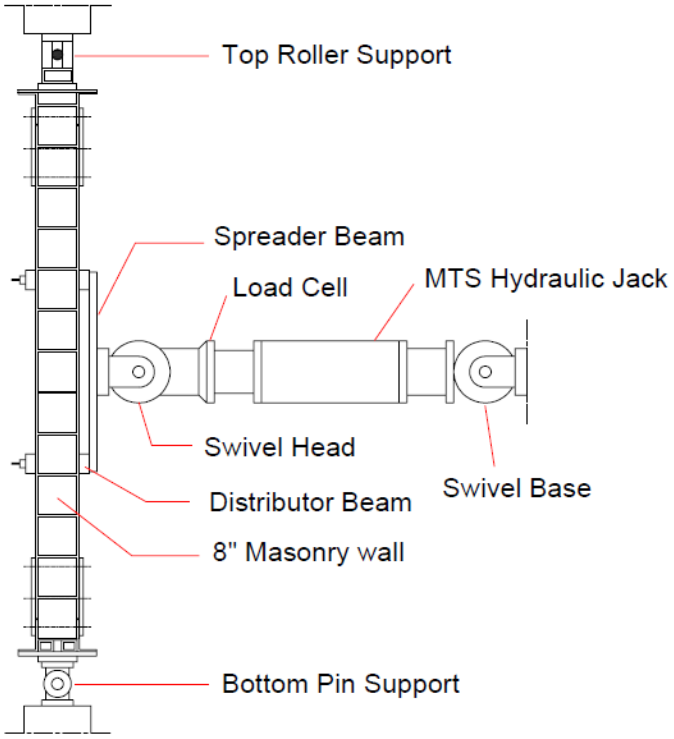

Figure 2-10: Test setup of Bhende and Ovadia (1994) [4]

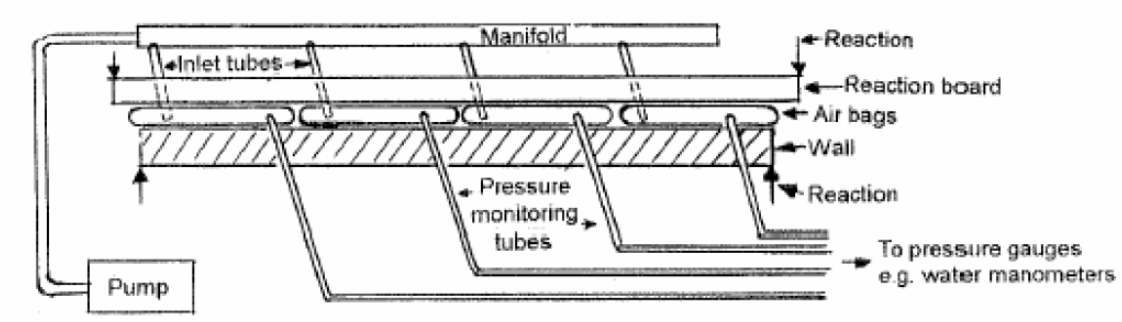

Figure 2-11: Out-of-plane test setups suggested by RILEM (1994) [5]

The out-of-plane behaviour of masonry walls has been evaluated through different experimental approaches such as

- Quasistatic monotonic or cyclic tests
- Dynamic shake table tests
- Pseudo dynamic tests

The quasi-static monotonic/cyclic tests are the most common technique used to evaluate the behaviour of Masonry walls. They are simple, relatively inexpensive, and do not require special apparatus. The test on simple elements or assemblages is performed by controlling the displacement due to the larger uncertainties in predicting the restoring forces in the nonlinear regime. It excludes the higher frequency modes of vibration. According to Gerardin and Negro [21], the main limitation of the static tests concerns the impossibility of simulating the inertial forces. They also said that the dynamic shake-table tests are the most realistic way of subjecting a structural model to any particular base motion as they're the closest to mimicking the earthquake accelerations.

Another approach that provides appreciable dynamic results consists of performing pseudo-dynamic tests. They are simpler than shaking table tests and it's a combination of a quasi-static test with a computer model which calibrates the load level to consider the dynamic responses. The masonry walls were subjected to a real earthquake excitation at a relatively slow speed, to observe the progressive damage by Paquette and Bruneau [22] as a part of their research program. The dynamic characteristics of the structure, equivalent mass and damping, were numerically simulated on a computer model, while the characteristics of the restoring force were directly measured in the tested specimens.

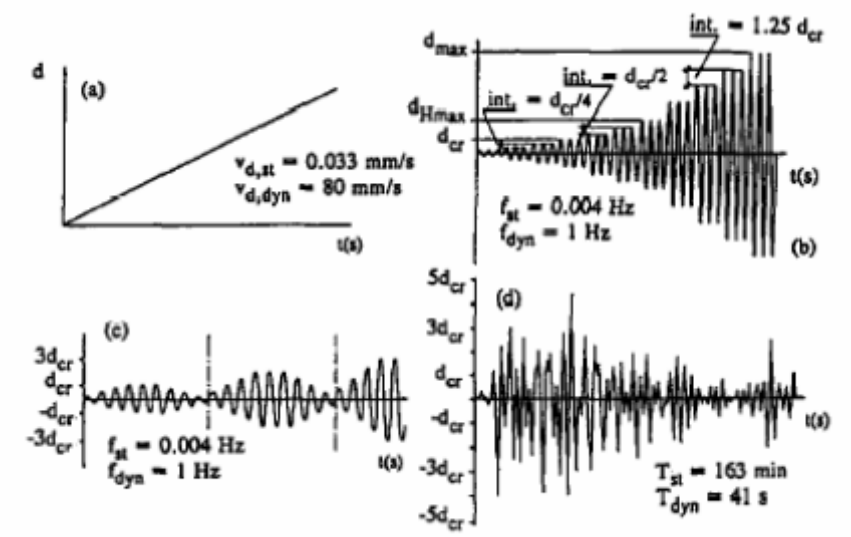

Figure 2-12: Typical lateral displacement time histories used to simulate seismic loading (Tomazevic [6])

Several lateral displacement histories have been used to simulate the seismic loads as shown in Figure 2-12. Tomazevic et al. [6] investigated the influence of the distinct displacement time histories on the in-plane behaviour of masonry walls by comparing the results obtained for each of the time displacement history on in-plane behaviour and deduced that monotonic loading gives highest lateral resistance and deformation whereas real earthquake accelerogram showed brittle failure. Boundary conditions also have an important role in the response. This study can be taken as precursor for the out of plane study in this thesis and it's decided to choose a benchmark which sticks to quasistatic and cyclic monotonic loading in the out of plane of the wall in order to observe the post peak deformation capacity of Masonry walls clearly.

When a wall is subjected to loading in the out of plane by earthquakes it undergoes bending and the orientation of internal principal stresses and the resulting crack pattern depend heavily on the supports. The walls are generally classified as one way spanning which undergo uniaxial bending and two way spanning walls which undergo biaxial bending, for which the out of plane flexure causes crack patterns as shown in the Figure 2-14. The biaxial bending case is more complex due to anisotropy of the masonry and the structural indeterminacy of the wall configurations as illustrated by Drysdale et al [23]. flexural stresses act in both the directions. The majority of the experimental research until now has been carried out on one way spanning walls by the likes of Doherty et al. [24], Griffith et al. [25], Derakshan et al. [20]. However the case of two way spanning walls find sparingly few investigations like Van der Pluijm [12] and Griffith, Vaculijk et al [13].

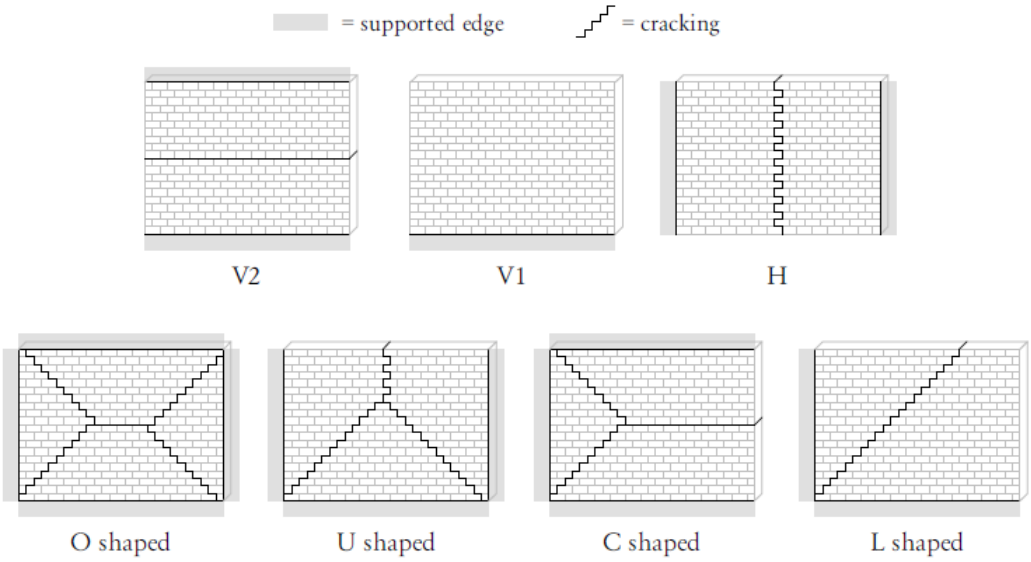

Figure 2-13: Vertically (V1, V2) and horizontally (H) spanning one-way walls and the two-way spanning walls [7]

Van der Pluijm's work on *"Tests on Laterally Loaded Clay Brick Panels, Nov* 2000*"* and *"Cyclic testing of unreinforced masonry walls in two-way bending,* 2006*"* by *Griffith et al.* are chosen as benchmarks to validate the computational model developed to simulate the behavior of walls in out of plane flexure. This decision is taken bearing in mind loading characteristic being Monotonic/Cyclic and the factor that the walls are spanning in two directions.

Source	Note	Country	Total no. walls	Reo *	Scale †	Material ‡ clay	Material ‡ conc.	Material ‡ CS	Support shape § O	Support shape § U	Support shape § C	Support shape § L	Support shape § V2	Support shape § H	No. walls with openings	No. walls with precomp.
Satti [1972]	a.	UK	19	U	1/6	19	-	-	6	13	-	-	-	-	-	-
Anderson [1976]		UK	6	U	1	-	6	-	-	6	-	-	-	-	-	-
BCRA (1977 - 1986)	b.	UK	239	U	1	176	51	12	11	209	9	-	2	8	15	3
Cairns [1983]		Australia	9	R	1	-	9	-	4	5	-	-	-	-	-	-
Lawrence [1983]		Australia	32	U	1	32	-	-	21	11	-	-	-	-	-	-
Baker [1984]		Australia	4	R	1	-	4	-	4	-	-	-	-	-	-	-
Anderson [1985]		UK	9	U	1	5	4	-	8	-	1	-	-	-	8	-
Tapp [1985]	c.	UK	6	U	1	6	-	-	-	6	-	-	-	-	5	-
Cairns and Scrivener [1987]		Australia	7	U	1	2	5	-	7	-	-	-	-	-	-	-
Drysdale and Essawy [1988]		Canada	21	R	1	-	21	-	12	3	-	-	3	3	-	3
Southcombe and Tapp [1988]		UK	5	U	1	5	-	-	-	5	-	-	-	-	5	-
Candy et al. [1989]		Australia	9	U	1	2	7	-	-	8	-	1	-	-	6	-
Chong [1993]		UK	16	U	1	13	3	-	2	10	4	-	-	-	11	-
Abrams et al. [1996]		USA	8	U	1/2	6	2	-	8	-	-	-	-	-	-	-
Edgell and Kjær [2000]		UK	37	U	1	22	15	-	14	12	11	-	-	-	11	-
Griffith [2000]		Australia	2	U	1	2	-	-	1	1	-	-	-	-	-	1
Chen [2002]	d.	Canada	8	U	1	-	8	-	8	-	-	-	-	-	7	-
Korany [2004]		Canada	4	U	1	4	-	-	2	2	-	-	-	-	1	1
Total no. walls:			441			294	135	12	108	291	25	1	5	11	69	8

*Unreinforced or reinforced. The reinforced masonry walls reported here are included only for completeness, as they were used by *Lawrence and Marshall* [1996] in validating the virtual work method.
†Specimen scale factor.
‡Unit material, as either clay brick, concrete block (including AAC and various types of aggregate concrete), or calcium silicate (CS) brick.
a. As reported by *Hendry* [1973].
b. Tests conducted by the British Ceramic Research Association have been reported throughout numerous publications, including *West et al.* [1977]; *Haseltine et al.* [1978]; *West et al.* [1979b,a]; *Hodgkinson et al.* [1982b]; *West et al.* [1986]; *de Vekey et al.* [1986]; *Haseltine and Tutt* [1986].
c. As reported by *Chong* [1993].
d. As reported by *Baker et al.* [2005]; *Ghobarah and El Mandooh Galal* [2004].

Figure 2-14: The summary of past experimental work on out of plane testing of single leaf masonry walls where V1, V2, H, O, U, C and L are crack patterns shown in previous figure [7]

2-5 Numerical Modelling

An unreinforced masonry wall can be analysed with analytical and numerical methods. The analytical models aren't discussed in this thesis as analytical validation isn't in the scope of this study. Moreover the existing methods available like the yield line method and the strip method help deduce the ultimate capacity of the wall and not the post peak behaviour which is the focus of the current study. The thesis focuses on the numerical modelling of the out of plane behaviour of Masonry walls. Masonry is a composite material that can be modelled on a macro scale or where individual parts are modelled on a micro scale i.e the bricks, mortar and the interface. Generally, the numerical methods are categorized into three main categories based on the level of accuracy and simplicity needed, as suggested by Rots [8] . :

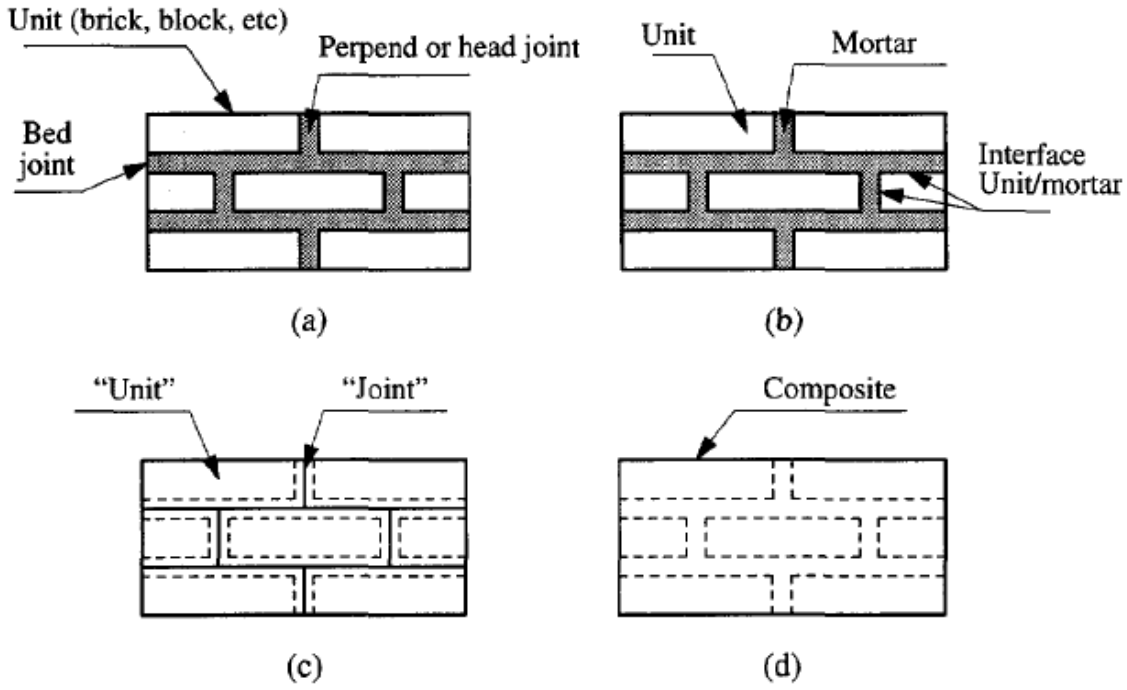

Figure 2-15: Modelling strategies for Masonry structures: a) Masonry sample b)Detailed micro modelling c) simplified micro modelling and d) Macro modelling [8]

- Detailed Micro modelling : Units and joints are represented by continuum elements and the brick mortar interface is modelled as discontinuum elements. The material properties of both the units and the joints like the Young's modulus, poisson's ratio and the inelastic properties are taken into account and the interface is provided with high initial dummy stiffness and acts as a potential crack/slip plane.
- Simplified Micro modelling : Units are represented by continuum elements and the mortar joint and the brick mortar interface are lumped into discontinous elements. Here each joint consisting of the mortar and two brick mortar interface is depicted by an average interface keeping the global geomtery consistent. Accuracy is lesser than the previous case as the poisson's effect of the mortar is not included.

- Macro modelling : Units, mortar and unit-mortar interface are lumped into continuum. Masonry is treated here as a homogenous anisotropic continuum.

The type of modelling used depends on the necessity to study local or global behaviour of masonry structures. Macro modelling provides a good balance between accuracy and simplicity due to the less computational memory and time requirements.

2-5-1 Discretization methods - Out of plane masonry modelling

Yield line method The case of out of plane behaviour of masonry walls subjected to Static/Quasistatic loading can be modelled by all of the above methods and additionally by Yield line method suggested by Brinker [9] wherein using the ductility observed in the experiments conducted and the crack patterns in the form of yield lines as shown in Figure 2-16, the upper bound ultimate resistance of the Masonry wall is deduced. But Lourenco [26] states that at peak load a distributed failure pattern is observed and only at ultimate failure a yield line is formed and hence talks about its unsuitability. Van der Pluijm [12] also talks about the method being suitable to find the ultimate load to a certain accuracy but stark differences in crack patterns from reality and suggests the need to consider that horizontal cracks still have some capacity after initial cracking and that the moment curvature diagram should be used to estimate the same. Nevertheless, this concept can be used to create a discrete cracking model for the out of plane bending case.

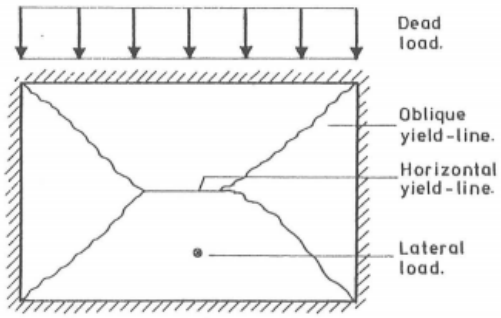

Figure 2-16: Laterally loaded masonry walls with yield lines [9]

Equivalent frame method This was first implemented by Roca et al. [27] and then later simplified in The TREMURI Program explained by Lagomarsino et al. [10]. The method uses one dimensional elements to describe a system of piers and spandrels of which a wall is built up. In this approach Timoshenko beam elements are used with two nodes, each six degrees of freedom. The initial stress state and the applied forces over the beam contribute to the stress vector at a certain cross-section. Through a stiffness matrix these stresses are related to the strains which determine the deformation of the beam and finally the displacement of the end node.

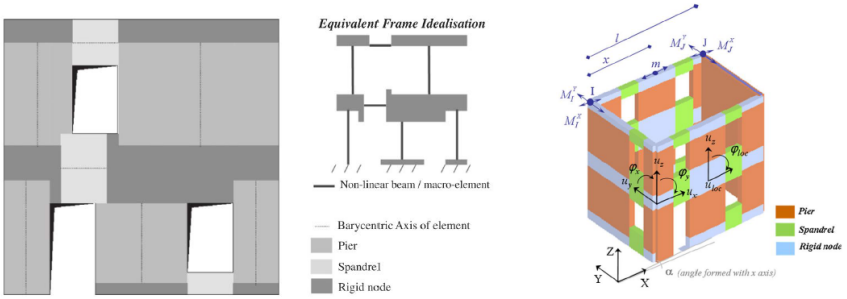

Figure 2-17: Idealisation from facade components to 1D elements and simplification of the Tremuri implementation [10]

The accuracy of the equivalent frame method is found to be sufficient in situations where local failure mechanisms are prevented. The method is able to correctly predict the global failure mechanism as mentioned in The TREMURI program. The approach was simplified by reducing the number of degrees of freedom per node to three, two translations and one in-plane rotation.

Multi-surface Interface model This Model developed by Lourenco and Rots [28] is the example of a micro modelling approach. It's called the interface cap model, see Figure 2-18 that includes all the possible failure mechanisms of masonry structures as shown in Figure 2-20. Application of the model to experiments on in-plane loaded walls showed good agreement. The model was able to reproduce the complete path of the structures until total degradation without numerical difficulties with global convergence. However, since there are too many interfaces and elements, a lot of degrees of freedom is created in the Finite element model. This significantly increases the computation costs. It is possible to reliably use this material model for the out of plane behaviour using shell elements with more integration points in the thickness direction but the computational memory and time constraints force the exclusion of this model as an option.

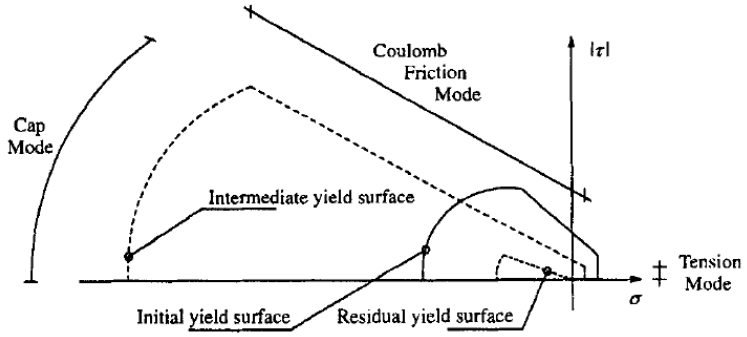

Figure 2-18: Proposed Interface Cap Model

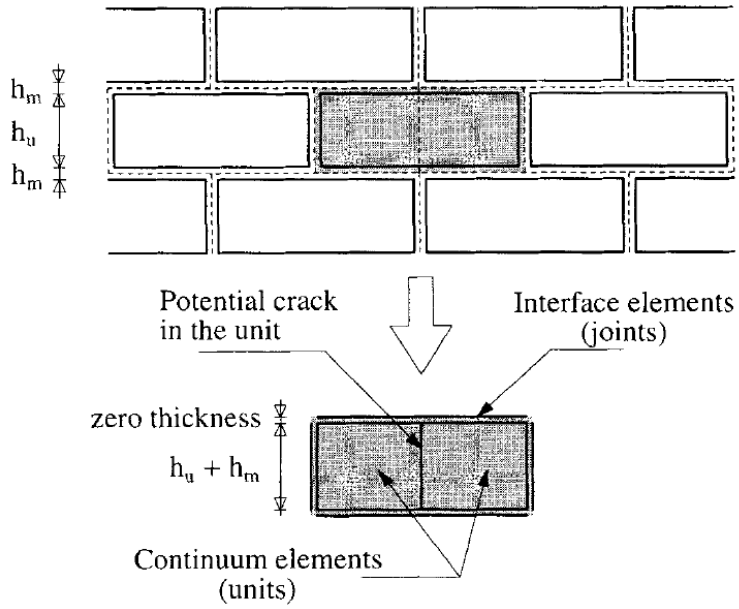

Figure 2-19: Suggested Modeling Strategy [Units (u), which are expanded in both directions by mortar thickness, are modelled with Continuum Elements; Mortar Joints (m) and Potential Cracks in Units are modeled with zero-thickness Interface elements

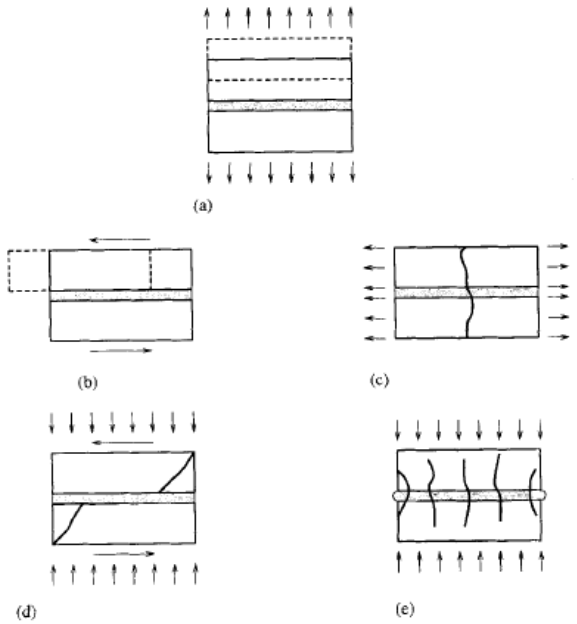

Figure 2-20: Failure Mechanisms of Masonry: (a) Joint Tension Cracking; (b) Joint Slip; (c) Unit Direct Tension Crack; (d) Unit Diagonal Tension Crack; (e) Masonry Crushing

Rigid element model The wall is modelled as a set of elements connected with rotation springs. This is in essence a simplification of the multisurface interface model, with bigger elements and only out-of-plane degrees of freedom. This makes it suitable for the out of plane behaviour of masonry walls considered in this study. The model was developed by Casolo [11] for suitability to dynamic analysis of out of plane loaded masonry walls.

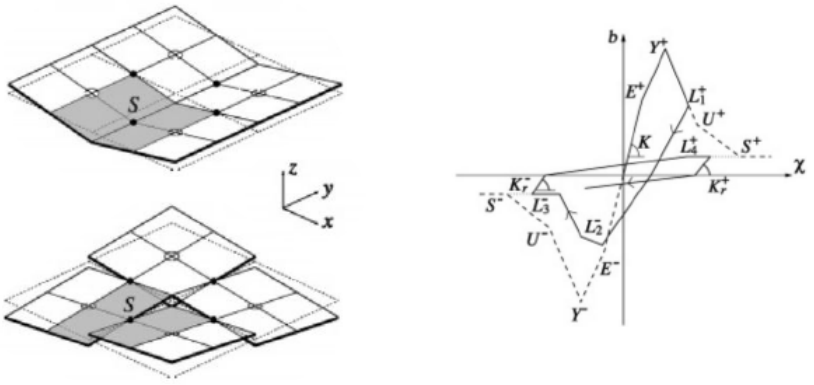

Figure 2-21: Discretization with four square elements subjected to pure flexural bending (top), and pure twisting (bottom); The hysteresis behaviour of the connection joint [11]

Rigid quadrilateral elements are connected using spherical hinges at the mid-side nodes of the quadrilateral elements and these hinges are subjected to bending and twisting between the two elements, see Figure 2-21. The elastic and plastic behaviour are defined by a moment-curvature relation, the consitutive relation with hysteresis effects, which is enforced in the hinges. The deformation of each elements can be described using three parameters with which the lateral displacement of the element is defined. When the internal compatibility and external constraint equations are applied the total number of degrees of freedom reduces to less than the number of elements and hence fits the bill from a computational point of view.

Anisotropic continuum model This model was developed by Lourenco [26] combines the material and geometrical properties of the mortar and bricks into effective material parameters in two orthogonal directions considering orthotropy. A smeared cracking approach is applied in this model to carry out the computations. This means that a crack is smeared out over a part of the element. When stress state computed at the integration point exceeds the yield criterion obtained from the constitutive relationship, which for tension is a Rankine-type criterion and for compression is a Hill-type criterion. as shown in Figure 2-22 , the part of the element belonging to that integration point is considered to be cracked. The crack opening is then smeared out over the element as a plastic strain. The orientation of the crack is in the direction normal to the principal stress.

The model as such is suitable for large structures where global behaviour is more critical and is very useful to reduce computational time as the number of degrees of freedom are also less as compared to a micro model like the Multi surface interface model. But for local failure modes, it should be used with care as this in comparison to discrete modelling approach would have a difference due to the smearing out of the cracks. This model would be suitable for the

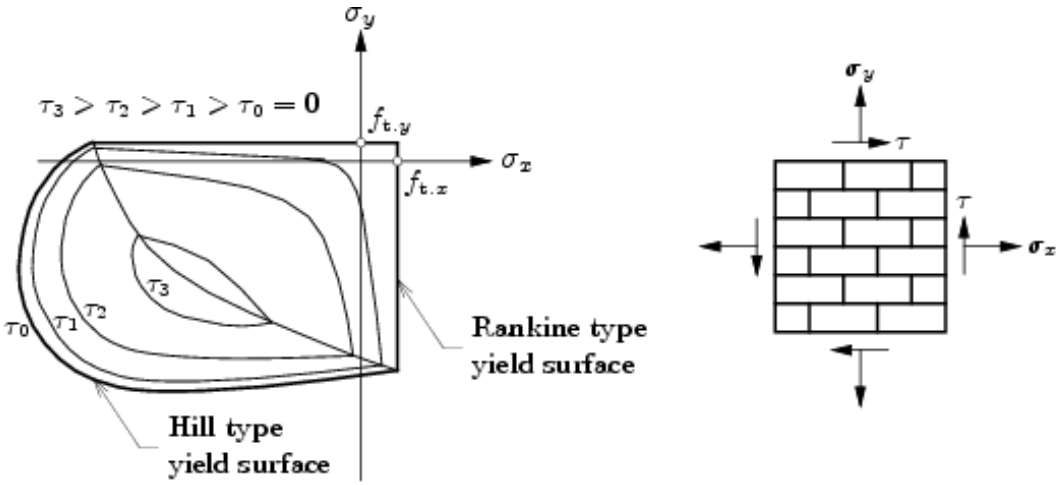

Figure 2-22: Rankine-Hill Yield criterion, Lourenco (2000)

case of Out of plane bending of the Masonry walls depending on the availability of effective parameters in orthogonal directions. In the absence of it, a simple continuum model (Total strain Based cracking model) can be used.

2-6 Conclusions

The various failure modes and behaviour in tension and compression associated with Unreinforced masonry has been reviewed. Masonry walls subjected to out of plane testing were reviewed, ranging from testing methods, loading histories to crack patterns obtained for different boundary conditions, to decide upon the benchmarks for the validation of the numerical model to be created. The constitutive models available to simulate the behaviour of masonry have also been presented and the choices are presented below

1. The Isotropic smeared cracking continuum model is used to simulate the two way bending although the orthotropy of the material is a key. The results vis-a-vis crack patterns could be used in a different modelling approach to simulate the orthotropy. The use of anistropic continuum models would require parameters like the tensile, compressive strengths and fracture energies, yield surface rounding off parameters and the plastic strain at peak compressive stress. This would lead to the need for sensitivity analysis of several of these parameters and hence an attempt is instead made to simulate the orthotropy using a variation of the model to be created. (See Localized model)
2. The two benchmarks as mentioned earlier - Van der Pluijm experiment and the Griffith experiment.

Chapter 3

Model - Van der Pluijm panel

3-1 Van der Pluijm's Experiment

One of the two benchmarks chosen for this study is the Lateral testing on Clay brick wall panels by R. Van der Pluijm, 2000 which has been described in detail in this section. This is one of the rare experiments conducted in The Netherlands with regards to Out of plane study of Masonry panels.

In this report two tests on laterally loaded panels are described. The tests were carried out in the Pieter van Musschenbroek laboratory of the Eindhoven University of Technology. The panels were made with wire cut clay bricks and a general purpose mortar designed in the laboratory. The dimensions of the panels were $4 * 1.75 * 0.1\ m^3$. The tension and the compression sides of the wall, the loading set up with air bags and the positions of strain and deflection measurements are shown in in Figure 3-1. The panels were simply supported on 4 sides and loaded with air bags, simulating wind induced pressures assuming a quasi static response of the panels. Additional tensile bond and bond wrench tests were carried out, to obtain a complete data set that makes simulation of the tests possible without having to guess important parameters as the tensile bond strength f_{tb}, flexural strength and Mode I fracture energy G_f^1.

Two panels have been tested and analysed. The material properties of the masonry and the behaviour of the panels were recorded in a detailed manner, allowing for a full non-linear evaluation with the finite element method, the important results of which are listed in Table 3-1, which are average values for Panel-II. The average value of density of the Mortar and brick was found to be 1854 Kg/m^3 and is approximated to 1900 Kg/m^3. It was concluded that the air pressure in the matresses was not equal to the load on Panel-I due to failure of one of the pressure gauges which led to the working gauge measuring higher loads than expected. The results for Panel-I was expressed relative to the failure load and hence is excluded for validation studies of the finite element model to be created owing to reliability.

Another important comment from the author was that the Panel-II was stronger than that suggested by results of tensile specimens. It's also suggested that the tensile strength and the post-peak behaviour + fracture energy must be used carefully chosen to result in the flexural bond wrench strength. The crack patterns of Panel-II after testing and the load displacement curve are shown in Figure 3-3 and Figure 3-2 respectively.

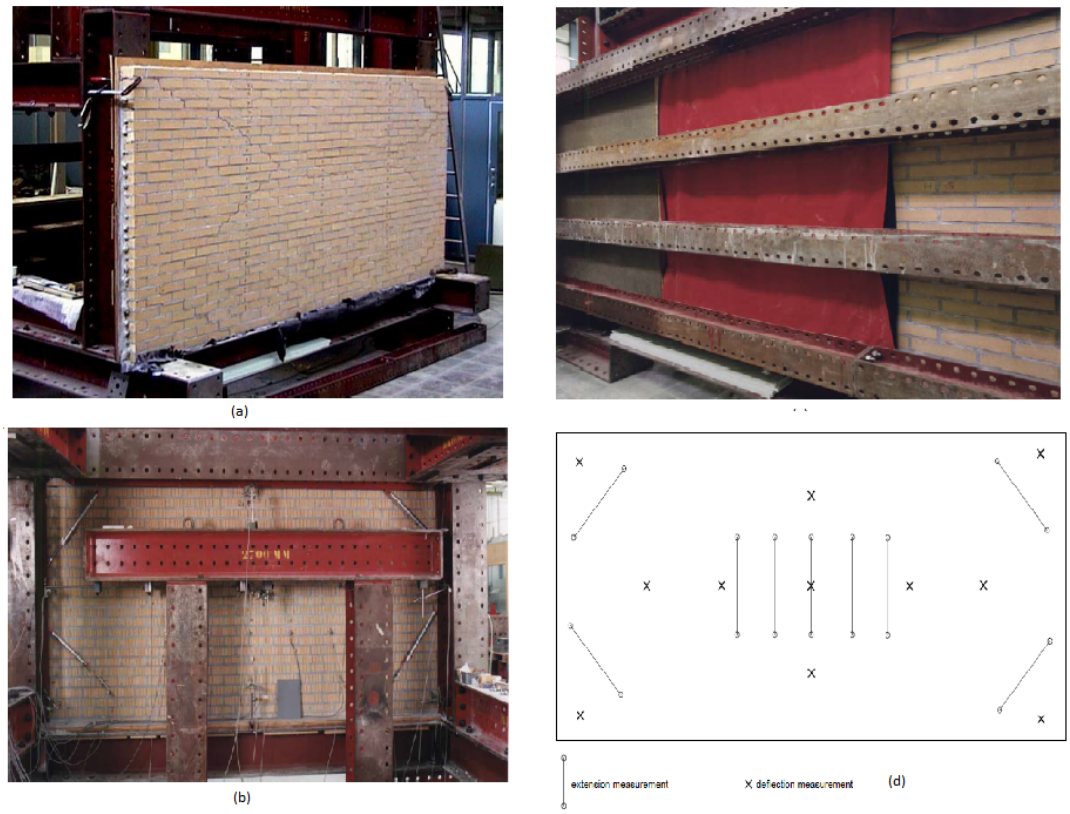

Figure 3-1: Compression side (a) and the Tension side (b) of the Panel-test arrangement (without loading arrangement), (c) Air bags used for loading and (d) Positions for transducers

Table 3-1: Masonry properties - Average values from VdP tests

Parameters	Values
Density $[Kg/m^3]$	1900
Young's Modulus E_o^{j+u} $[N/mm^2]$	3527
Tensile bond strength f_{tb} $[N/mm^2]$	0.13
Mode I fracture energy G_f^1 $[N/mm]$	0.0011
Flexural bond wrench strength $[N/mm^2]$	0.3

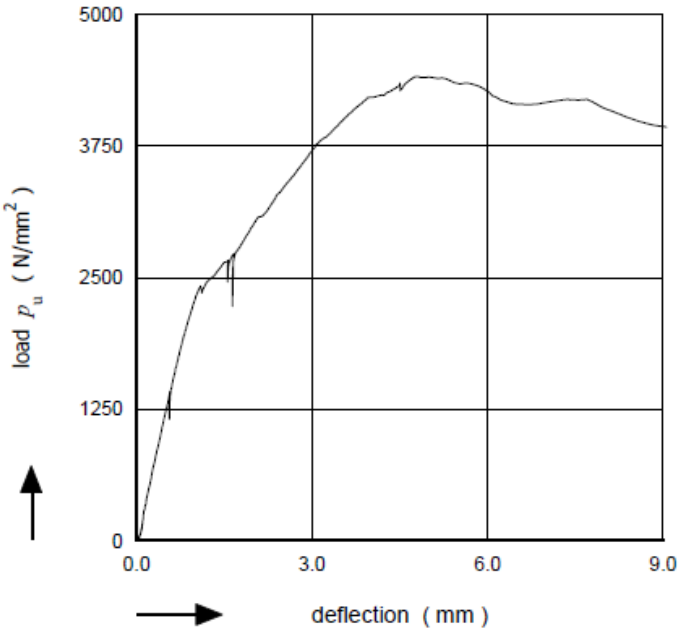

Figure 3-2: Load-deflection diagram of panel-II

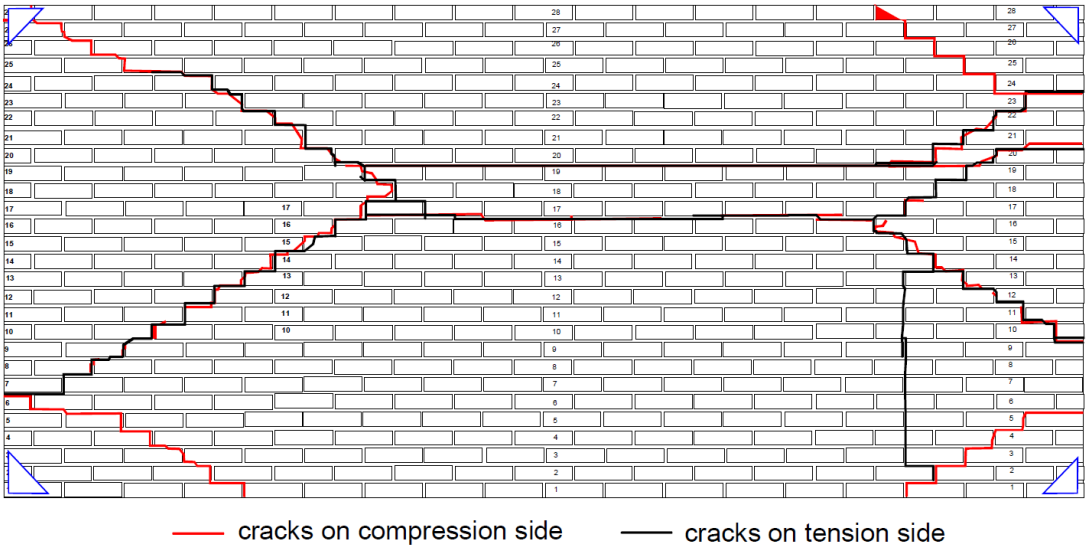

Figure 3-3: Crack pattern in panel-II after testing

3-2 Numerical Modelling - An Overview

3-2-1 Finite Element Discretization

In this section, an overview of the finite element discretization / modelling approaches and the different solution procedures employed in this study, to obtain a stable post peak behaviour close to the experimental observation, is presented. The wall can be discretized using finite elements of different kinds. Considering the geometry of the wall, where the thickness is very small as compared to the two main dimensions of the wall, use of shell elements could prove useful. Solid elements also can be used to model the wall but would require greater computational time and memory when compared to shell elements.

The failure of the wall when subjected to out of plane uniformly distributed loads undergoes two way bending and the crack patterns (like the one shown in the previous section) post the breach of the limiting strength in the tension and compression regimes of the masonry depend on the boundary conditions of the wall. Typically, the crack patterns in two way bending cases end up being analogous to the Yield line cracking in the concrete slabs, see Figure 2-14. Keeping this aspect of the two way bending in mind, the modelling of the wall as a thin strip / column (which has widely used in the modelling of out of plane bending of walls), as shown in Figure 3-4 (d), is ruled out. This is because it would reflect the case of One way bending

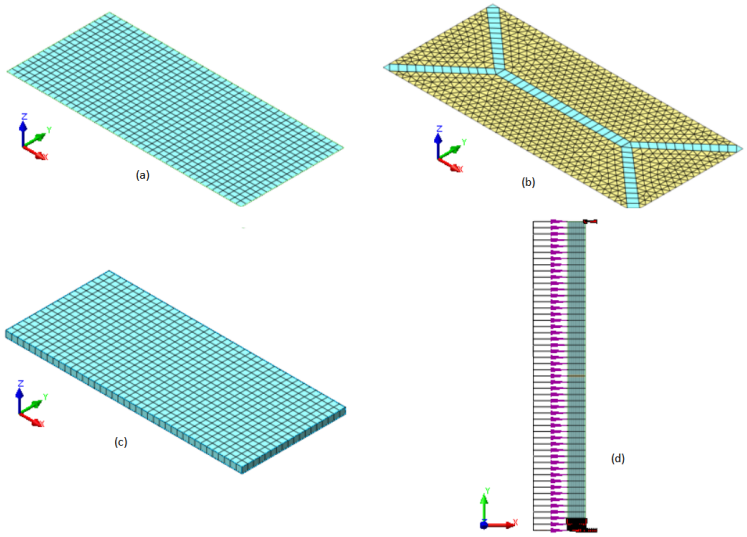

Figure 3-4: Different modelling approaches for the case considered : (a) Shell element model (b) Localized model (c) Solid element model (d) Equivalent thickness model of wall using plane strain elements

A variation of the shell element model could also be considered where a local zone close to the cracking yield line is made inhomogenous with all material non linearities being lumped and the rest of the wall having linear properties. Also, a discrete crack model using Interface elements compatible to shell elements along the cracking line could be an alternative, where all the material non linearity could be lumped.

A decision is thus made to include the following discretization ideas for the study at hand and the models are created using MIDAS FX+ which could be used for post-processing of results as well, also shown in Figure 3-4 :

- Shell element Model
- Localized non-homogenous model with Shell elements, referred to as Localized model from hereon.
- Solid Element Model

3-2-2 Solution procedures

In order to analyse the Models created using the different approaches listed in the previous section, various analysis procedures are available, of which the following have been zeroed into for this study to reliably obtain post peak behaviour of out of plane two way bending.

- Non linear static analysis
  - Force controlled incremental procedure
  - Arc length controlled incremental procedure
- Quasi-dynamic Analysis - including the inertia and damping effects.

A consummate overview of the study is as follows:

Table 3-2: Numerical Modelling overview - VdP Models

		Finite Element Discretization		
		Shell Element Model	Localized Model	Solid Element Model
Solution Procedures	1) Non linear static analysis			
	• Force control	3-3-1	-	-
	• Arc length control	3-3-1	3-4-1	3-5-1
	2) Quasi-dynamic analysis	3-3-2	3-4-2	3-5-2

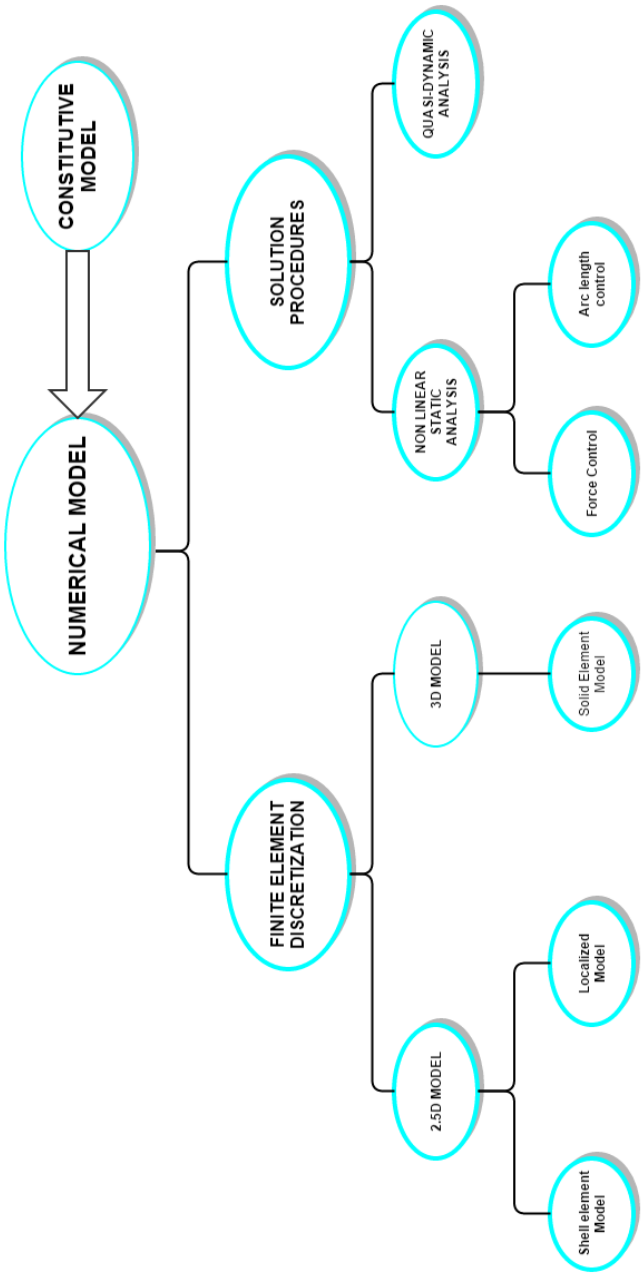

Figure 3-5: Flowchart showing an overview of the Numerical modelling

3-3 Shell Element Model

Preprocessing

Geometry The geometry of panel-II is created using the pre-processor Midas Fx+ version 3.3.0 with the dimensions of $4 * 1.75\ m^2$. The thickness of the wall, $0.1\ m$ is incorporated in the thickness of the curved shell elements used to create a 2.5D Model. The geometry of the wall along with the Meshing is shown in Figure 3-7.

Meshing and Elements The geometry of the Panel is then meshed using Isoparamteric quadrilateral curved shell elements shown in Figure 3-6 as the thickness of the wall is very small as compared to the two main dimensions of the wall. These elements are chosen as they allow for out of plane loads. It has five degrees of freedom per node, three translation and two rotations as shown. The CQ40S element is the eight-node quadrilateral isoparametric curved shell element which is based on quadratic interpolation and Gauss integration over the $\eta\ \xi$ element area. The integration in ζ direction (thickness) may be Gauss or Simpson. The default integration scheme in the element plane is 2x2 Gaussian to avoid membrane and shear locking and a 3 point Simpson's integration in the ζ direction but more number of points are employed in case of non-linear analysis.
The face of the wall is map meshed using these CQ40S elements to a fine level keeping in mind the aspect ratios of the elements. 40 elements were provided in the longitudinal direction of the wall and 20 elements in the direction of height of the wall.

Boundary conditions and Loads The wall is simply supported along all edges to restrain out plane displacements and hence is given restraints all along the edges of the model in the global Z direction. The bottom of the wall is supported in the Global Y direction for the gravity load and in the Global X direction to avoid axial displacements if any. The corners of the walls are clamped to prevent the lifting up in order to achieve the theoretical boundary condition of a simply supported plate where concentrated forces exist in the corners. These inputs are considering the description by the Van der Pluijm in his report.
The loading applied using the air matresses, placed between the reaction frame and the panel

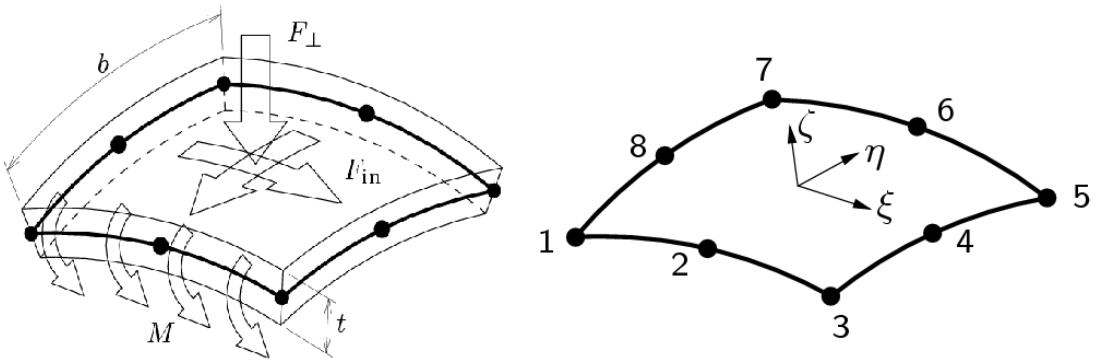

Figure 3-6: Default quadrilateral curved shell element and the CQ40S element

to create a uniform distributed load, is simulated using a distributed face load in Midas FX+ and a value of 5000 N/m^2 is given which is well above the failure load as seen in the load displacement curve, see Figure 3-2. Also, dead load of the wall is added as gravity load in the Global negative Y direction. Refer Figure 3-7 for the model generated with the meshing and boundary conditions. The distributed load is applied on the face in the Global negative Z direction and has not been shown for clarity of Boundary conditions and meshing.

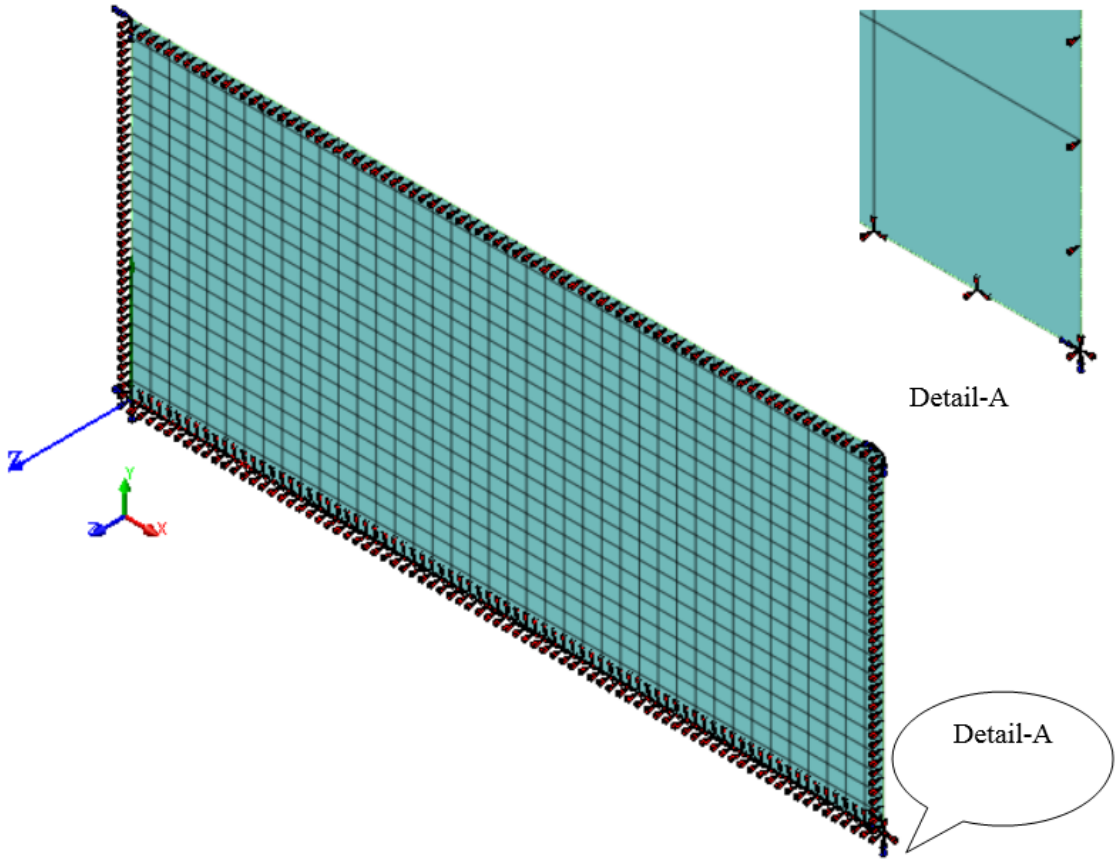

Figure 3-7: Finite element model with boundary conditions created using Midas FX+

Constitutive model The Modelling is done at a macro scale to save computational time and memory and hence the bricks, mortar and the interface are smeared into continuum. The model created is treated with the assumption that Masonry is isotropic which could be safe for a one way bending case. It is extended to the two way bending case as a start although it is expected to not simulate the behaviour. The concept of Total strain based smeared cracking model, see Figure 3-8, where the crack is spread over a region of the element whose gaussian integration point experiences stresses greater than the limiting stress, helps in getting quite good results considering the computational time constraint. The clay brick masonry used in the Van der Pluijm panels have been tested for parameters like Young's moduli, strength, fracture energy etc. in the tensile regime alone as shown in Table 3-1. The compression regime has not been touched upon and as described in the literature study section, it's decided that the elastic behaviour would be employed. This would also imply that the crack pattern on the

compressive side of the wall would not be similar to the real pattern and the crack pattern in the tensile side is looked into with more attention. With regards to the tensile regime, the exponential softening model available in TNO Diana is used which requires the input of tensile strength f_{tb} and Mode I Fracture energy G_f^1. The constitutive model effectively looks as shown in Figure 3-8. Parameters assumed are Poisson's ratio $v = 0.15$ and constant shear retention function for the shear behaviour with a factor of 0.01 for initial analysis.

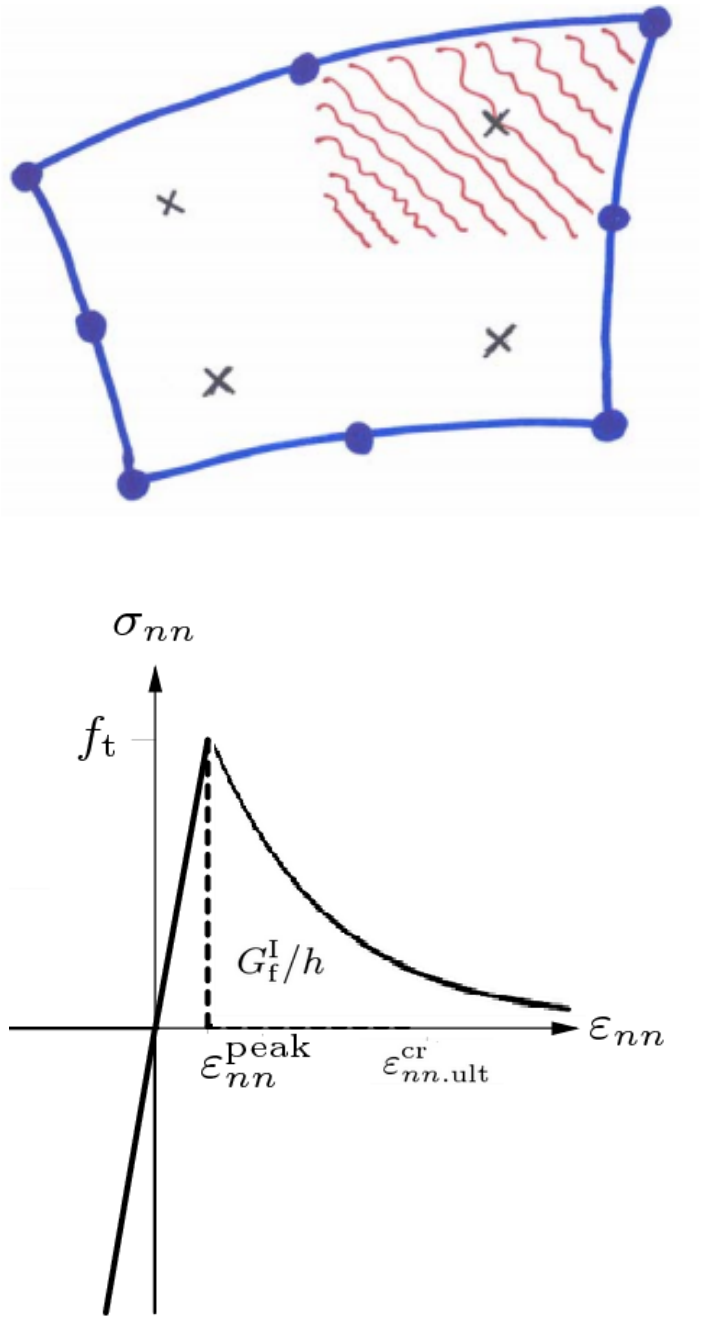

Figure 3-8: Smeared cracking, Course CIE5148 and Constitutive Model

3-3-1 Non linear Static Analysis

Force control

The Linear analysis are run to check for singularities in the Finite element model and check whether the analysis results (deformed shapes, stress and strain fields) are realistic, i.e., whether the structural behaviour of the model, for the loading level applied, is found within the bounds of its structural response.

Then the Non-linear static analysis are run using Force-control incremental procedure to obtain the peak load and the arc length incremental procedure to possibly obtain a post-peak behaviour. As a norm, Newton raphson method is the iterative procedure used with the number of iterations set to 150. Force and displacement convergence norms of 0.01, the default value in DIANA, are used. Automatic solver is used by default and the type of analysis run is physically non-linear combined with goemetric non-linearity. The load is applied in uniform small steps which are $\frac{1}{100}th$ of the load applied - 5000 N/mm^2.

Post-processing and Results

Initially the material properties obtained from the test results of the work by Van der Pluijm were used with the load being applied in Force controlled incremental procedure. The default 2x2 Gaussian in-plane integration and the 3 point Simpson's integration scheme was used. The peak load obtained was way lower as compared to the peak load obtained in the results. This is shown in Figure 3-9 and confirms the comment by the author that the reported tensile material properties have to be lower than expected. It was also deduced that there is a need for a better integration scheme in the plane, i.e 3x3 and more number of integration points in the thickness direction. As a common feature with all force control results, the procedure failed to converge beyond 150 iterations or diverged as can been seen in the ensuing load displacement curves.

Hence, trials for higher value of material parameters with the default integration scheme were performed and the load displacement curve is as shown in Figure 3-10. This reiterates the need for higher material parameters and a possible sensitivity analysis to deduce the parameters to be used for the Finite element model.

Effect of Integration schemes The same model was run with higher integration points in the thickness direction as the out plane behaviour of Masonry walls depends on the cracking of the various layers along the thickness of the wall. Also, the in-plane 3x3 Gaussian integration scheme is used instead of the default 2x2 scheme for accurate extrapolation of result to the nodes. The study is shown in Figure 3-11 which leads us to the conclusion that the use of 3 integration points in the thickness direction overestimates the peak load and hence is unsuitable for the modelling of Out of plane bending of Masonry. Based on this study, 11 integration points will be used in the thickness direction for all analysis from here on.

Sensitivity Analysis for G_f^1 Based on the inferences of the preliminary analysis, the tensile bond strength f_{tb} is low and hence the highest value of $f_{tb} = 0.33N/mm^2$ obtained in the

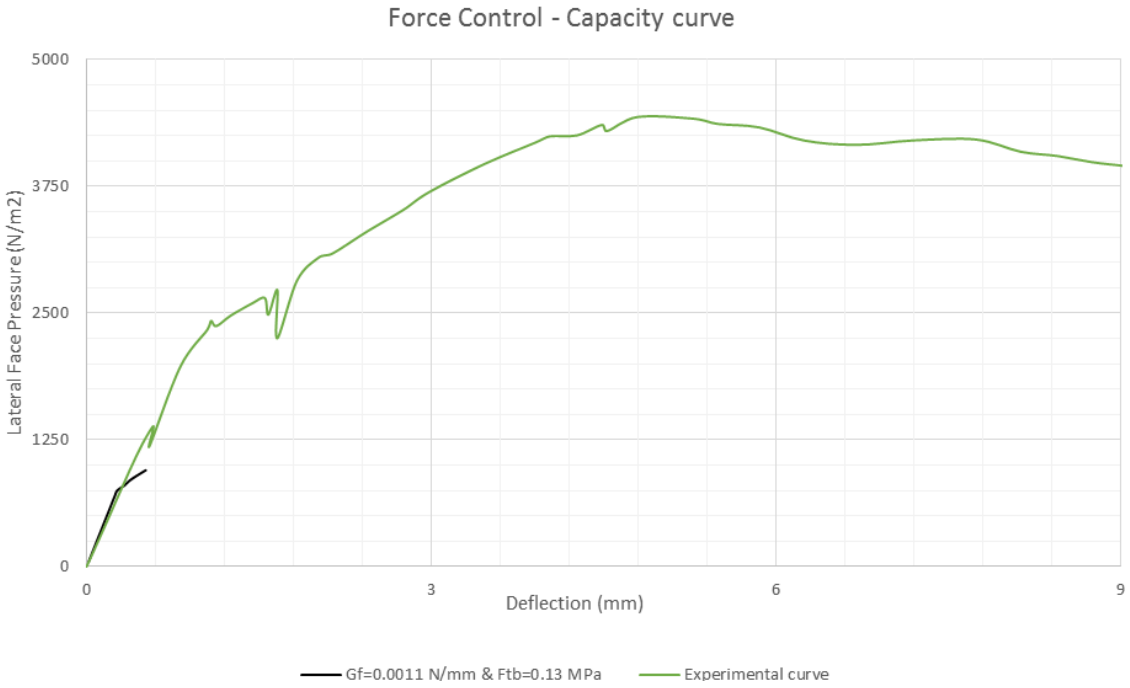

Figure 3-9: Force displacement curve with original parameters

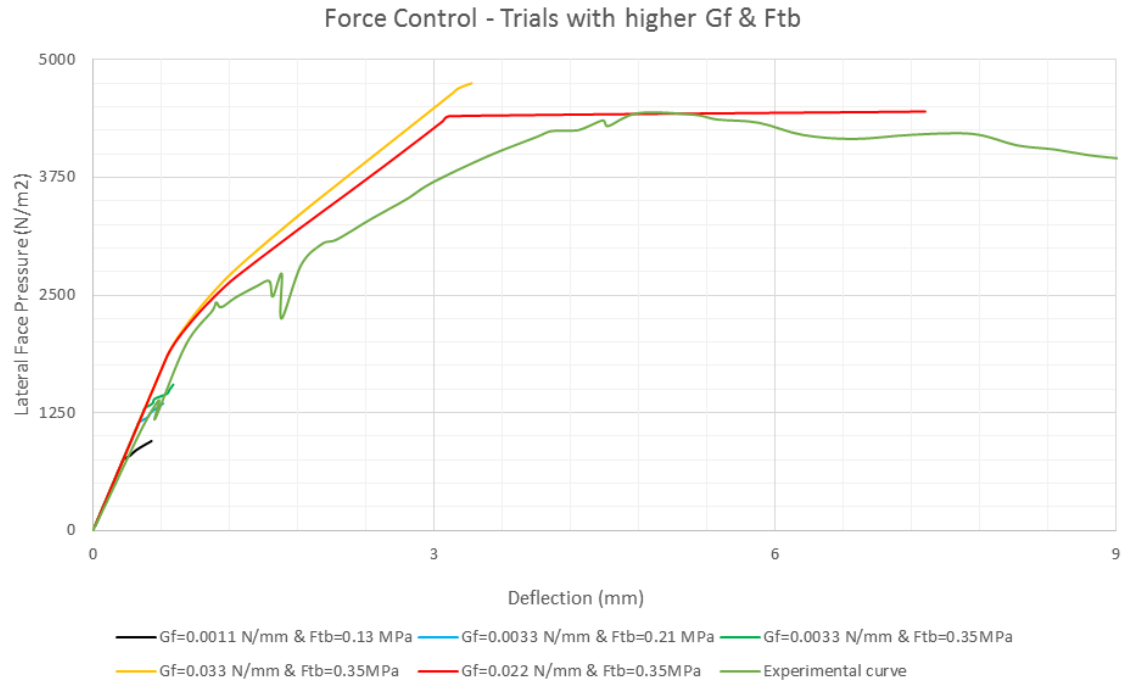

Figure 3-10: Force displacement curve with higher G_f^1 and f_{tb}

tensile test results of the experiment is fixed as a constant and effect of G_f^1 variation is studied. This is shown in Figure 3-12. It was observed that with increasing G_f^1, not only does the ultimate strain increase but the peak load increased as well. But even with a value

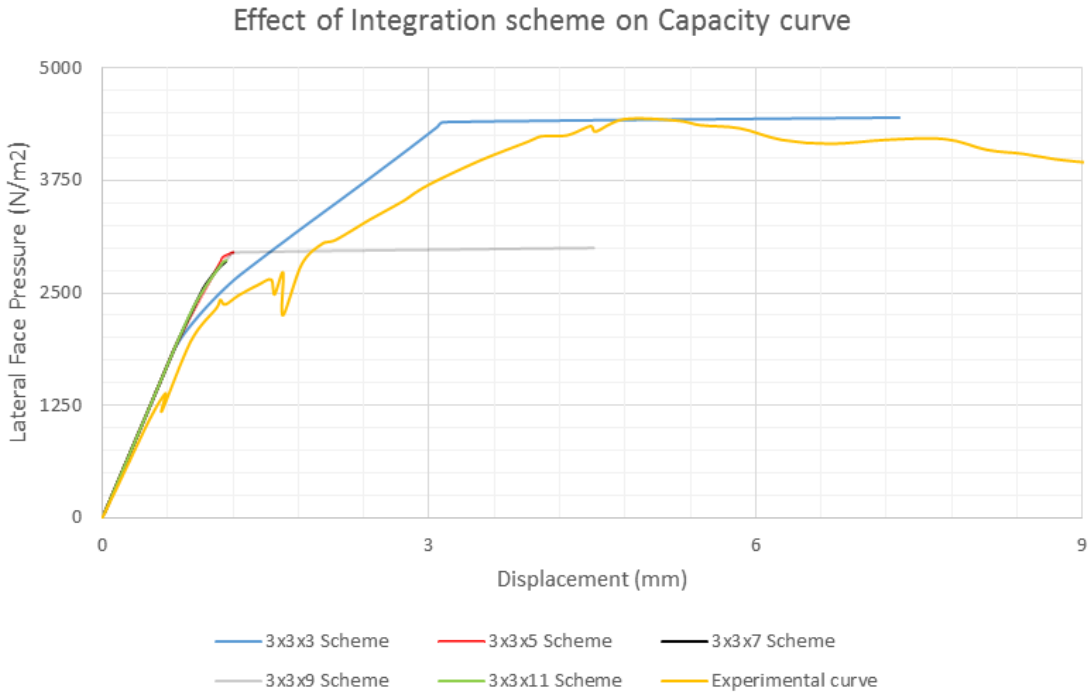

Figure 3-11: Force displacement curve - Effect of Integration schemes

Table 3-3: VdP model masonry parameters - deduced from parametric analysis

Parameters	Values
Density $[Kg/m^3]$	1900
Young's Modulus E_o^{j+u} $[N/mm^2]$	3527
Tensile bond strength f_{tb} $[N/mm^2]$	0.5
Mode I fracture energy G_f^1 $[N/mm]$	0.035
Crack bandwidth h $[mm]$	93.54

of $G_f^1 = 0.07N/mm$ the peak load reached is around 3750 N/mm^2 and not the actual peak load of 4410 N/mm^2 which leads us to a conclusion that f_{tb} also ought to be increased. Rots [29] states that there is no evident relation between the Mode 1 Fracture energy and the tensile bond strength which implies there needs to be a careful choice of the parameters for the modelling as both values in this case seem low. Lourenco [30], states that for a range of $G_f^1 = 0.005$ to 0.02 N/mm the variation of f_{tb} is 0.3 to 0.9 N/mm^2. Taking this into account and the result of the sensitivity analysis that very high values of G_f^1 also doesn't yield the peak load, the assumption is made to fix $G_f^1 = 0.035N/mm$ which is the Fracture energy value suggested for Continuum modelling in the Groningen Masonry research program and a tensile strength of $f_{tb} = 0.5N/mm^2$ which is higher than the highest value of tensile bond strength observed in the test results. These values will be used for the remaining analysis in this study as shown in Table 3-3.

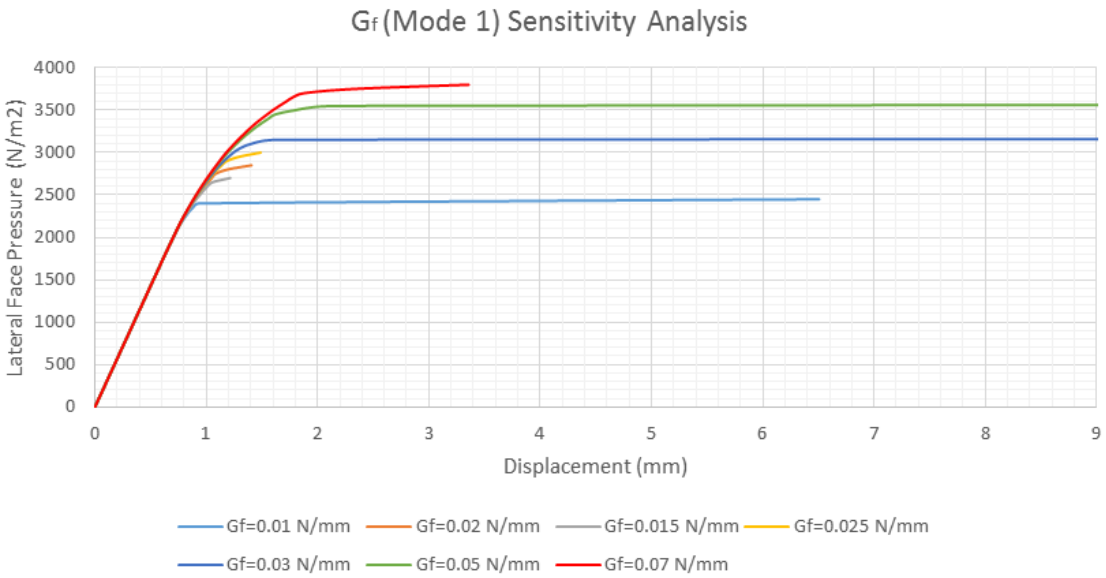

Figure 3-12: Sensitivity Analysis for Mode-I Fracture energy for a constant tensile bond strength of 0.33 MPa

Arc length Control Procedure

Since the Force control procedure yields only the peak load and diverges post peak, the Arc length control procedure is used for obtaining post peak behaviour of the Masonry walls. A global arc length procedure enhanced with line search option for stabilizing the convergence behaviour and increasing the rate of convergence is used. The displacement control would be ideal to yield good post peak results but as shown in Appendix, various patterns of displacement loads to simulate the actual behaviour and crack patterns is not accurately obtained despite yielding post peak behaviour. The arc length control is carried out with the Newton raphson iterative process with a maximum of 150 iterations per load step for three different meshes of different mesh density. The load is applied in uniform small steps which are $\frac{1}{200}th$ of the load applied - 5000 N/mm^2.

Post-processing and Results

Mesh Objectivity It was observed that with mesh refinement the peak load obtained increased and in the case of the finest mesh, the actual experimental peak load was very close to the numerical peak load as shown in Figure 3-13.

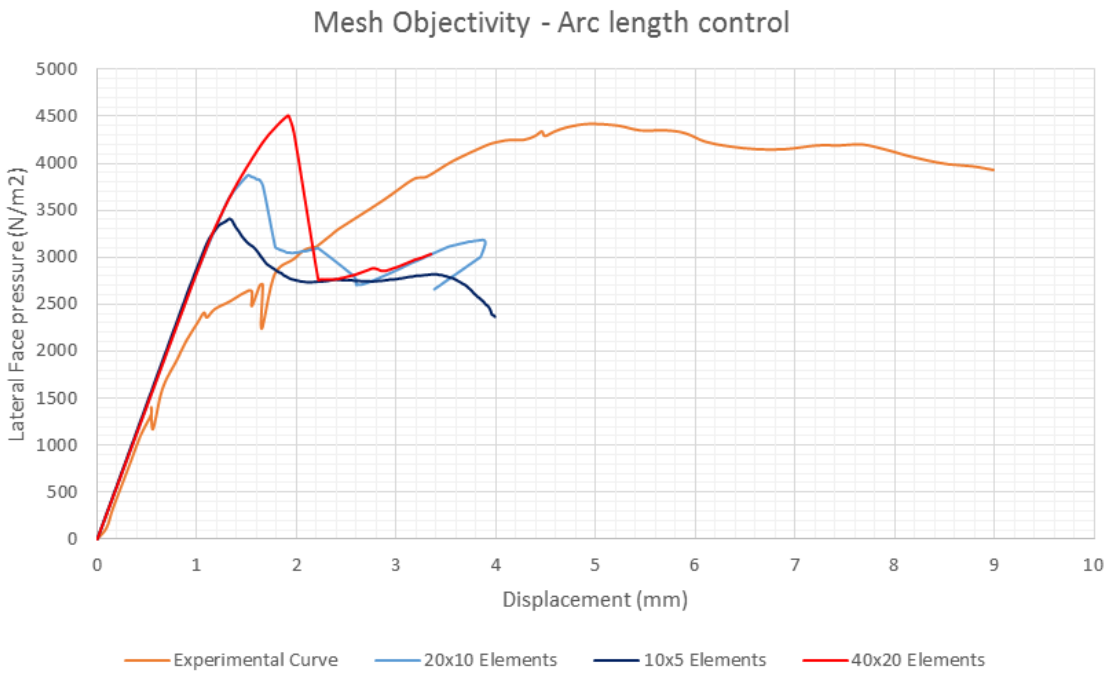

Figure 3-13: Mesh Objective results for Arc length control procedure

The Mode-I fracture energy will be released in an element if the tensile strength is violated and the deformations localize in the element. With this approach the results which are obtained with the analysis are bound to be objective with regard to mesh refinement. It is possible that the elements of the discretization are so large that the equivalent length of an element results in a snap-back in the constitutive model and the concept of objective fracture energy

which has been assumed is no longer satisfied. As a solution, firstly, it is possible to decrease the equivalent length h (the crack bandwidth) , but this property is an element property and consequently a fixed value. Secondly, it is possible to increase the fracture energy G_f^1 since this will result in an increase in the ductility of the material but the value is already fixed at a higher magnitude based on the sensitivity analysis. The final possibility is to decrease the tensile strength f_{tb} which results implicitly in an increase of the ductility since the fracture energy remains constant in this case according to the expression for ultimate strain from the exponential softening model.The crack bandwidth is expressed as $h = \sqrt{A}$ where A is the planar area of the shell element.

$$\varepsilon_{ult.nn}^{cr} = \frac{G_f^1}{h * f_{tb}}$$

$$\varepsilon_{ult.nn}^{cr} = \frac{0.035 N/mm}{93.54 * 0.5} = 7.49 \times 10^{-04}$$

$$\varepsilon_{nn}^{peak} = \frac{f_{tb}}{E_o^{j+u}} = 1.417 \times 10^{-04}$$

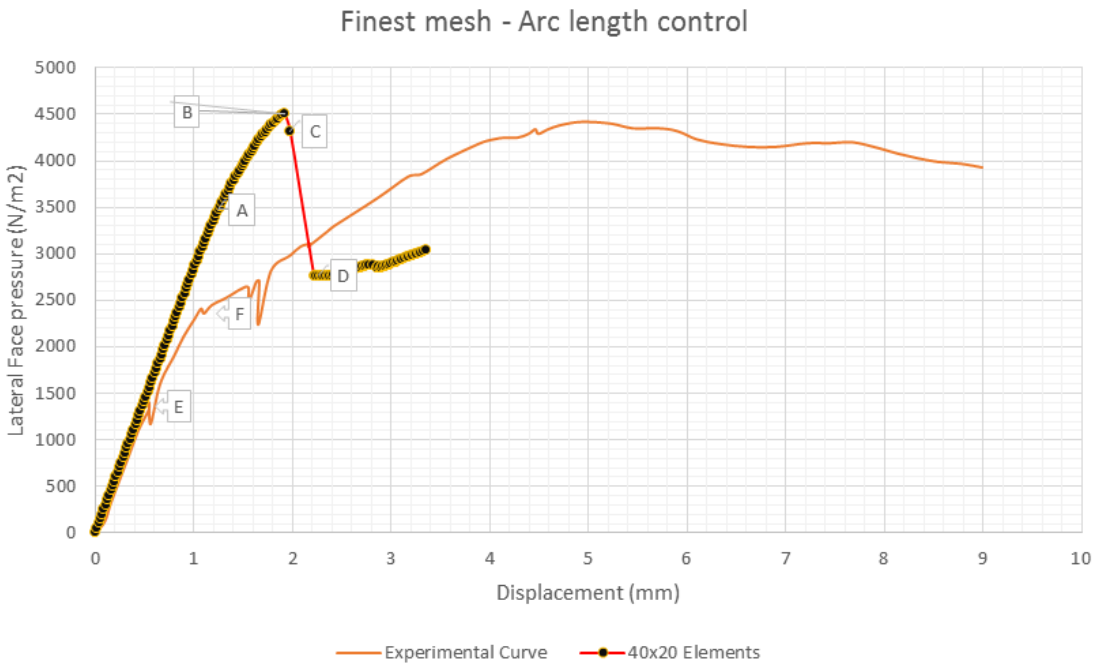

Figure 3-14: Finest Mesh - 40x20 Elements -load displacement curve

Principal strain plots and Crack patterns The legend for the principal strain plots used is a norm as shown below. However, the crack strain plots have not been shown with respect to a generic legend.

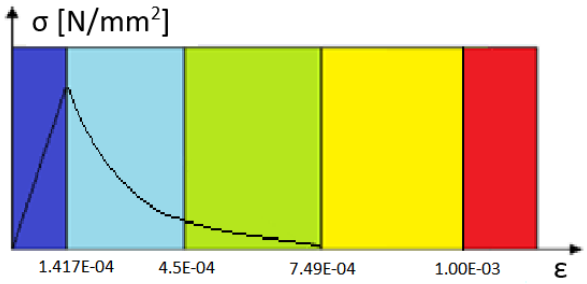

Figure 3-15: Legend for the principal strain plots - Shell element model

Figure 3-14 is the load displacement curve for the finest mesh created. It is observed that the ascending branch of the curve has stiffness close to the experimental curve. However, the stiffness doesn't reduce at a load of around 1250 N/mm^2 (point E) and again at around 2400 N/mm^2 (point F) as can be seen in the experimental curve. Van der Pluijm notes that these two points are the onset of micro cracking and that of serious cracking (starting of the horizontal crack) although the opened horizontal crack is observed only at around 85-90 % of the ultimate load. The difference in the curves can be attributed to the absence of the orthotropic character of the masonry. Nevertheless, the response is interpreted in terms of the strain plots and crack patterns.

Point C shown in the capacity curve, see Figure 3-14, is a point just below the peak load, point B, which is in good accordance with the experimental failure load of 4410 N/mm^2 but is the first non-converged step after 150 iterations. The Force and displacement variation seem to be increasing away from the convergence tolerance and would have led to divergence if the number of iterations is increased. But as the load steps were continued, the behaviour is seen in the load displacement curve. There are three more non-converged steps post point D. The principal strain plots and the crack pattern corresponding to points A, B, C and D are shown in Figure 3-16 and Figure 3-17 respectively. The principal strain plots are in accordance with Figure 3-15 and shows the complete formation of the horizontal crack and the deformed elements along the crack. The crack pattern shows the smeared out cracks starting at the centre of the wall and progressing horizontally. This then leads to serious cracking and opening of the crack and continuation to form the diagonal cracks. The pattern cannot be clearly understood as a yield line pattern as this is not a discrete crack but certainly the crack strains are greater along a yield line as compared to its neighbouring elements.

The post peak response obtained using the arc length controlled non-linear static analysis isn't stable despite use of very small load steps and very high number of iterations. It has to be noted that even with the default tolerance value of 0.01 the post peak is unstable, which leads us to the conclusion that use of tighter convergence tolerance wouldn't be of any improvement.

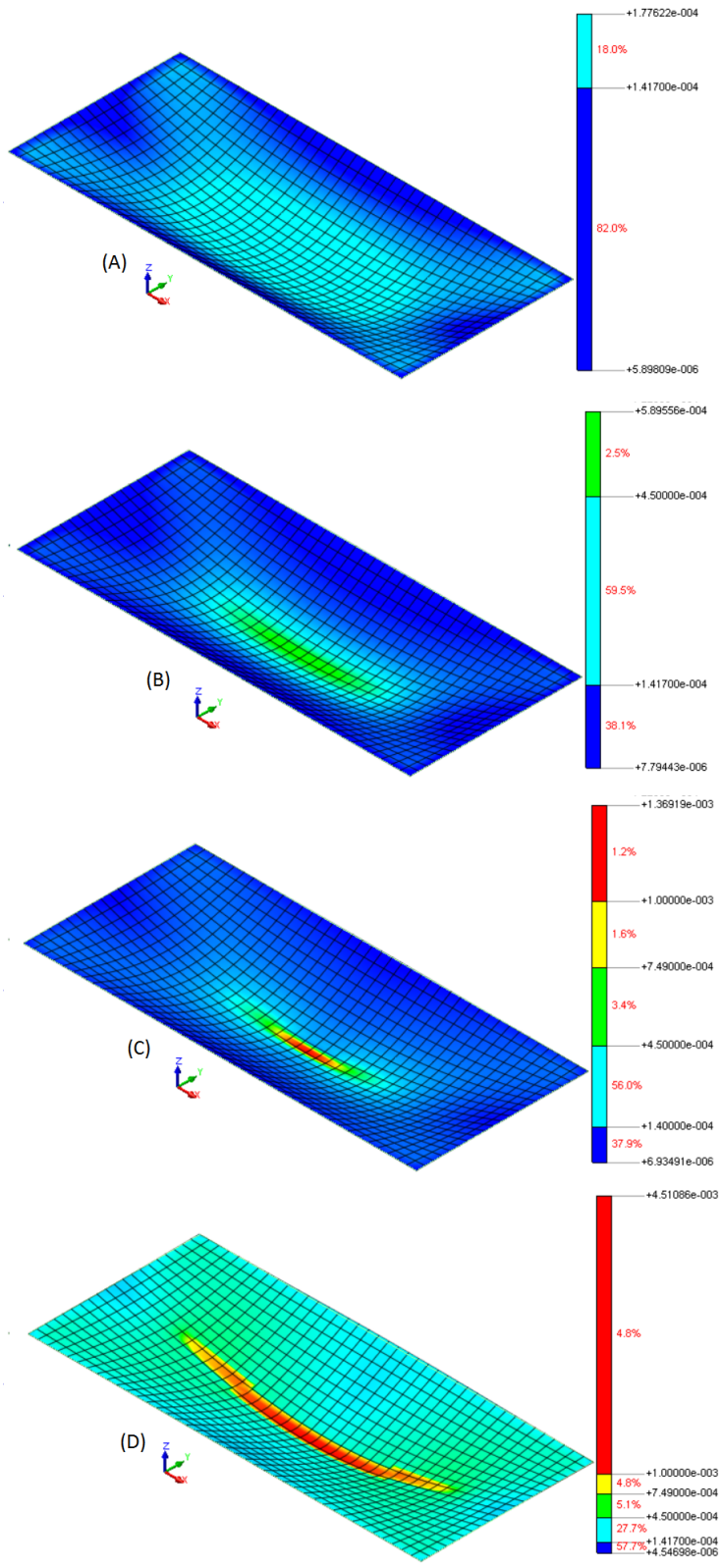

Figure 3-16: Principal strains at points A, B, C and D of the load displacement curve

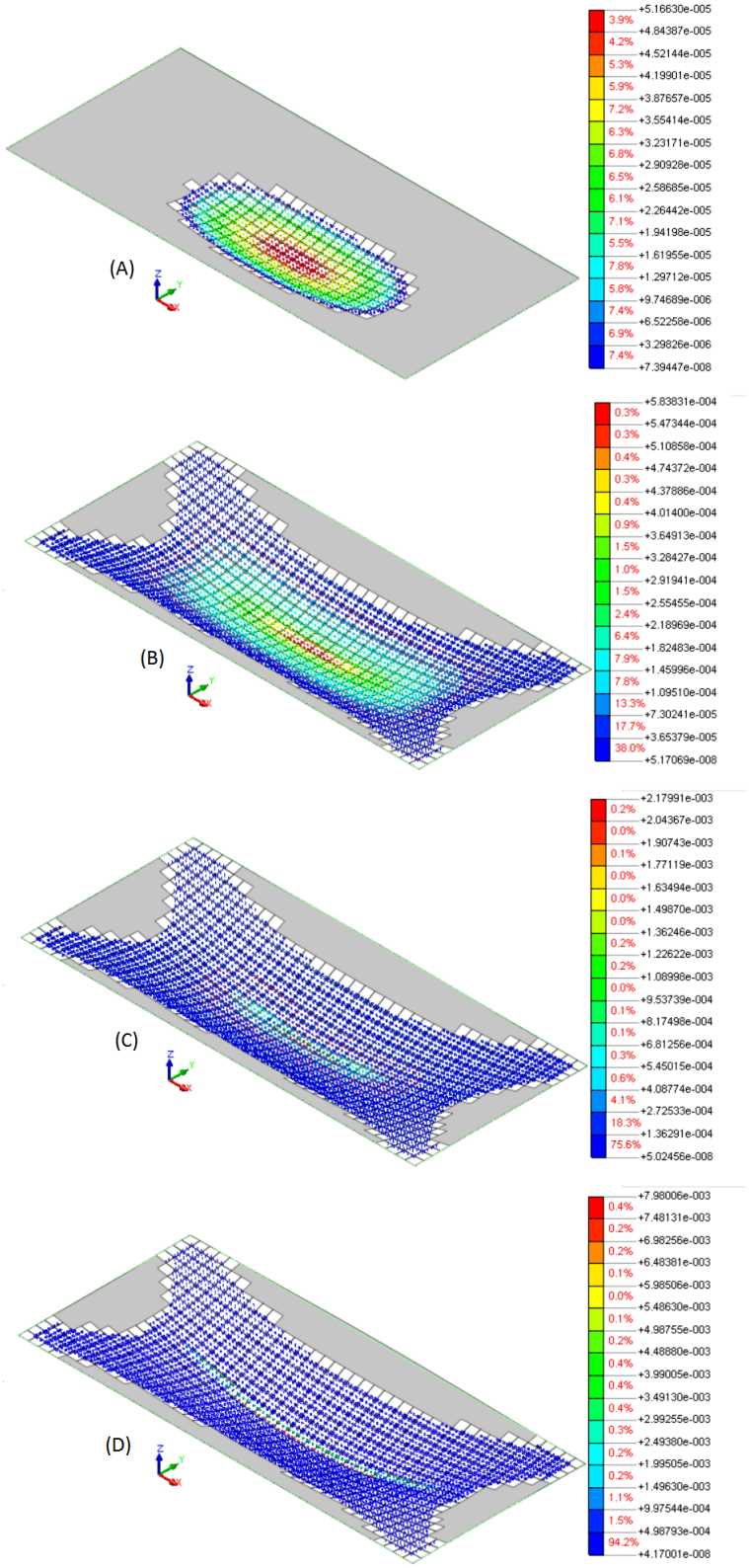

Figure 3-17: Crack pattern at points A, B, C and D of the load displacement curve with legend showing crack strain values

3-3-2 Quasi-dynamic Analysis

The post peak behaviour obtained in the non-linear static analysis is highly unstable showing the quasi-brittle nature of the Masonry. The post peak behaviour is very important to our study as the deformation capacity of walls assumes great importance in the topic of seismic engineering. It should be noted from Figure 3-16 that post peak there is a sudden increase in the principal strain which could be attributed to the step not converging. There is an acceleration of crack formation taking place and the formation of macrocracks begins. The macrocracks are unstable, which means that the load has to decrease to avoid an uncontrolled growth. The sudden opening of the crack could also involve inertia effects. It's therefore important to not neglect the effect of inertia and try to see if a dynamic analysis helps achieve post peak behaviour.

Consequently, an approach is taken up in which the application of load is done with respect to time slowly to cause low strain rate in the wall to ensure a quasistatic response but the transient effects of inertia and damping are also included to be able to understand the stability of the post peak response of the finite shell element model in a different way. This is referred to as Quasi-dynamic analysis from here on.

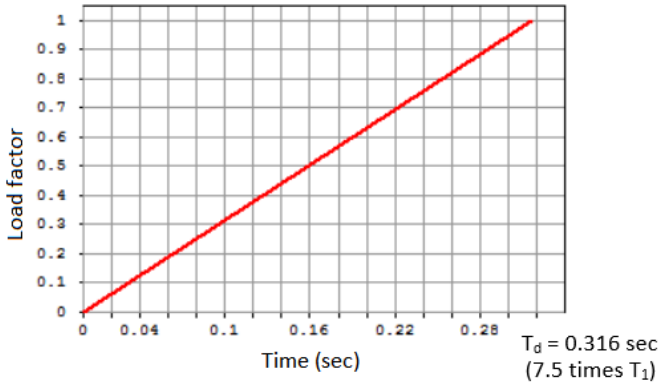

Figure 3-18: Load applied with respect to time

The load here is applied as a ramp function i.e load is applied as a function of time as shown in Figure 3-18. The maximum load (load factor of 1) is set to 5000 N/mm^2 which is the same as the non-linear static analysis and is higher than the failure load of 4410 N/mm^2. The load is increased to its maximum over a period of time called the rise time T_d. The load is applied in time steps that are very small post peak as compared to the ones in the pre peak zone. It is observed that the use of smaller time steps in the post peak zone is very essential to obtain a reliable response as is explained in the parametric study for time steps in this section at a later stage. Also, the use of tighter convergence tolerance for force and displacement norm is essential and hence a value of 0.001 is used instead of the default 0.01.

First an eigen value analysis is run and the rayleigh damping coefficients a and b are deduced taking into account the first mode and the third mode which cumulatively contribute to 73 % of the response in the direction of the load and a damping ratio ζ. The contribution of higher modes is minimal and is not considered. Mode 1 and 3 shapes are shown in Figure 3-19 and Figure 3-20. The mass damping coefficent a is set to zero to avoid mass damping effects and only the stiffness damping is taken into account using b. Consistent mass and damping matrices are used. The Newmark integration scheme is used for time integration with integration constants $\gamma = 0.5$ $\beta = 0.25$ are used, as it is second order accurate. The rayleigh damping coefficients a and b corresponding to $\zeta = 0.05$ are found in the eigen value analysis.

Table 3-4: Quasi-dynamic analysis parameters - VdP model

Parameters	Values
Rise Time T_d $[s]$	0.316
Mode 1 Time period T_1 $[s]$	0.0418
Damping ratio ζ	0.05
Rayleigh Stiffness damping coefficient b $[s]$	2.05E-04
Young's Modulus E_o^{j+u} $[N/mm^2]$	3527
Tensile bond strength f_{tb} $[N/mm^2]$	0.5
Mode I fracture energy G_f^1 $[N/mm]$	0.035
Crack bandwidth h $[mm]$	93.54

The key to this solution procedure is the magnitude of the rise time $T_d >> T_1$ where $T_1 = 0.0418s$ is the time period of the first mode of vibration. This ensures the fact that there are no dynamic effects in the initial stages of load application. Thus the presence of dynamic effects, if any, would arise from a phenomenon not related to the frequency of the first mode of vibration. The rise time is set to $T_d = 0.316s$ which is 7.5 times $T_1 = 0.0418s$. The load steps are applied in 34 equal steps of 0.0079 s and 150 equal steps 3.16E-04 s for the stable post peak response.

The convergence criteria is the same as the arc length procedure where a Newton raphson iteration procedure is used. This is done with 75 iterations per step and the convergence norm used are displacement and force with the tighter tolerance of 0.001 as compared to the default value. The parameters used for the Quasi-dynamic analysis are listed in Table 3-4.

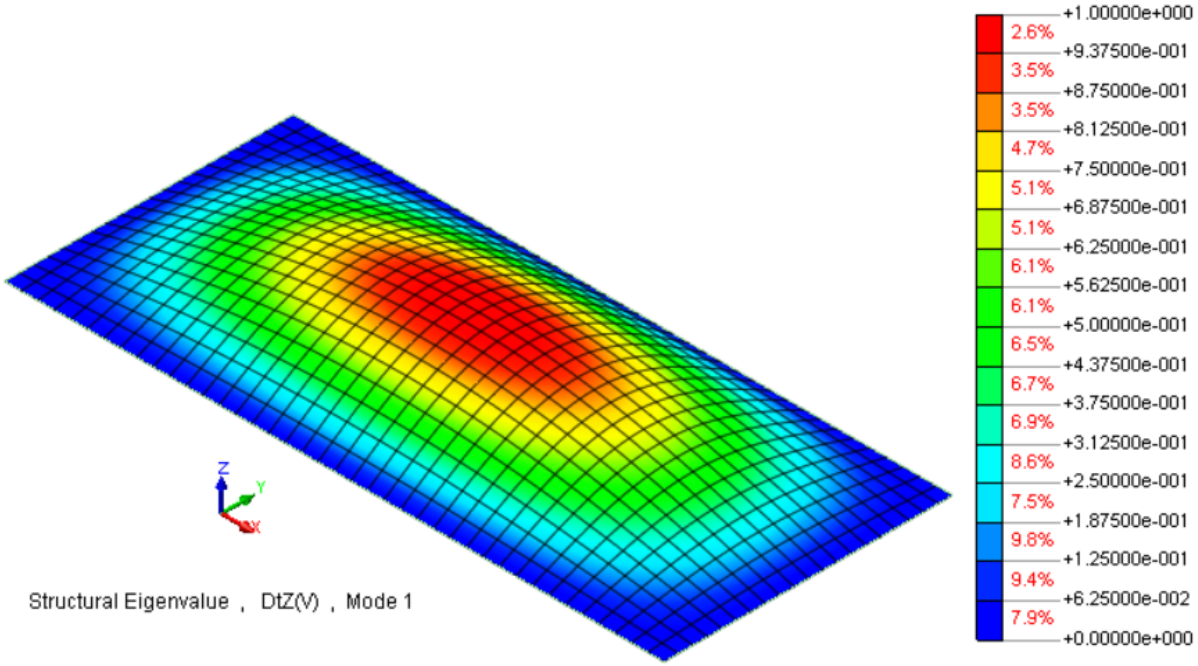

Figure 3-19: Mode 1 shape, Time period = 0.0418 s

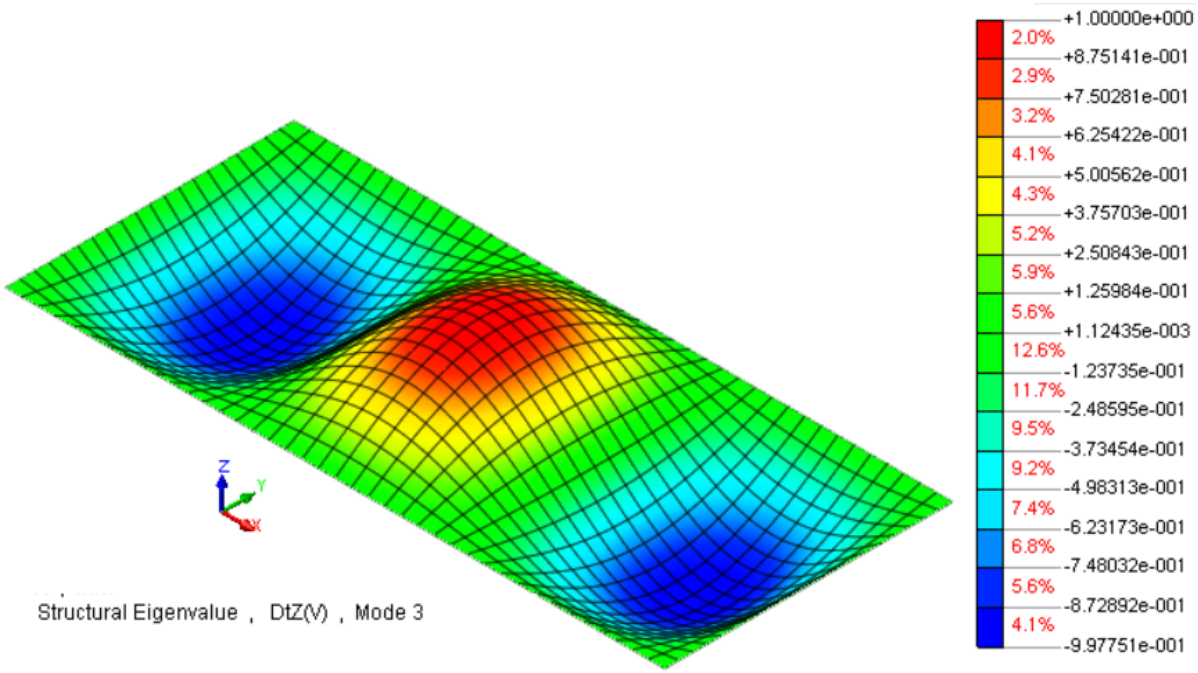

Figure 3-20: Mode 3 shape, Time period = 0.0186 s

Post-processing and Results

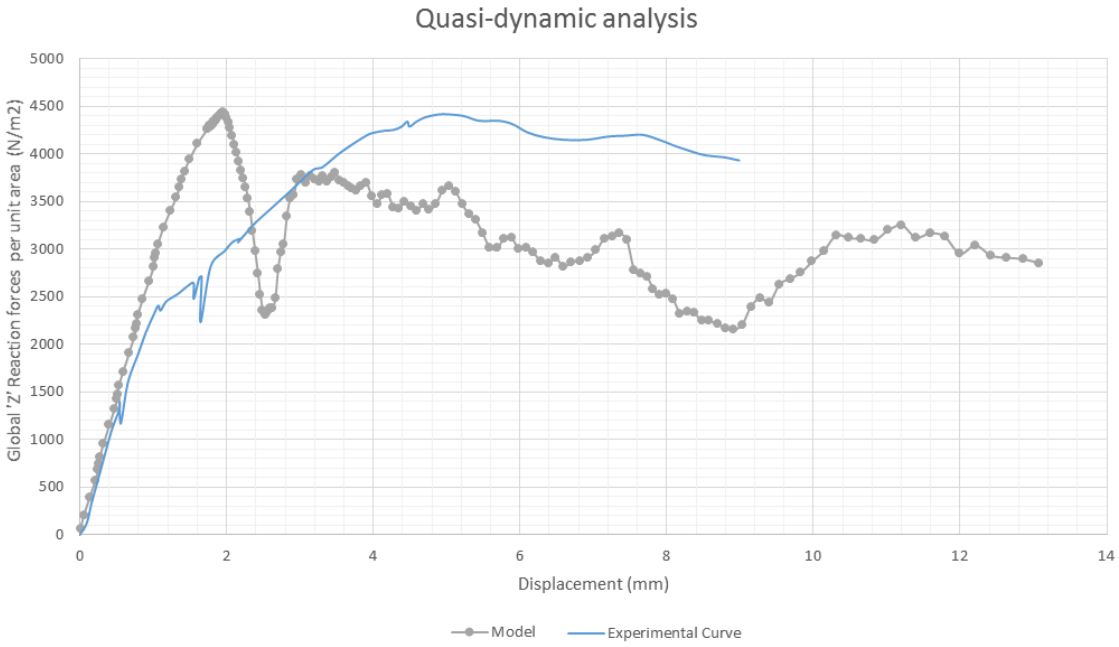

Figure 3-21: Load displacement curve obtained using Quasi-dynamic analysis - Global 'Z' reaction forces per unit area taken as the equivalent face pressure

The load displacement curve obtained for the Quasi-dynamic analysis is as shown in Figure 3-21. The applied load is increasing as is shown in the ramp input function, see Figure 3-18, to a valued of 5000 N/mm^2. However, the response of the model to the Quasi dynamic analysis shows the decrease of load beyond the peak where the macro crack propagation begins. This response has been obtained as a measure of the reaction forces from the supports for out of plane displacements against the out of plane displacement at the middle of the panel. The sum of reaction forces from the supports divided by the area is taken to be the distributed load on the panel for the loading to be presented in a capacity curve. It shows a post peak response unlike the non-linear static analysis. The effect of inertia (dynamic effects) is seen post peak as was expected and is negligible in the ascending part of the curve.

Figure 3-22 illustrates the effect of inertia after the peak labelled as point A. The decrease of the reaction forces (represented as the uniform distributed face pressure) in relation to increase of the applied load shows the violation of static equilibrium and the onset of dynamic equilibrium. The acceleration vs time graph, Figure 3-23, also shows the acceleration experienced by the wall post peak. The interpretation is shown in terms of calculations in the next page. This dynamic effect could be attributed to the sudden release of energy due to the formation of the macro crack. The energy triggers the vibrations but it is damped out due to the viscous damping factor added in the model. However, the acceleration values are quite high with one peak touching a value of 30 times g which could be reasoned as the effect of one of the higher modes getting excited. Addition of mass damping may help in this regard. The behaviour is not globally convergent as discussed in 3-3-2 but is appreciable as

most of the non converged steps, shown as red marks in Figure 3-27, approach the tolerance of displacement norm.

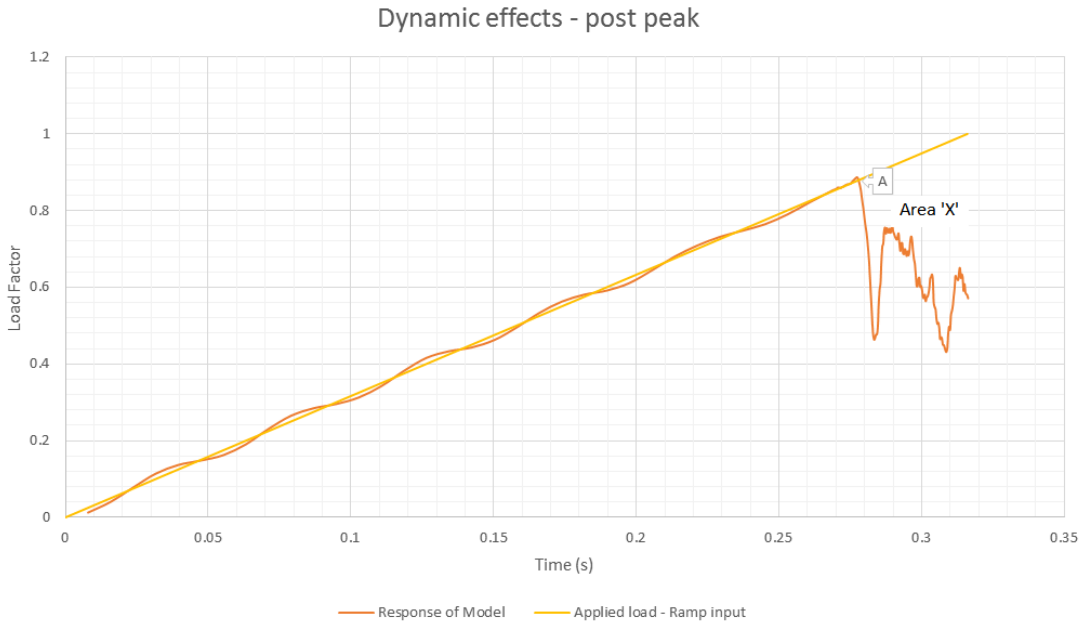

Figure 3-22: Dynamic equilibrium observed post peak - Applied load and the Global 'Z' reaction forces per unit area represented in relation to the maximum load applied 5000 N/m^2 as load factor

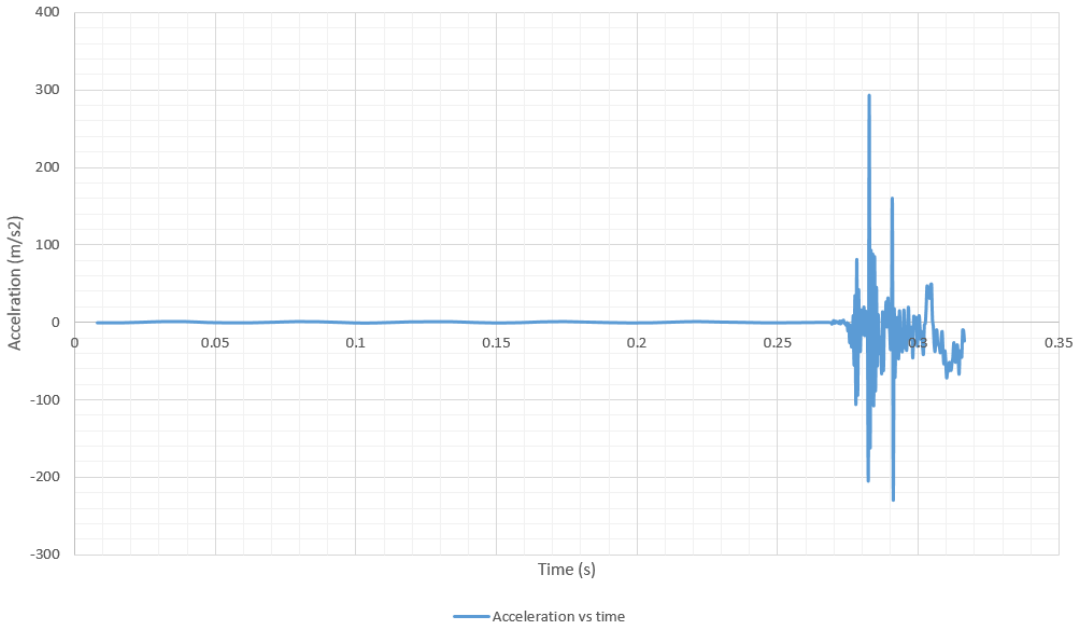

Figure 3-23: Inertia effects observed post peak

Calculations Area X in Figure 3-22 is the amount of Force F with regards to loss of static equilibrium considered.

$$F = AreaX * Load * Areaofwall = (0.5 * 0.4 * 2) * 5000N/m^2 * 7m^2 = 14000N$$

Mass of the wall:

$$M = Volumeofwall * Density = 0.7m^3 * 1900Kg/m^3 = 1330Kg$$

As an approximation (neglecting the damping force and the restoring force from stiffness),

$$F = M * acceleration$$
$$acceleration = F/M = 10.5m/s^2$$

The acceleration values as seen in Figure 3-23 are at an average around 10-20 m/s^2 but there are few peaks which are very high, one even touching close to $30g$. These could be some numerical problem in the solution procedure.

Effect of Time Steps It is observed in the post peak response obtained that there are 150 tiny time steps leading to the post peak behaviour as shown earlier. But when the size of the time steps are kept the same as in the pre-peak zone, i.e $0.0079s$, there are only three points time steps leading to the rise time T_d. The time steps are the markers on the curve and the curve clearly demarcates the need for smaller steps post peak to obtain a reliable and accurate curve. Also, the response in the equal step case is globally convergent due to the use of default convergence tolerance of 0.01 for both the force and displacement norms. The use of larger time steps has led to response not being a representation of interaction of the modes of vibration. When the time steps are very small, the oscillations are clearly captured. The tolerance could be improved to check if the obtained globally convergent result is obtained at lower tolerance levels of 0.001 and 0.0001. This leads us to a parametric analysis for the convergence tolerance to deduce a tight convergence tolerance which can be used for further analysis.

Effect of Convergence tolerance To increase the reliability of the curve obtained, a parametric study on the effect of convergence tolerance is done and is represented in Figure 3-26. When a tighter convergence tolerance of 0.001, 0.0001 and 0.00001 for force and displacement norms were used, the results were not globally convergent anymore unlike the default case of 0.01. But the analysis was not terminated upon loss of convergence and was continued to see the difference in the responses.

As it can be clearly seen in Figure 3-25, there is a clear difference in the response of model for different tolerance when larger time steps post peak are used. It's concluded that the second peak obtained in the response of the default case is thus not true. However the difference is comparatively lower when smaller time steps are used as is seen in Figure 3-26. Also, since

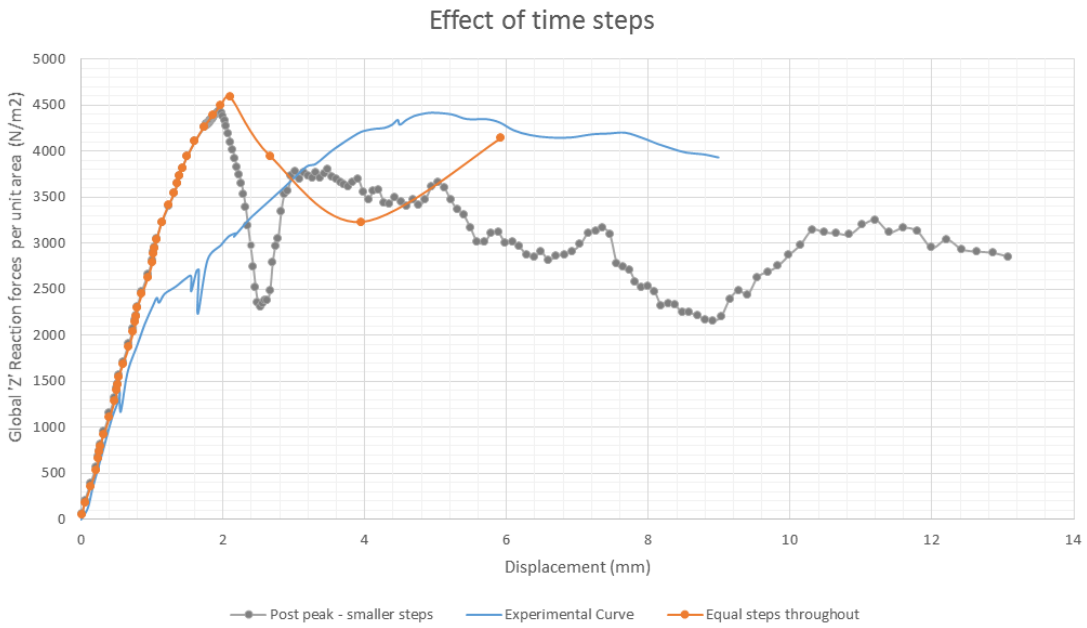

Figure 3-24: Effect of time steps post peak - Quasi-dynamic analysis

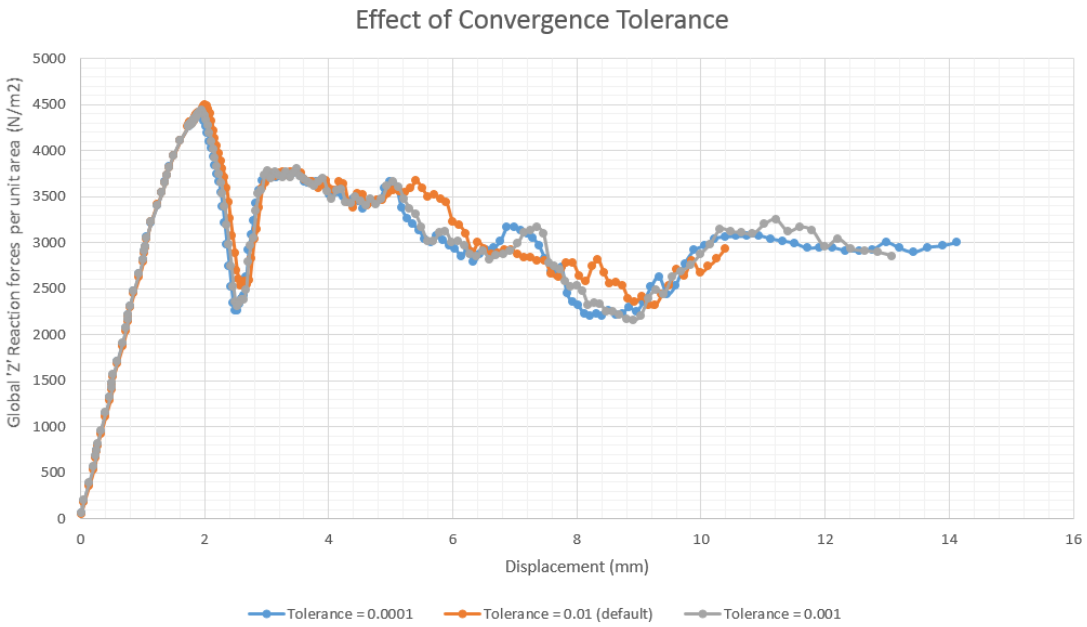

Figure 3-25: Effect of convergence tolerance - smaller steps post peak, Global 'Z' reaction forces per unit area taken as the equivalent face pressure

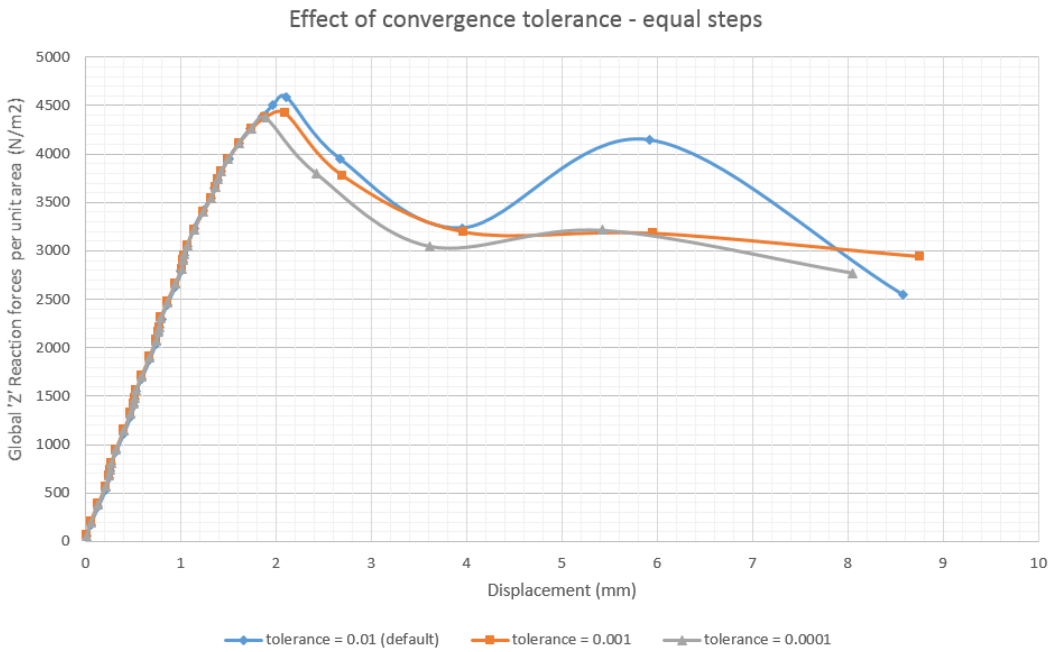

Figure 3-26: Effect of convergence tolerance - larger steps post peak,Global 'Z' reaction forces per unit area taken as the equivalent face pressure

the behaviour of the cases with tolerance 0.001 and 0.0001 are identical, the decision to use tolerance of 0.001 for all analysis is taken.

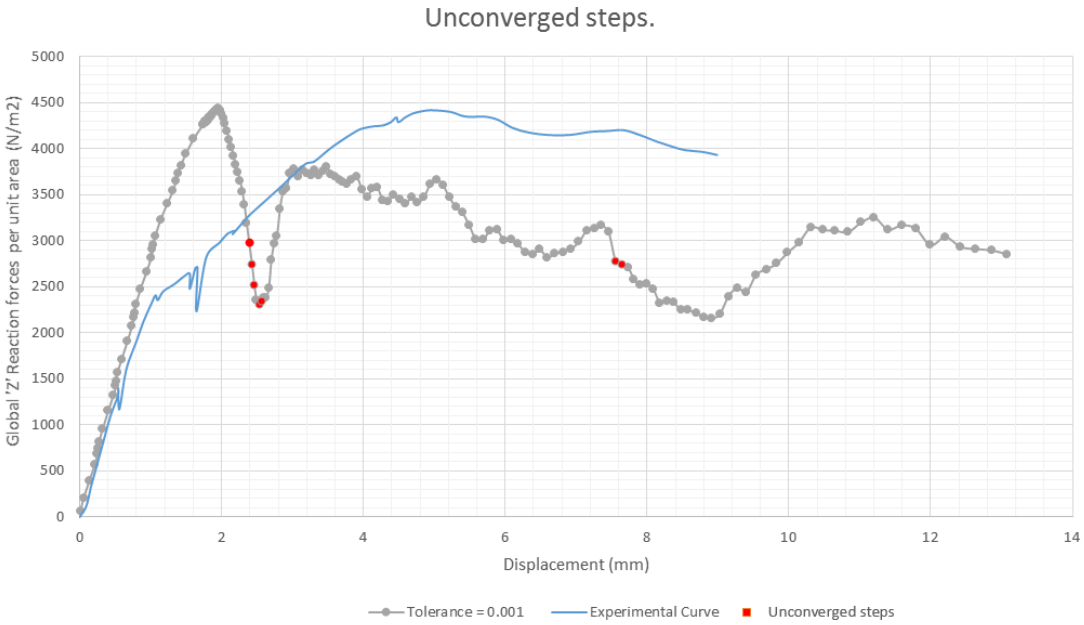

Figure 3-27: Unconverged steps in the 0.001 tolerance case, Global 'Z' reaction forces per unit area taken as the equivalent face pressure

Effect of Damping The effect of damping ratios can be seen in Figure 3-28. It can be seen that the load applied for the same period of time with different damping ratios (resulting in different rayleigh stiffness damping coefficients) leads to similar response containing the response of the modes (small oscillations). The only significant difference noticed is the first fall in load that corresponds to the start of dynamic equilibirum and it is lesser when the damping ratios are increased. Also, the displacement obtained for the same time of the applied load decreases with increasing damping ratios because the oscillations are damped faster (lower velocities as against the case of lower damping ratio with relatively higher velocities).

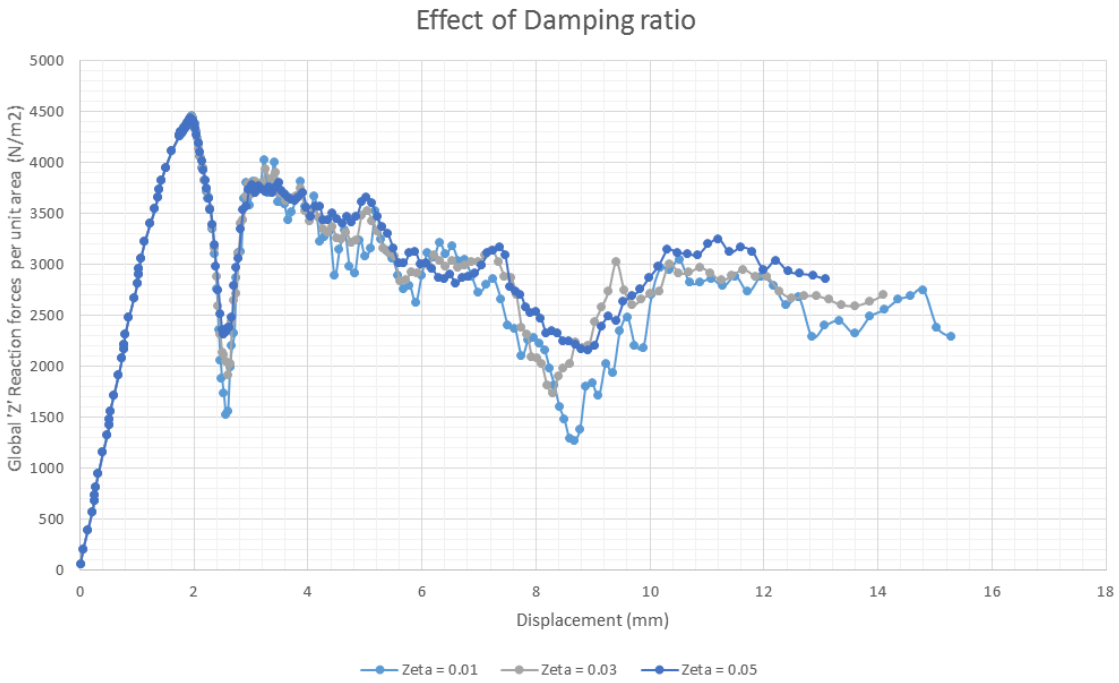

Figure 3-28: Effect of increasing damping ratios, Global 'Z' reaction forces per unit area taken as the equivalent face pressure

Principal strain plots The legend for the principal strain plots used is a norm deduced based on calculations as shown below.

$$\varepsilon_{ult.nn}^{cr} = \frac{G_f^1}{h * f_{tb}}$$

$$\varepsilon_{ult.nn}^{cr} = \frac{0.035N/mm}{93.54 * 0.5} = 7.49 \times 10^{-04}$$

$$\varepsilon_{nn}^{peak} = \frac{f_{tb}}{E_o^{j+u}} = 1.417 \times 10^{-04}$$

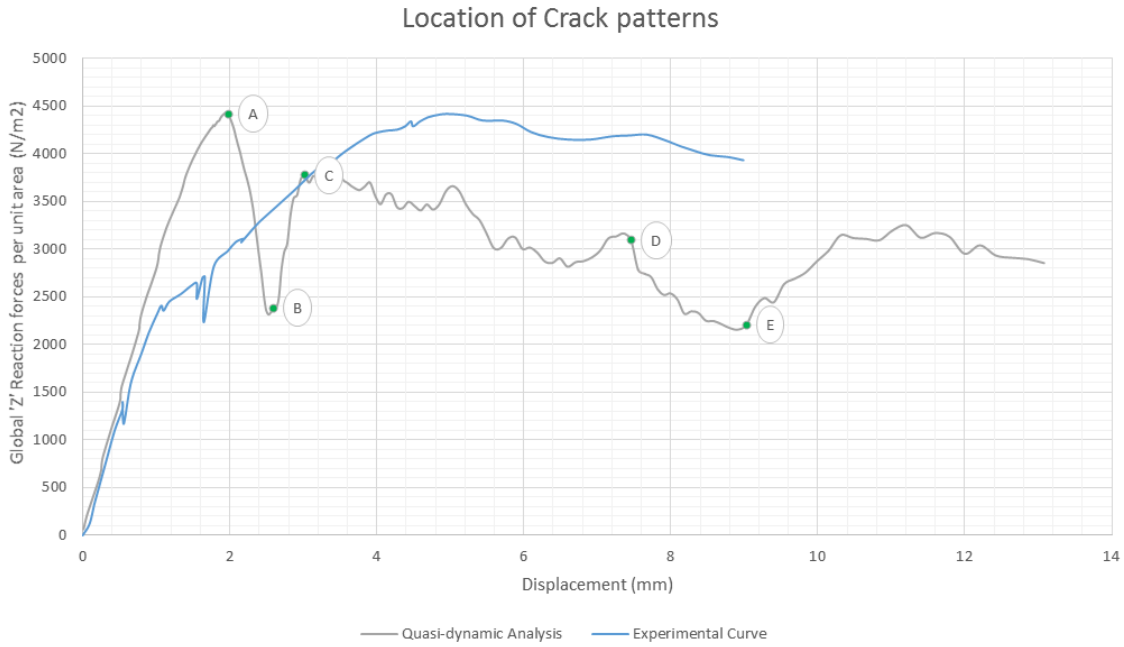

Figure 3-29: Finest Mesh - 40x20 Elements -load displacement curve

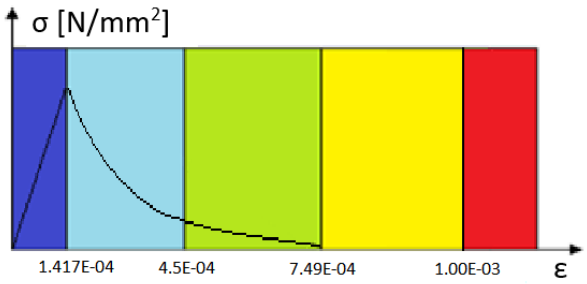

Figure 3-30: Legend for the principal strain plots - Shell element model, Global 'Z' reaction forces per unit area taken as the equivalent face pressure

Figure 3-29 is the load displacement curve from the quasi dynamic analysis of the shell element model. The reaction forces have been plotted against the displacement of the mid node of the

wall. It is observed that pre peak, the response is very similar to the arc length controlled non-linear static analysis which is due to the absence of the orthotropic character of the masonry. Nevertheless, the response is interpreted in terms of the strain plots. Crack patterns aren't shown for this study as the smeared cracks, over the entire wall in the post peak, make it really difficult to understand the crack patterns with the crack strain contours on it.

The key points of the response identified for investigation are points A, B, C, D and E where the point A is the peak load reached followed by inertia effects showing the drop in reaction forces. At Point A, the macro crack formation has already begun as can be seen in the strain plots. Point B shows the stark difference in bending (see the contorted elements along the horizontal crack) and also the progression of the horizontal crack. Point C marks the onset of the diagonal cracking and redistribution of moments and therefore the regain of capacity as is seen in the curve. Points D and E are interesting as they show that the entire wall has cracked seriously, although relatively lesser as compared to the yield line pattern of horizontal crack. The principal strain plots from points A is shown in Figure 3-31, B and C are shown in Figure 3-32 and for point D and E in Figure 3-33

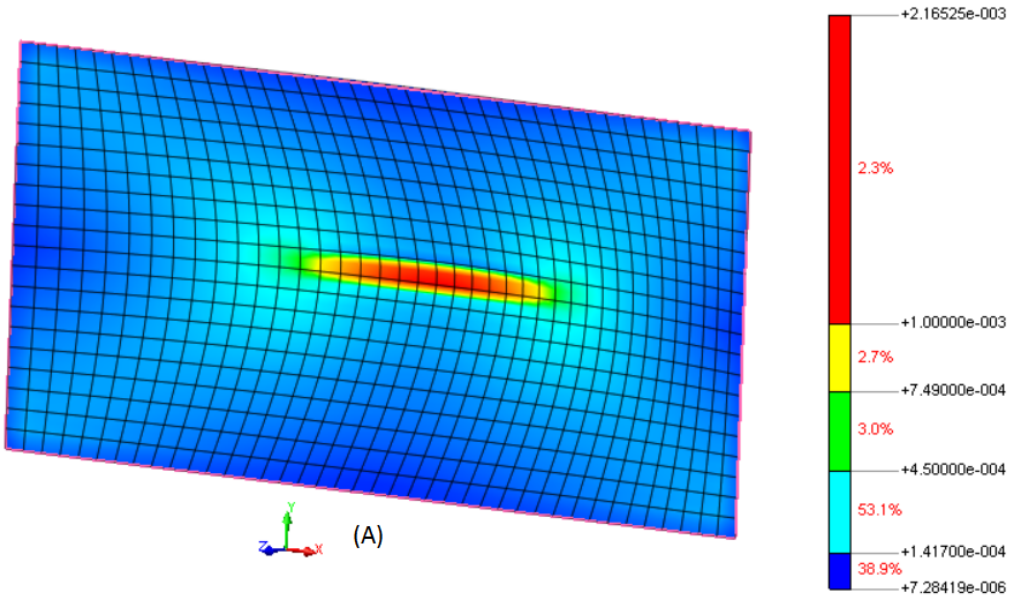

Figure 3-31: Principal strains at points A and B of the load displacement curve

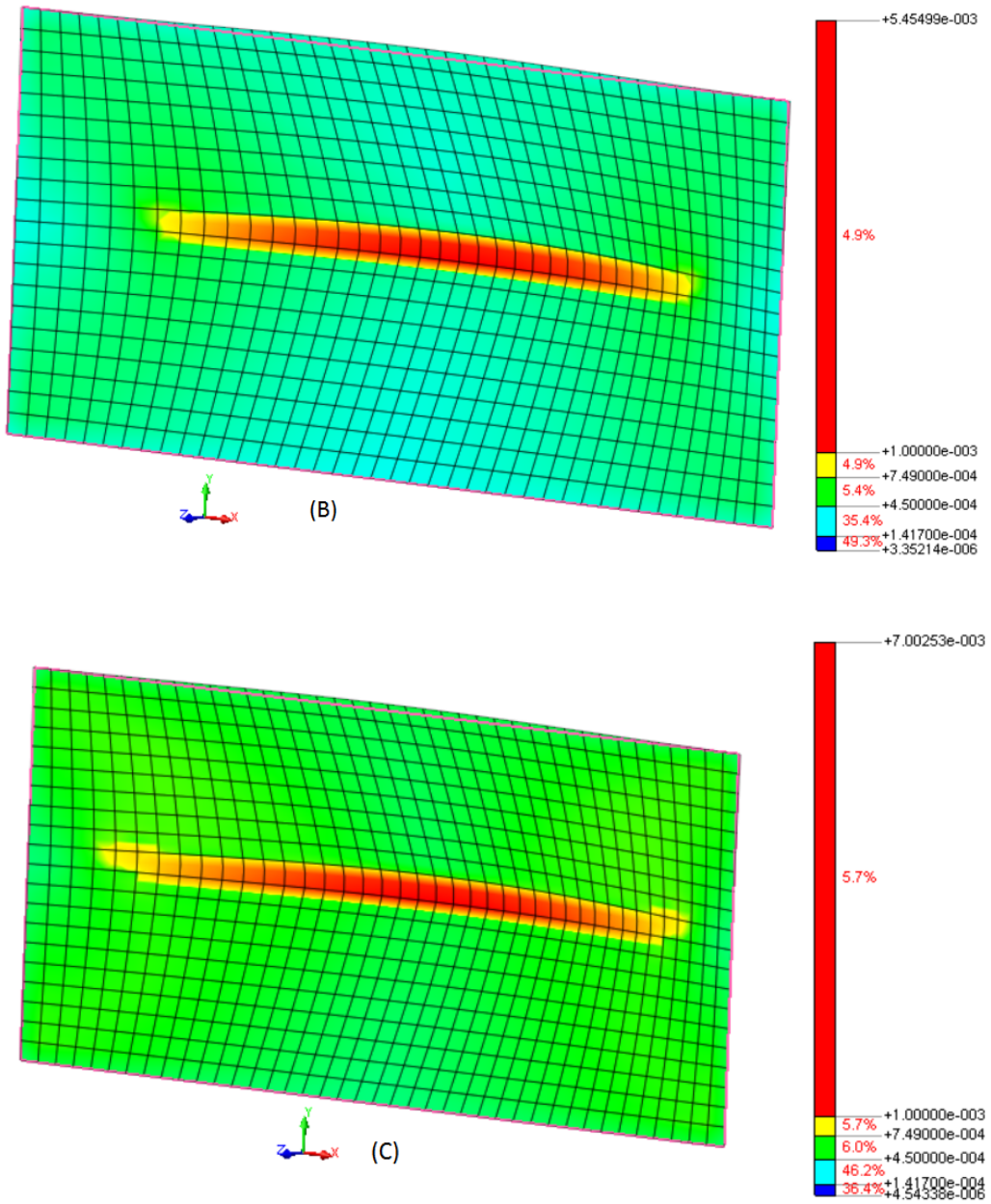

Figure 3-32: Principal strains at points B and C of the load displacement curve

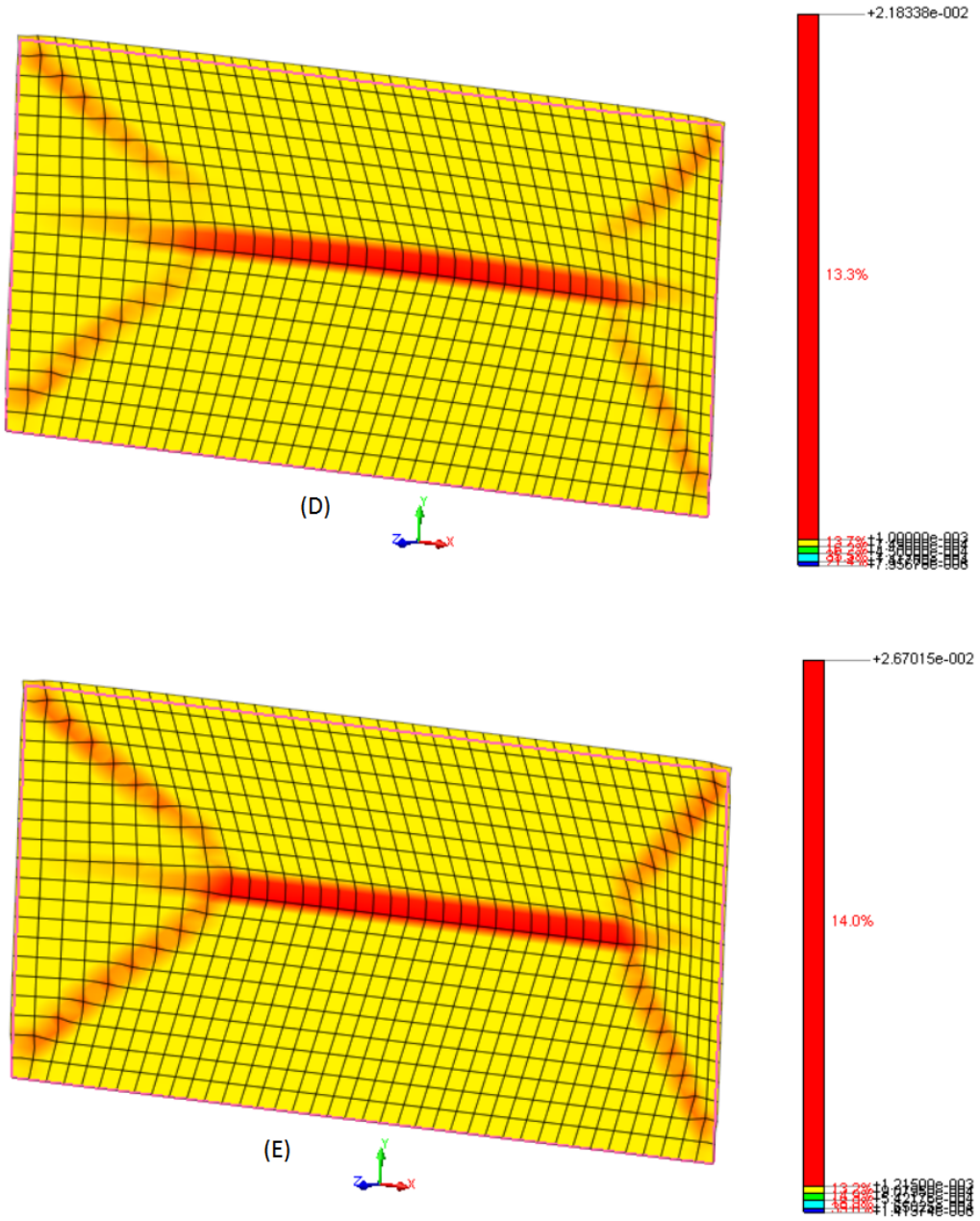

Figure 3-33: Principal strains at points D and E of the load displacement curve

Compression side crack pattern The assumption of elastic behaviour was made for compression regime. To be sure that the assumption was right and the crushing of the wall doesn't happen at the loaded face, the crack patterns at the last step of loading in the quasidynamic analysis is checked. It can be clearly seen that the range of stresses on the compression face of the wall is in the range of 0.54 MPa (compression) to 1.26 MPa in tension. Actually the tensile stresses are found on the loaded face as well and this has led to the crack pattern as shown in Figure 3-34.

According to Eurocode 6 - Design of masonry structures - Part 1-1: General rules for reinforced and unreinforced masonry structures, the characteristic compressive strength f_k of the masonry is established by the relation

$$f_k = K * f_b^{\alpha} * f_m^{\beta}$$

K, α and β are constants and f_m is the normalised compressive strength of the brick and f_m is the compressive strength of the mortar. As the mortar used is general purpose mortar, α is 0.7 and β is 0.3. The normalised compressive strength is reported to be 72 MPa and the average mortar compressive strength used for panel II is 8.75 MPa. Factor K is 0.55 for group I class units masonry and an additional factor of 0.8 according to 3.6.1.2 (6). This results in

$$f_k = 16.83 N/mm^2$$

, which is much higher than the values observed in the wall at the last loaded step. Thus the assumption of elastic behaviour in compression was safe.

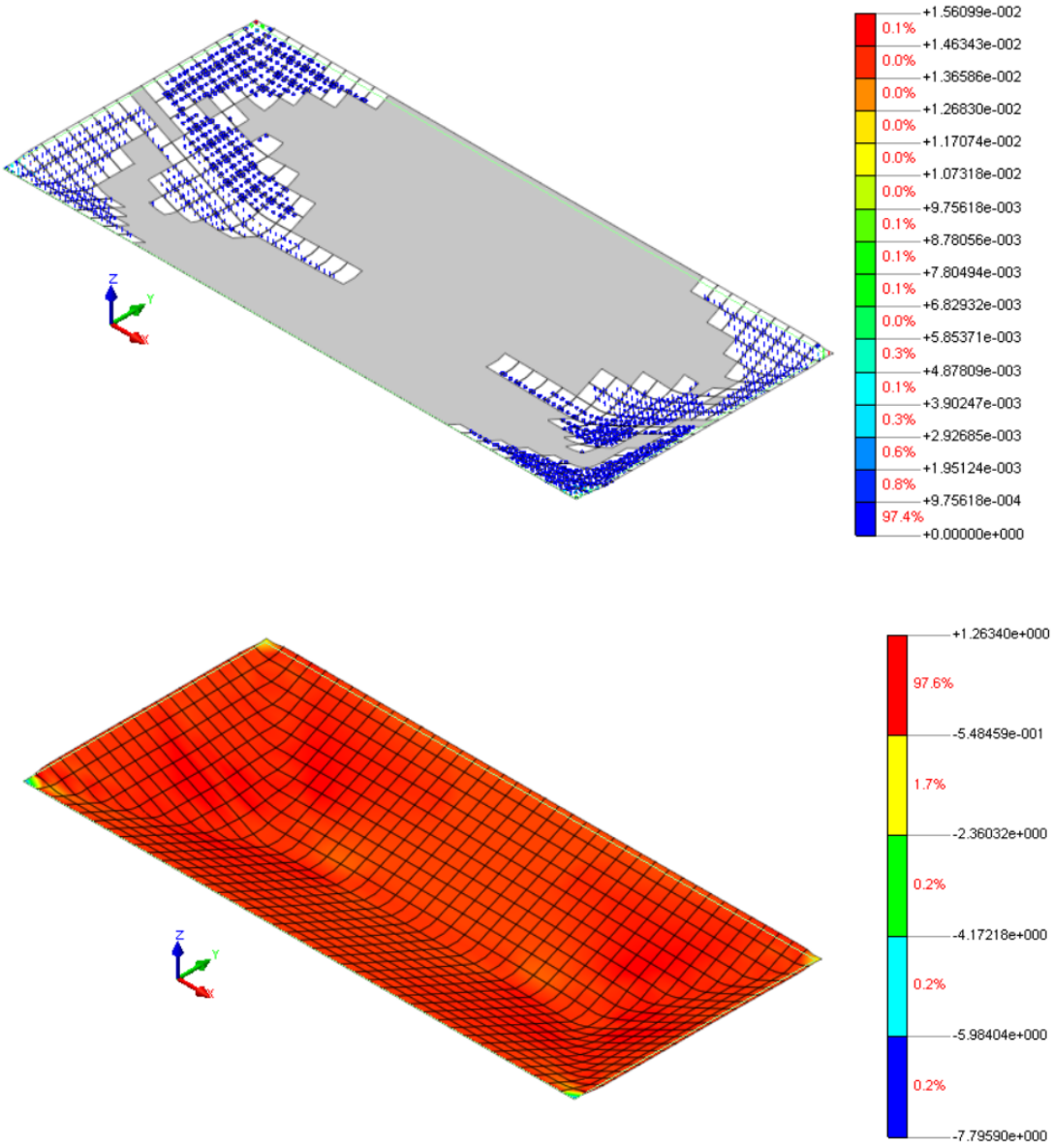

Figure 3-34: Crack pattern in the compressive side of the wall at the LAST step in the analysis and the corresponding principal stress

3-3-3 Conclusions

The isotropic continuum model is used as a base for the further investigation of orthotropy using the localized model, a variation of the shell element model. As can be seen in Figure 3-35, the Quasi-dynamic analysis yields post peak behaviour but has a certain amount of deviation from the actual post peak owing to the lack of orthotropy which results in the moment redistribution in the walls from the diagonal cracks. Although the deviation is around 20-25 % roughly through the post peak region, its a positive step towards understanding the response aided by the diagonal cracking. Further exploration in this avenue could help achieve refinement of the quasi-dynamic approach to increase reliability.

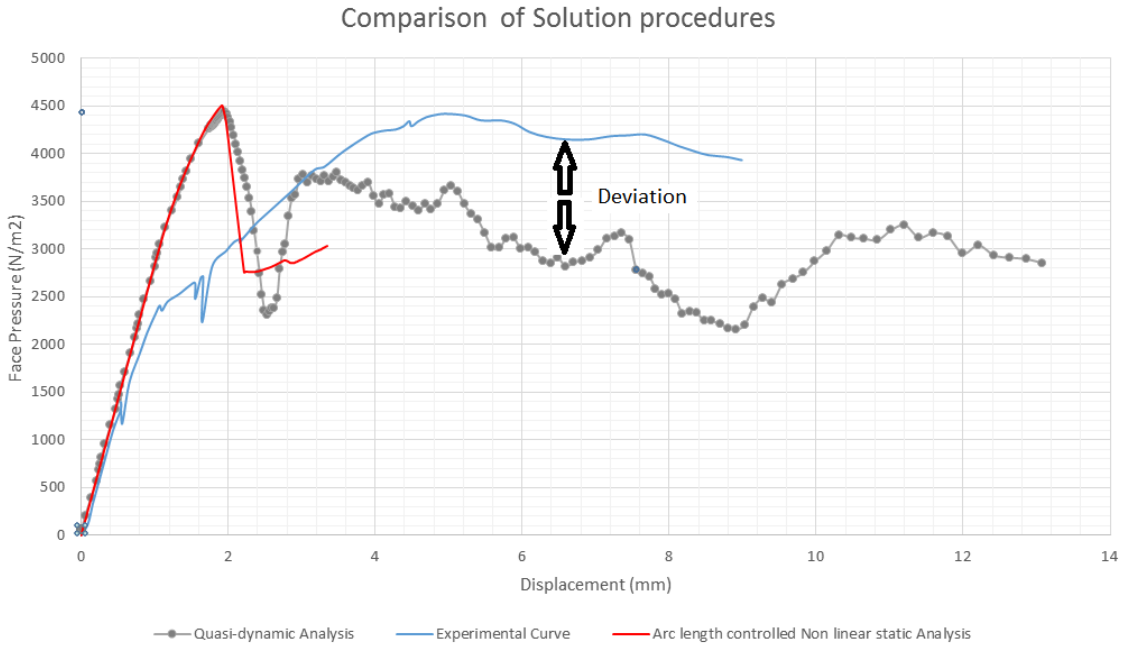

Figure 3-35: The non linear static and Quasi-dynamic analysis result comparison for Isotropic continuum shell model, Global 'Z' reaction forces per unit area taken as the equivalent face pressure in the Quasi-dynamic case

Some of the important conclusions drawn from this section are:

1. There is a need of more integration points along the thickness direction of the wall for accurate estimation of the capacity.
2. There is need for a sensitivity analysis for Mode I fracture energy every time to obtain response with the Isotropic masonry properties. This could be avoided with proper testing of masonry specimens in uniaxial tension. However, the model requires orthotropy to simulate the actual behaviour. Hence the testing could be done for masonry properties in the two orthogonal directions for tensile strength and Mode I fracture energy.
3. Arclength control is highly unstable post-peak and the quasi-dynamic approach yields a better post peak behaviour in comparison to the former.

3-4 Localized model

In this study, it is chosen to look into the nonlinear static and Quasi-dynamic analysis of the Wall in conjunction with Boundary conditions, Loading, constitutive model, Analysis types similar to the Isoparametric curved shell element model described in the previous section. The difference lies in the way the model is created wherein an area is created along the yield line, which is designated as the only portion of the wall with material properties for physical non linearity, as shown in Figure 3-37. The dimensions of the area are decided upon based on the crack pattern observed in the shell element model subjected to the arc length incremental procedure. This is essentially a variation of the shell element model to try simulate the orthotropic effect by giving higher tensile strength and Mode I fracture energy values for the diagonal strips as against the horizontal strip.

Preprocessing

The geometry of the Panel is then meshed using Isoparamteric quadrilateral and triangular curved shell elements with Quadratic interpolation in the localized area (blue elements) as shown. The integration scheme used is the 3x3x11 for these elements. The rest of the face of the wall when auto-meshed in Midas FX+ yields a combination of quadrilateral and triangular curved shell elements but some of the elements are highly skewed. The geometry of the model is deduced based on the line of thought presented in Figure 3-39.

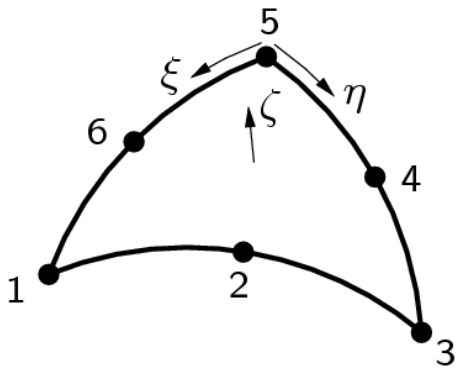

Figure 3-36: CT30S curved shell element

It's thus decided to mesh the rest of the face uniformly distributed with six-noded isoparamteric triangular curved shell element CT30S, shown in Figure 3-36, with the 3x11 integration scheme. The material behaviour in this zone is treated as linear. The localized zone consists of a combination of CQ40S element and CT30S element where non-linear constitutive model described in the previous section on shell element model is used. The boundary conditions are also the same as that for the shell element model and is shown in Figure 3-37. Figure 3-38 shows the dimensions of the local zone.

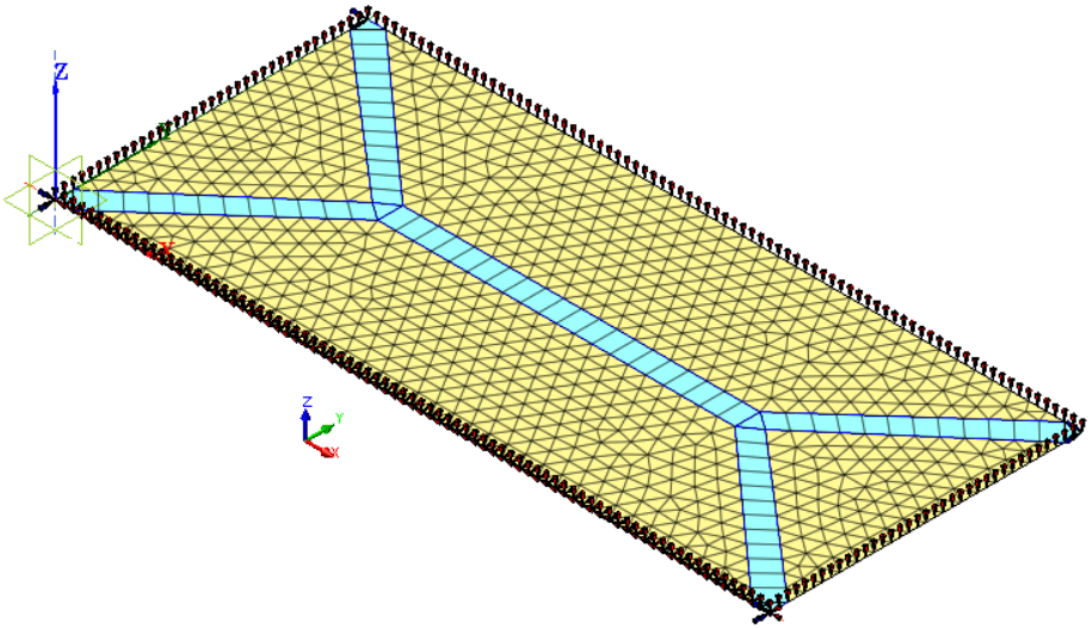

Figure 3-37: Localized Model with Boundary conditions

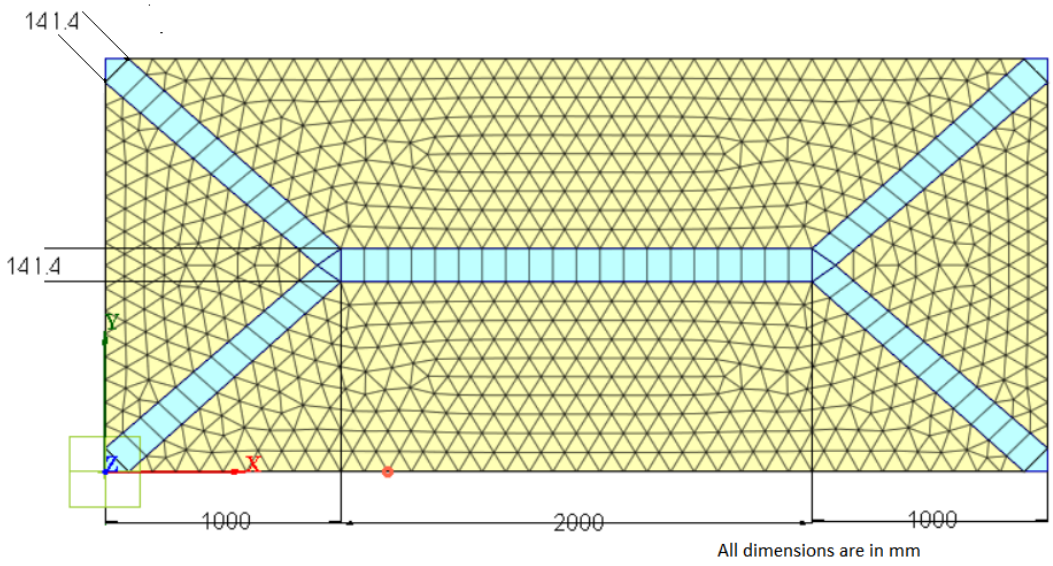

Figure 3-38: Local zone dimensions

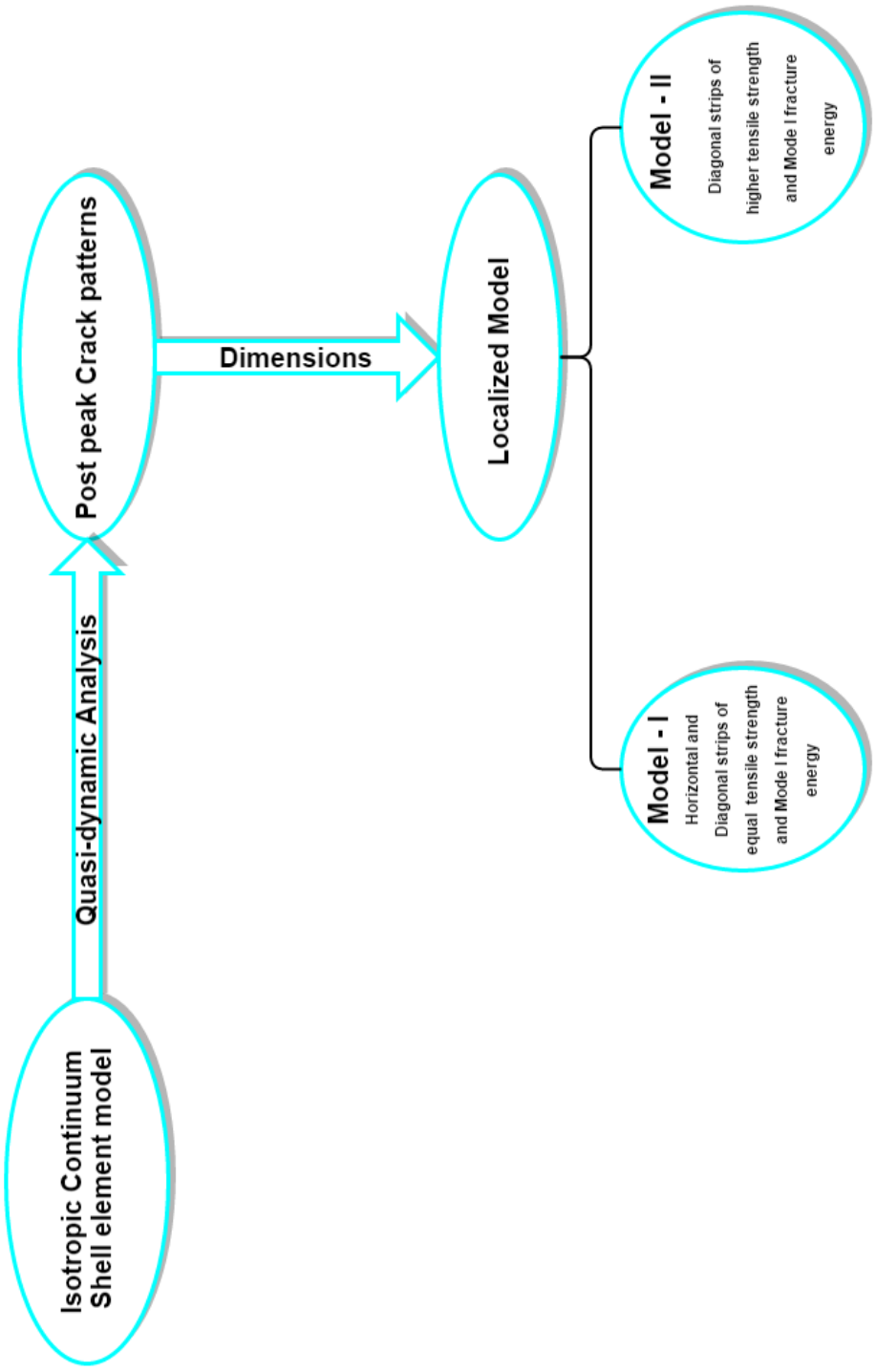

Figure 3-39: Localized model approach

3-4-1 Non-linear static analysis

Since the Force control procedure yields only the peak load and diverges post peak, and the post peak behaviour is looked into with more attention in this study, the Arc length control procedure is used for obtaining post peak behaviour of the Masonry walls. A global arc length procedure enhanced with line search option (for stabilizing the convergence behaviour and increasing the rate of convergence) is used. The arc length control is carried out with the Newton raphson iterative process with a maximum of 100 iterations per load step. A tolerance of 0.001 for the force and displacement norms is used instead of the default value of 0.01 to achieve results. The load is applied in uniform small steps which are $\frac{1}{200}th$ of the load applied - 5000 N/mm^2.

The model has two variations :

1. Local Model I - Model with horizontal and diagonal strips with equal G_f^1 and f_{tb} values of 0.035 N/mm and 0.5 N/mm^2 used in the shell element model.
2. Local Model II - Model with diagonal strips of higher strength and fracture energy values to indirectly simulate orthotropy. Since the test results don't have orthotropic values, orthogonal ratio is obtained as an approximation of the ratio of orthogonal moments which is close to ${l_x}^2/{l_y}^2 = 5.3$. The tensile strength of the horizontal strip is fixed at $f_{tb} = 0.3N/mm^2$ which is the average value of flexural bond wrench strength obtained from the tests as shown in Table 3-1 from which the diagonal strip's tensile strength is deduced using orthogonal ratio. The fracture energy values for the horizontal and diagonal strips are used initially for analysis, in accordance to the masonry properties listed for Continuum modelling in the Groningen Masonry research program.

The parameters used for the model are listed in Table 3-5:

Table 3-5: Masonry parameters - Localized VdP Models I and II

Model I uniform parameters	Values
Density $[Kg/m^3]$	1900
Young's Modulus E_o^{j+u} $[N/mm^2]$	3527
Tensile bond strength f_{tb} $[N/mm^2]$	0.5
Mode I fracture energy G_f^1 $[N/mm]$	0.035

Model II Parameters	Values
Density $[Kg/m^3]$	1900
Young's Modulus E_o^{j+u} $[N/mm^2]$	3527
Horizontal strip f_{tb} $[N/mm^2]$	0.3
Horizontal strip G_f^1 $[N/mm]$	0.01
Orthogonal ratio μ	5.3
Diagonal strip f_{tb} $[N/mm^2]$	1.6
Diagonal strip G_f^1 $[N/mm]$	0.06

Post processing and results

Figure 3-40: Load displacement curve for the Localized model I

Local Model I The Load displacement curve for the model is as shown in Figure 3-40. This is the response of the model when the horizontal and diagonal local strips are both provided with $G_f^1 = 0.035N/mm$ and $f_{tb} = 0.5N/mm^2$ which are the values used for the shell element model. The behaviour is then compared to that where the diagonal local zones are given higher strength and fracture energy values.

The response obtained is pretty similar to shell element response as the effect of orthotropy is key to simulate the two way bending case. The post peak also is very unstable as shown.

Effect of Orthotropy - Local Model II In the analytical calculations by Van der Pluijm using the Yield line method, he deduces the value of Orthogonal ratio of $R = 5.33$ and this is close to the approximation made. The final graph presented in Figure 3-41 has been deduced post a parametric analysis for the G_f^1 of the diagonal strips as with the assumed values for Localized Model-II, the response falls short of the peak load. Since the tensile bond strengths have been fixed upon, the diagonal strips' G_f^1 alone has been varied (shown in parametric analysis) to arrive at a value of $G_f^1 = 0.08N/mm$ which ultimately yields a response with peak of 97 % as that of the experimental peak.

It is to be noted that initially the elements of the discretization for the diagonal strip were large that the equivalent length of an element results in a snap-back in the constitutive model for the chosen paramteres and the concept of objective fracture energy which has been assumed is no longer satisfied. As a solution, based on the explanation in section for shell element model, the equivalent length h (the crack bandwidth) is reduced to 50 mm.

Points A, B, X, C and D are looked into with interest and their principal strain plots and crack patterns are shown in the next section where the response of the model is discussed in conjunction with the patterns.

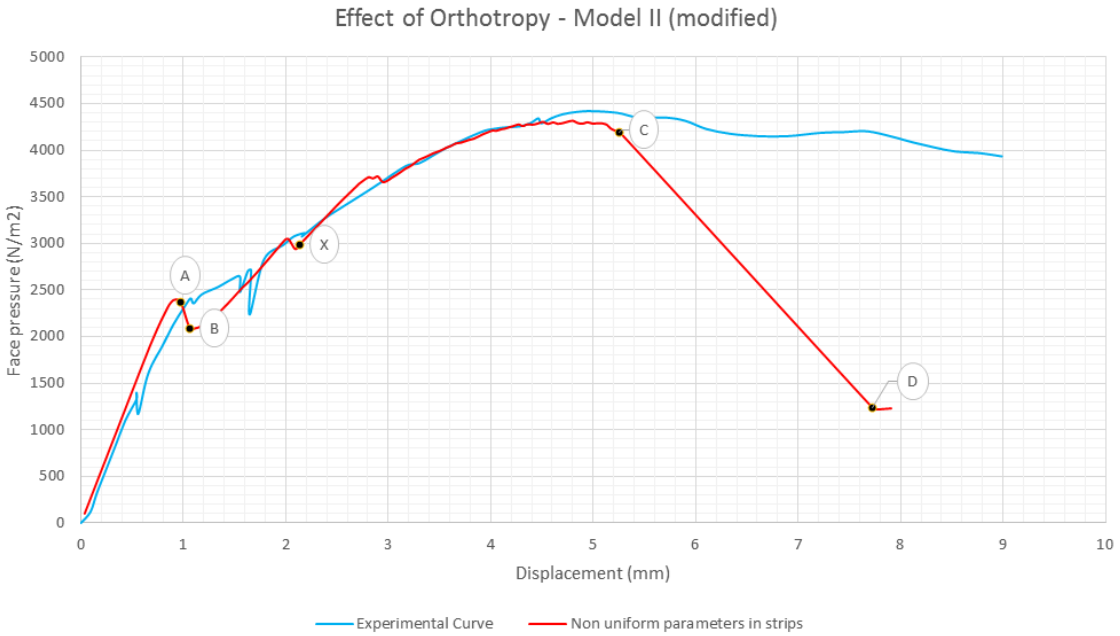

Figure 3-41: Localized model with Model-II parameters and Diagonal $G_f^1 = 0.08N/mm$

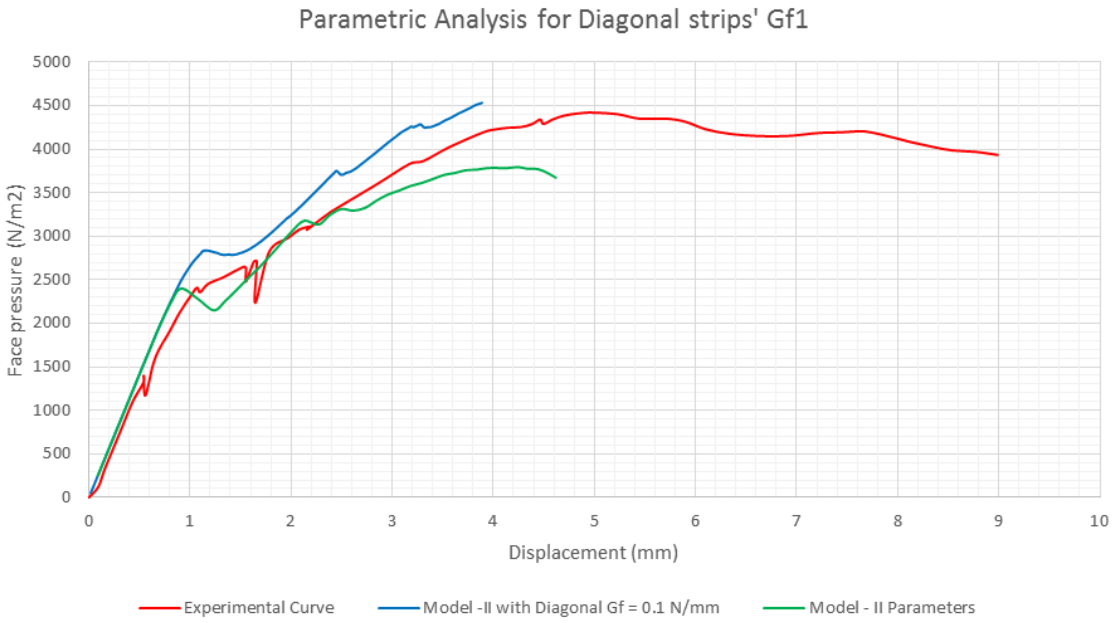

Figure 3-42: Localized model with Model-II - Parametric analysis for Diagonal G_f^1

Parametric analysis for Diagonal G_f^1 The model is made initially using the material parameters listed in Table 3-5 where the horizontal strip is given $G_f^1 = 0.01N/mm$ and $f_{tb} = 0.3N/mm^2$ and for the diagonal strips of the local zone $G_f^1 = 0.06N/mm$ and $f_{tb} = 1.6N/mm^2$ are given. This is done keeping in mind the fact that diagonal cracks have to propagate through head joints or the unit itself and bed joints in a stepped manner. But this yields a peak load which is 86 % of the experimental capacity. Hence a parametric analysis is done and the value of $G_f^1 = 0.08N/mm$ is fixed along with a crack bandwidth of 50mm for the diagonal cracks alone. This is shown in Figure 3-42.

Principal strain plots and Crack patterns The principal strain plots and crack patterns of Local model -II response is looked into to understand the changes in structural behaviour. Since the non-linearity is lumped in the local zone the cracking occurs only in that zone but when the principal stress values of the adjacent linear triangular elements are checked, they exceed $f_{tb} = 0.5N/mm^2$ which implies that this mode of simulating the behaviour may be fine in confining the failure zone but in reality the tensile strength is exceeded in adjacent elements too.

The values of ultimate peak strain and ultimate crack strain for the Horizontal strip are calculated as follows

$$\varepsilon_{ult.nn}^{cr} = \frac{G_f^1}{h * f_{tb}}$$

$$\varepsilon_{ult.nn}^{cr} = \frac{0.01N/mm}{118.9 * 0.3} = 2.803 \times 10^{-04}$$

$$\varepsilon_{nn}^{peak} = \frac{f_{tb}}{E_o^{j+u}} = 8.505 \times 10^{-05}$$

The legend for the principal strain plots used is a norm shown in Figure3-43. However the crack strains are not shown according to a generic legend in the crack patterns:

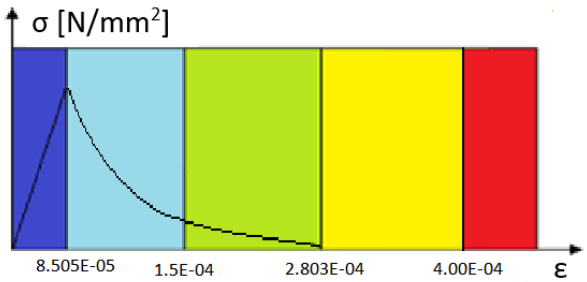

Figure 3-43: Legend for the principal strain plots - Local element Model-II Horizontal strip

The values of diagonal strips with the crack bandwidth calculated by DIANA according to $h = \sqrt[3]{A}$ where A is the planar area of the shell element will lead to the reduction of the tensile strength, which is not desired. Hence a crack bandwidth of 50mm is fixed for the

diagonal strip elements and the values of ultimate peak strain and ultimate crack strain for the diagonal strip are shown below:

$$\varepsilon^{cr}_{ult.nn} = \frac{G^1_f}{h * f_{tb}}$$

$$\varepsilon^{cr}_{ult.nn} = \frac{0.08N/mm}{50 * 1.6} = 1.00 \times 10^{-03}$$

$$\varepsilon^{peak}_{nn} = \frac{f_{tb}}{E^{j+u}_o} = 4.536 \times 10^{-04}$$

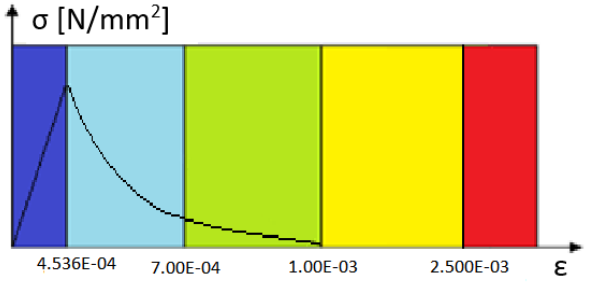

Figure 3-44: Legend for the principal strain plots - Local element Model-II Diagonal strip

Points A and B The principal strain plots are in accordance with Figure 3-43 and shows the progressive formation of the horizontal crack from point A to B and the deformed elements along the crack. The stage at which the crack is expected by Van der Pluijm to have started is close to the prediction by the localized model. The principal strain plot B shows the middle of the wall having the formation of the macro crack which is seen as the red zone at the centre of the wall. Since this is a zone of non linearity and the shell elements have 3x3 integration points in plane, the crack pattern shows smeared pattern within the element alond the three lines.

The formation of the crack leads to the drop in the load from point A to B and thus the unloading is justified. Post point B the response has reduced stiffness but the redistribution of the moment capacity due to the stronger and tougher diagonal zone leads the response of the wall to the peak load and thereafter the ductile region where the clear effect of the toughness of the diagonal zone is seen which adds to the overall deformation capacity of the wall.

Point X Point X marks the starts of the cracking of the diagonal zone and hence we see a drop in capacity and a further reduction in the stiffness of the response of the wall.

Points C and D The principal strain plots are in accordance with Figure 3-44 and shows the formation of the diagonal crack. The principal strain plot C shows the middle of the wall having the formation of the macro crack which is seen as the red zone at the centre of the wall. Due to difference in legend in the strain plots of the horizontal and diagonal strips, the extent to which the horizontal strip has seriously cracked is more than seen in plot C and D. It also has to be noted that the principal strains in the linear part of the wall seems to exceed the strain corresponding to the tensile strength and thus as explained before, the idea of confining the non linearity within the local zone is only a technique to simulate the behaviour.

The diagonal crack is beginning to be seen as a macro crack but there is a sudden drop of capacity of the wall leading to point D where the entire local zone seems to be cracked. The progressive failure of the diagonal strips is not understood clearly and warrants the need to study the post peak behaviour in detail using a better solution procedure.

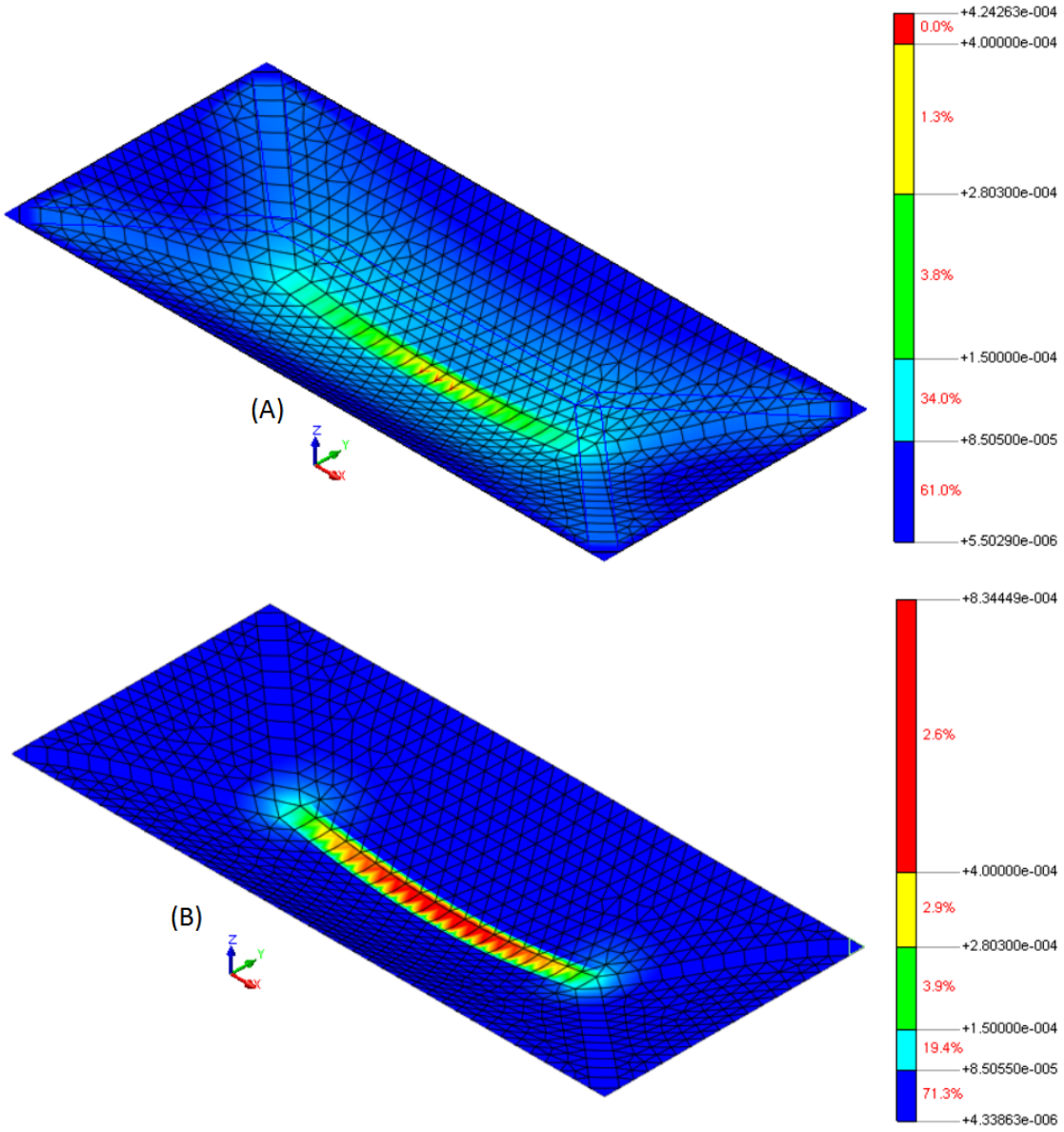

Figure 3-45: Principal strains at points A and B of the load displacement curve

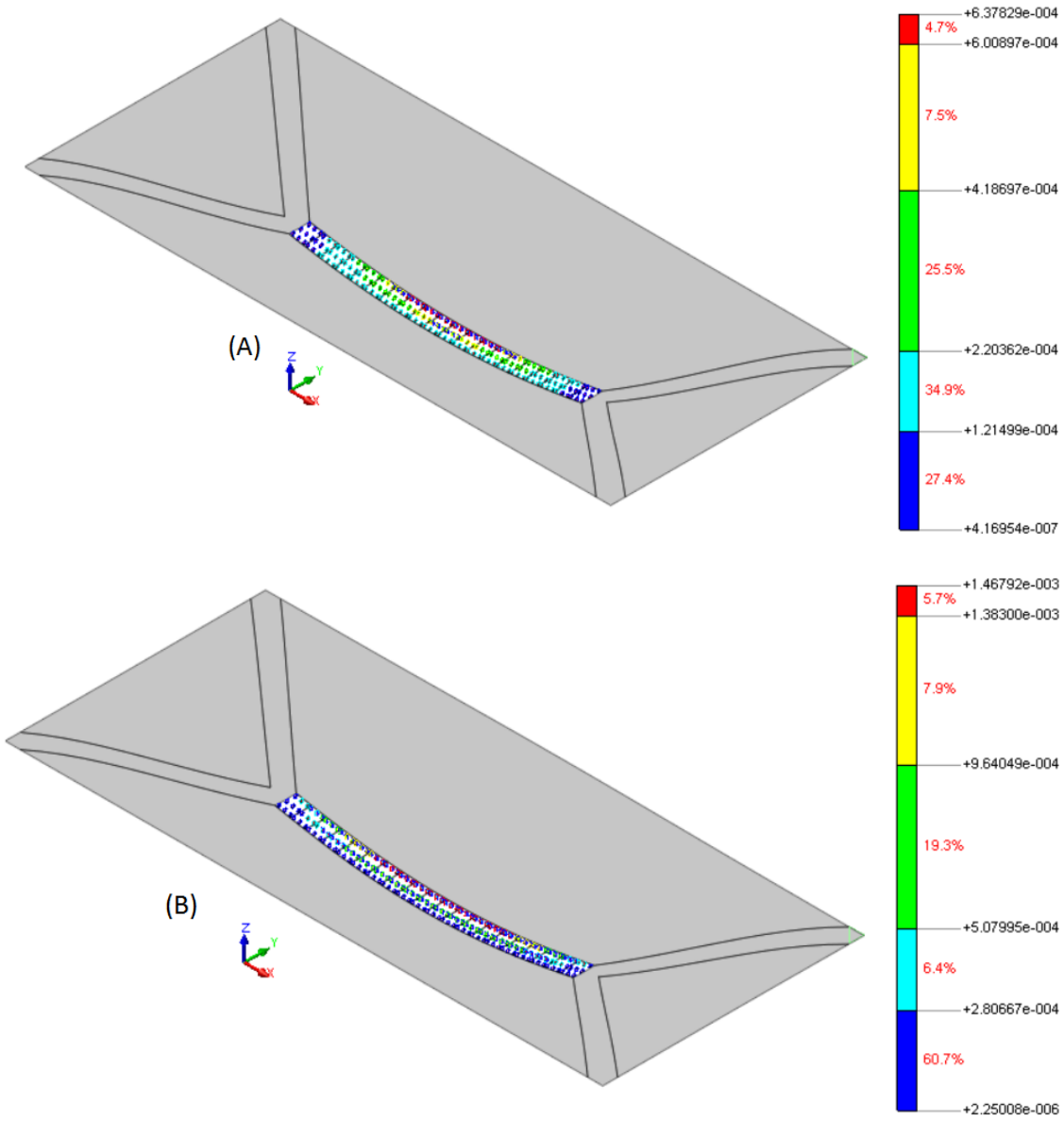

Figure 3-46: Crack pattern at points A and B of the load displacement curve and the crack strain legend.

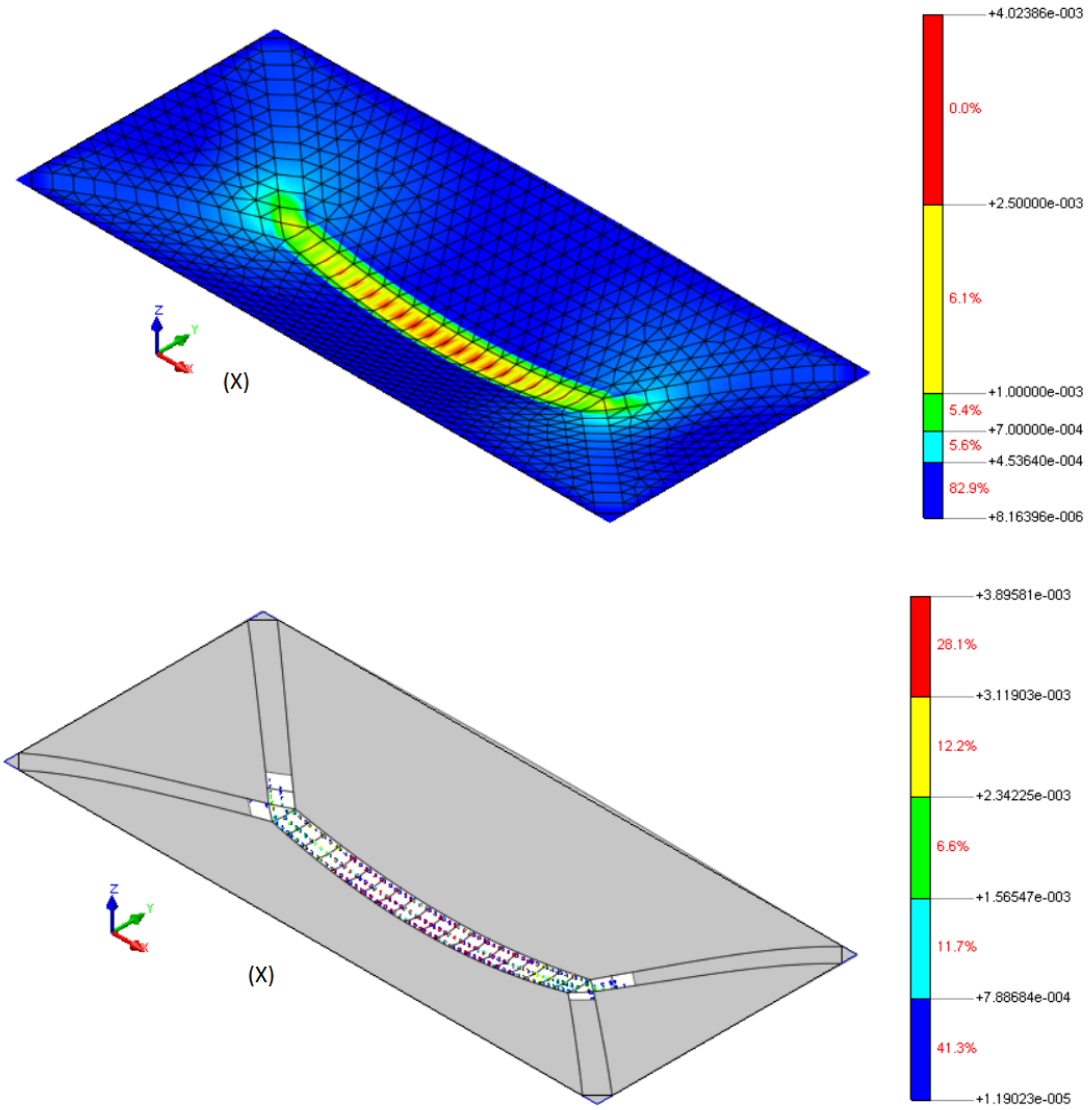

Figure 3-47: Principal strains and crack pattern at point X of the load displacement curve

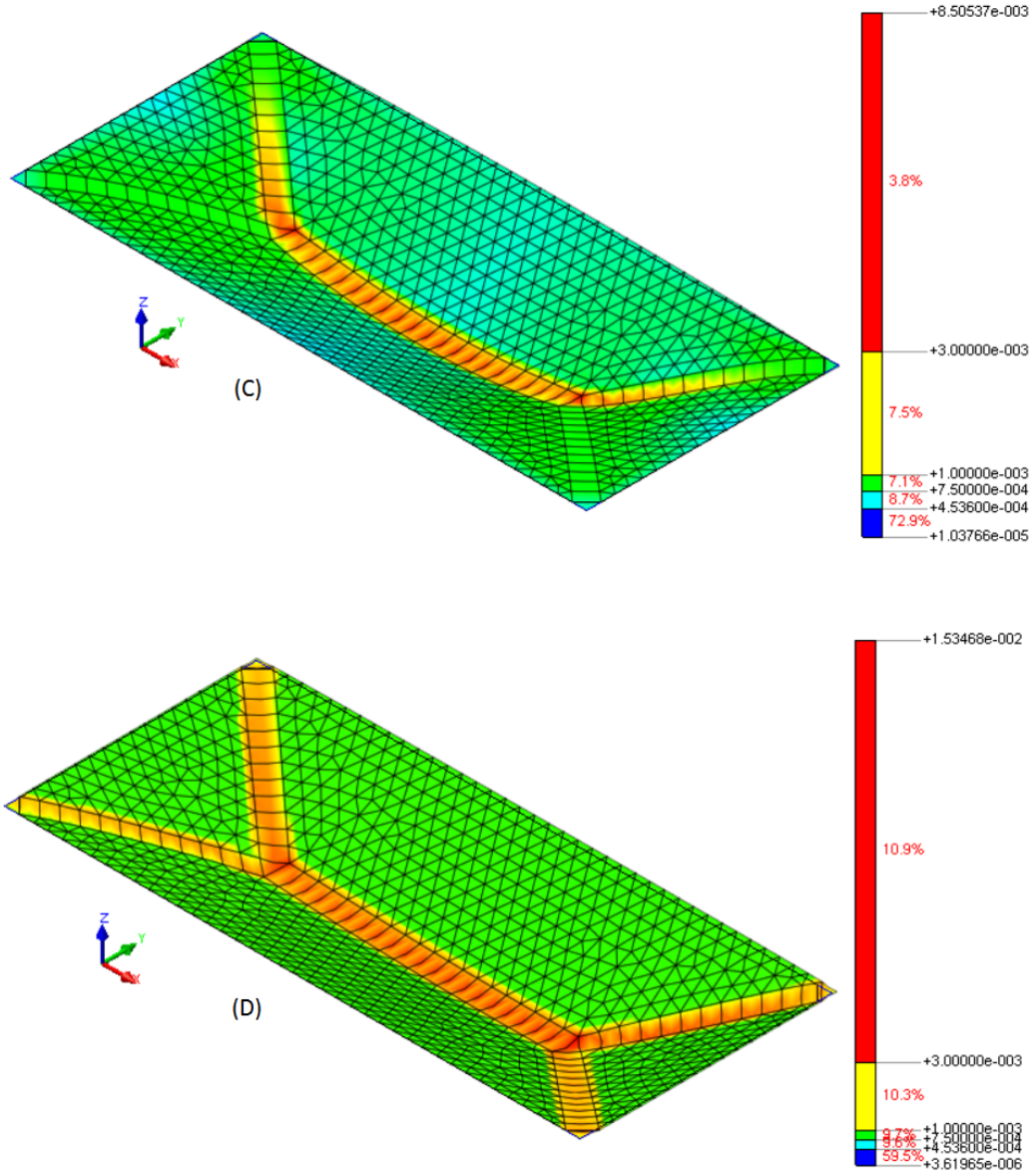

Figure 3-48: Principal strains at points C and D of the load displacement curve

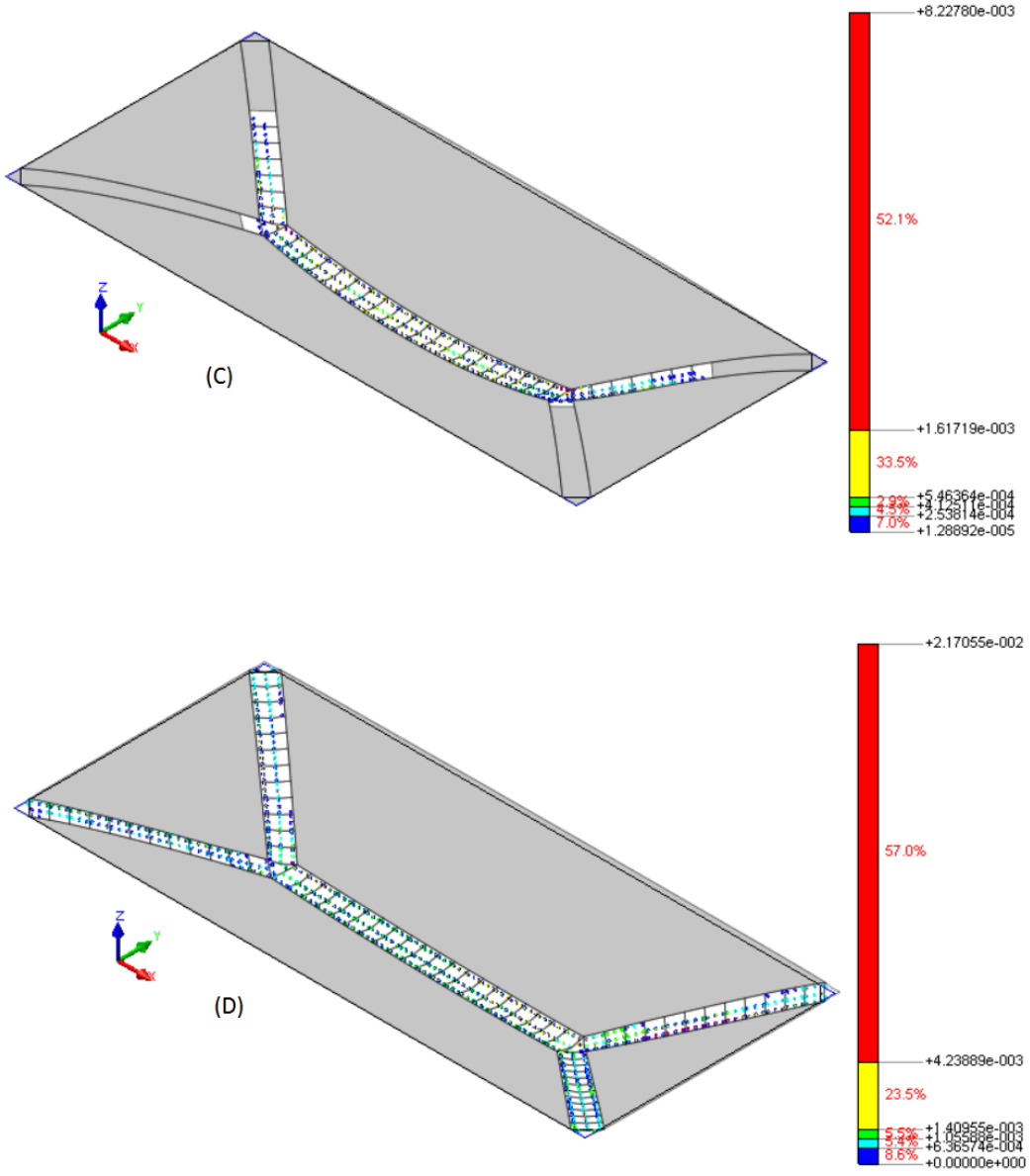

Figure 3-49: Crack pattern at points C and D of the load displacement curve and the crack strain legend.

3-4-2 Quasi-dynamic analysis

The Quasi-dynamic approach similar to the shell element model is undertaken to take into account the inertia effects caused by the macro crack formation. First an eigen value analysis is run to calculate the rayleigh damping coefficients a and b taking into account the first and third modes of vibrations contributing cumulatively to 73 % and a damping ratio $\zeta = 0.05$. Mode 1 and 3 shapes are shown in Figure 3-51 and Figure 3-52. The mass damping coefficent a is set to zero to avoid mass damping effects which are quite large and only the stiffness damping is taken into account using b. Consistent mass and damping matrices are used. The Newmark integration scheme is used for time integration with integration constants $\gamma = 0.5$ $\beta = 0.25$ are used, as it is second order accurate.

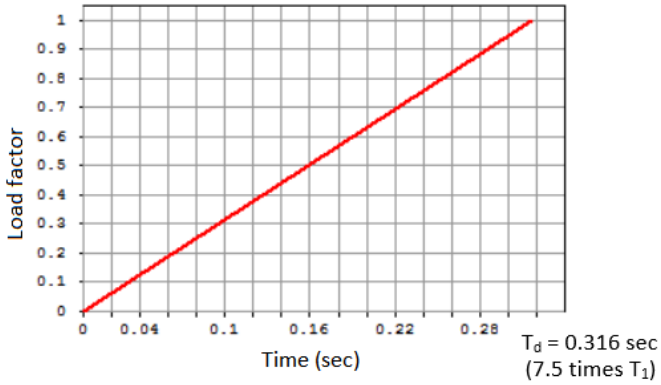

Figure 3-50: Load applied with respect to time

The load is applied as function of time as shown in Figure 3-50 where the maximum load (load factor of 1) is set to 5000 N/mm^2 which is the same as the non-linear static analysis and is higher than the failure load of 4410 N/mm^2 and the rise time is set to $T_d = 0.316s$ which is 7.5 times $T_1 = 0.0418s$. The load steps are applied in 34 equal steps of 0.0079 s and 150 equal steps 3.16E-04 s for the stable post peak response. Convergence tolerance of 0.001 is used based on the conclusion drawn from the shell element model for a tighter tolerance. The parameters used for the Quasi-dynamic analysis of the localized model are listed in Table 3-6.

Table 3-6: Quasi-dynamic analysis parameters - Localized VdP model-II

Parameters	Values
Rise Time T_d $[s]$	0.316
Mode 1 Time period T_1 $[s]$	0.0418
Damping ratio ζ	0.05
Rayleigh Stiffness damping coefficient b $[s]$	2.05E-04
Young's Modulus E_o^{j+u} $[N/mm^2]$	3527
Tensile bond strength f_{tb} $[N/mm^2]$	0.5
Mode I fracture energy G_f^1 $[N/mm]$	0.035

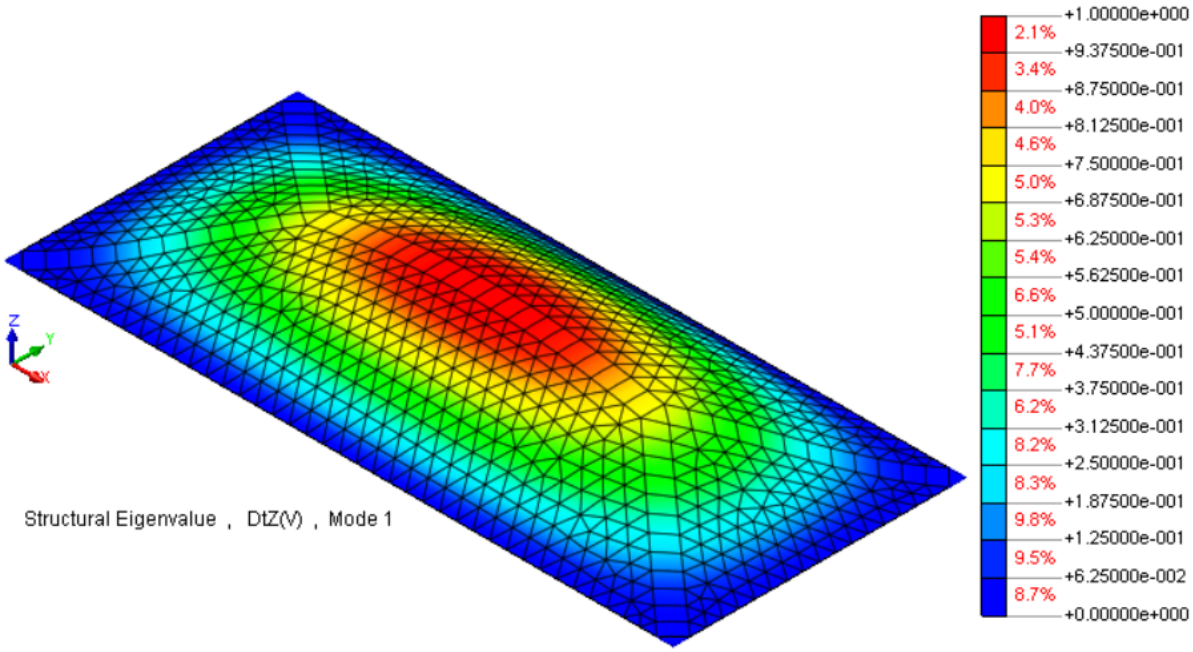

Figure 3-51: Mode 1 shape, Time period = 0.0418 s

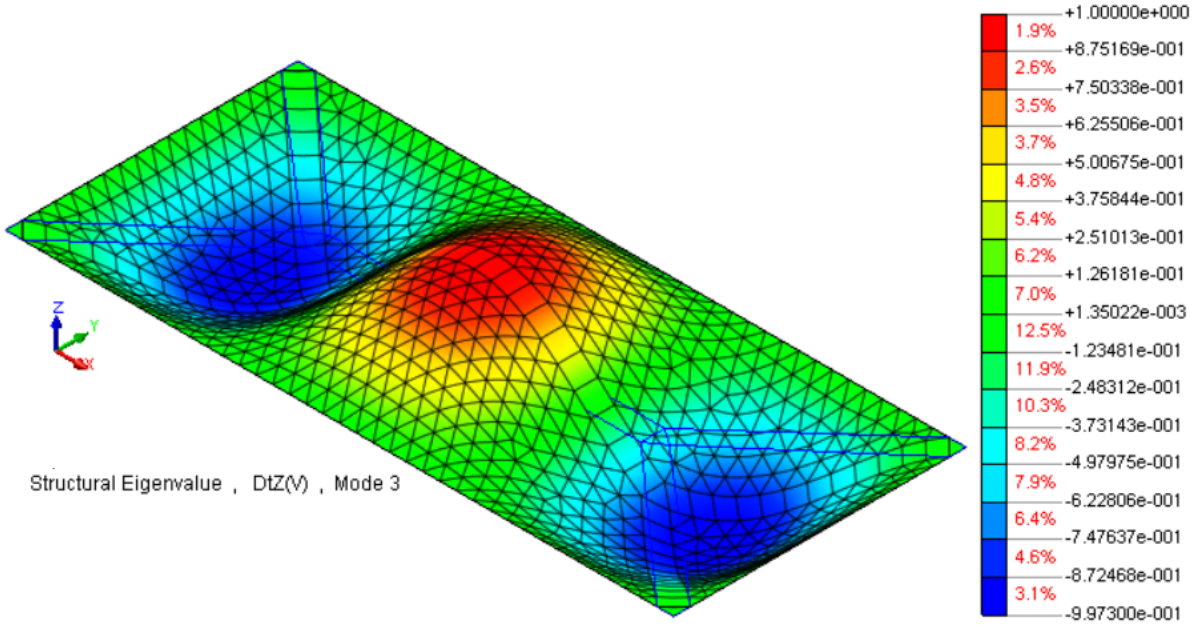

Figure 3-52: Mode 3 shape, Time period = 0.0186 s

Post processing and results

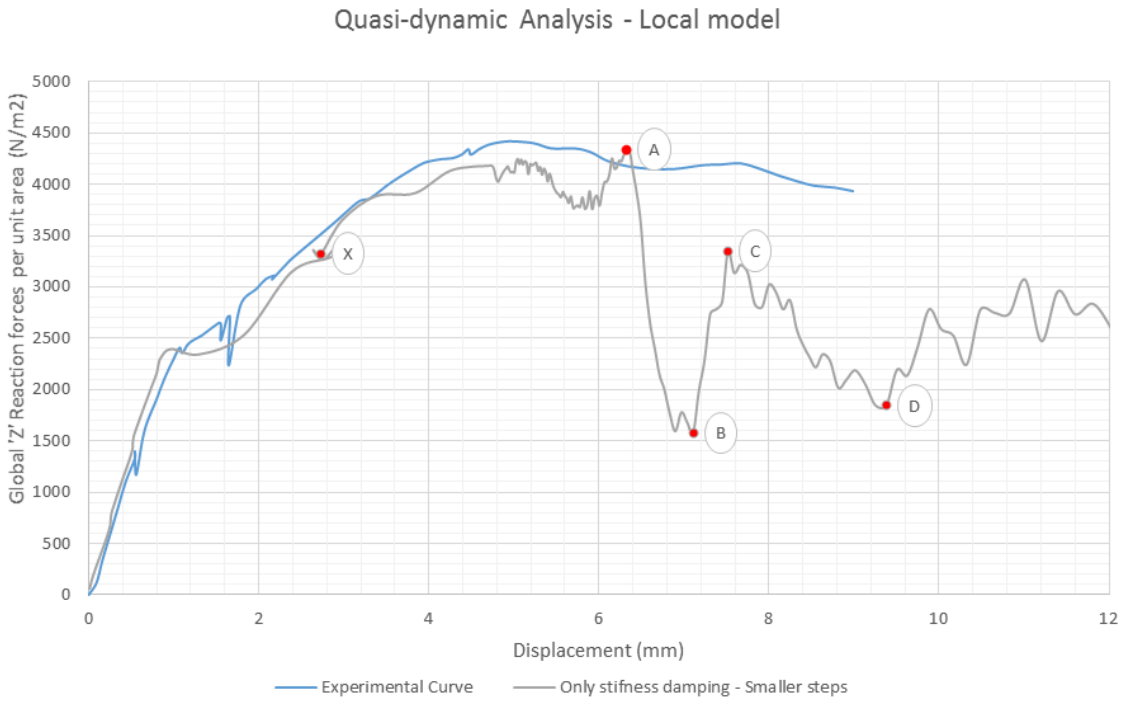

Figure 3-53: Load displacement curve for the Localized model - II, Global 'Z' reaction forces per unit area taken as the equivalent face pressure

The Load displacement curve for the model is as shown in Figure 3-53. This is the response of the model when the horizontal with $G_f^1 = 0.01N/mm$ and $f_{tb} = 0.3N/mm^2$ and diagonal strips are provided with $G_f^1 = 0.08N/mm$ and $f_{tb} = 1.6N/mm^2$ which are the values used for the response obtained in the non-linear static analysis shown in Figure 3-41.

The pre peak behaviour is close to that obtained from the experimental result and the non-linear static analysis but is highly distorted at a certain point labelled X in the plot which marks the beginning of the cracking of diagonal strip as was observed in the non-linear static analysis as well. The post peak behaviour shows dynamic effects and this can be attributed to the formation of macro crack in the diagonal zone. The principal strain plots are shown for the horizontal and diagonal portions according to Figure 3-43 and Figure 3-44 respectively. Even in this case, a crack bandwidth of 50 mm is chosen for the diagonal cracks to avoid snap back in the constitutive model.

Principal strain plots and Crack patterns The principal strain plots are shown in Figure 3-54. Point A refers to the macro crack formation in upper diagonal zone which leads to sudden loss of capacity as was seen in the non-linear static analysis as well. Point B shows the diagonal cracking in the lower zones. There is a very small difference between B and C. If observed very carefully, the cracking of the lower diagonal zone after point B has caused the lower portion of the wall to bend stiffer. That is, there is redistribution of moment capacity of the lower diagonal crack. Point D shows greater strains and serious cracking throughout

the local zone. The thing to be noted is that the rest of the wall also is undergoing softening but as the non-linearity isn't present, the elements are not deformed as compared to the local zone.

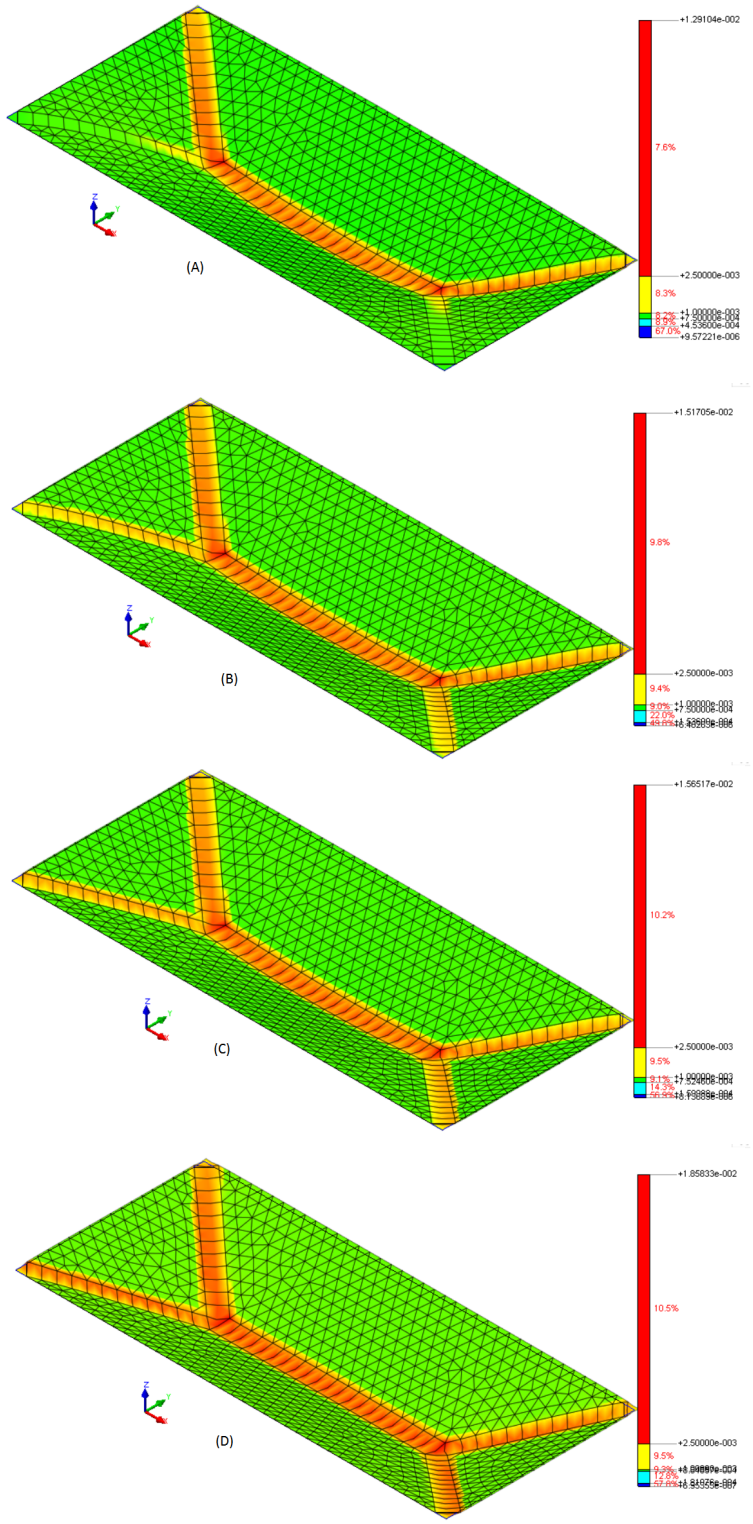

Figure 3-54: Principal strains at points A, B, C and D of the load displacement curve

3-4-3 Conclusions

The effect of orthotropy is introduced indirectly into the shell element model using the localized zone having different strength parameters along the horizontal and diagonal strips. As can be seen in Figure 3-55, the behaviour very close to the experimental curve in the pre peak zone and the post peak is obtained with some deviation in the Quasi-dynamic analysis.

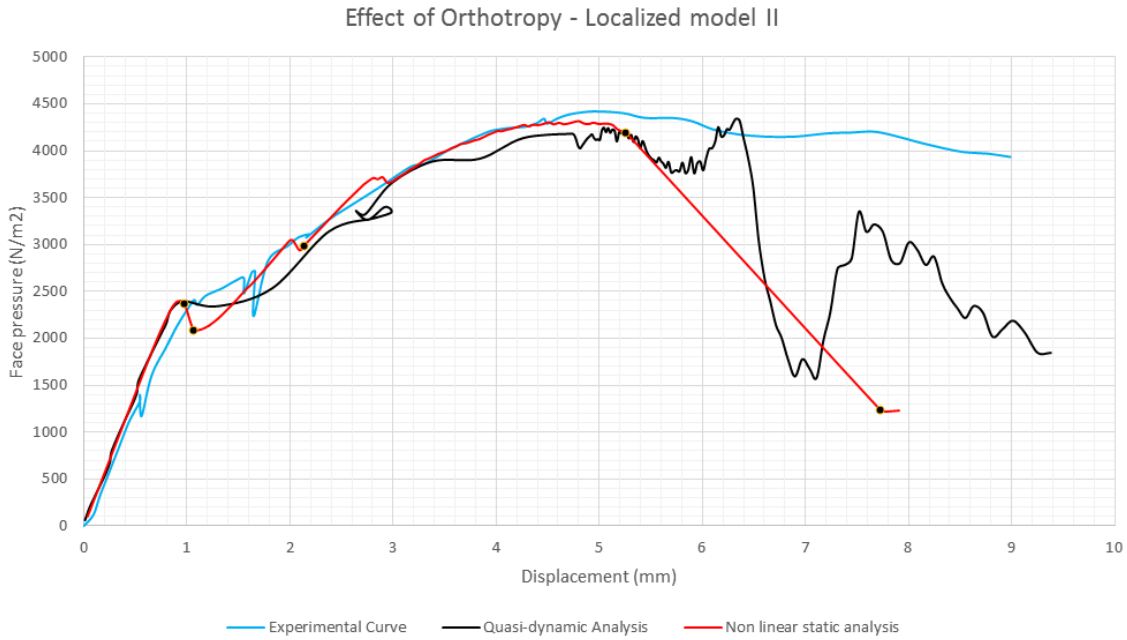

Figure 3-55: The non linear static and Quasi-dynamic analysis result comparison for Isotropic continuum Localized shell model -II

Some of the important conclusions drawn from this section are:

1. There is need for a sensitivity analysis for Mode I fracture energy every time to obtain response with both the horizontal and diagonal strips. This section reiterates the need for proper testing of masonry specimens in the two orthogonal directions for tensile strength and Mode I fracture energy. When these parameters are available in both directions, the use of Rankine hill anisotropy model is also possible.
2. Arc-length control is highly unstable post-peak and the quasi-dynamic approach yields a better post peak behaviour in comparison to the former as was observed in the case of shell element model as well.

3-5 Solid Element Model

Preprocessing

Geometry The geometry of panel-II with the dimensions of $4 * 1.75\ m^2$ is modelled in this section using Solid elements instead of Shell elements. It is thus a 3D model. The geometry of the wall along with the Meshing is shown in Figure 3-57.

Meshing and Elements The geometry of the Panel is then meshed using isoparametric solid brick elements shown in Figure 3-56. These elements allow for out of plane loads just like the shell elements. The difference is just that the element is three dimensional. It has three degrees of freedom per node which are the three translations as shown. The CHX60 element is the twenty-node quadrilateral solid brick shell element which is based on quadratic interpolation and Gauss integration over the η ξ element area. The integration in ζ direction (thickness) may be Gauss or Simpson. The default integration scheme in the element area is 3x3 Gaussian and a 3 point Simpson's integration in the ζ direction. The 2x2x2 scheme is supported and yields optimal results but 3x3x3 scheme is used for accuracy.

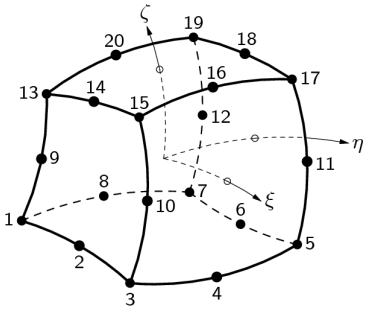

Figure 3-56: CHX60 element

The wall is map meshed using these CHX60 elements to a fine level keeping in mind the aspect ratios of the elements. 40 elements were provided in the longitudinal direction of the wall, 18 elements in the direction of height of the wall and 3 elements in the thickness direction to ensure more integration points for accurate results.

Boundary conditions and Loads The wall is simply supported along all edges to restrain out plane displacements and hence is given restraints all along the edges of the model in the global z direction. These are given to the nodes of the elements at the back side of the wall as the loading is applied on the front side. The bottom of the wall is supported in the Global Y direction for the gravity load and in the Global X direction to avoid axial displacements if any. This is done in accordance to Van der Pluijm's set up.

The loading applied is simulated using a distributed face load on the front side of the the 3D solid element model with a value of 5000 N/m^2 which is well above the failure load as seen in

Table 3-7: Masonry parameters - Solid element VdP Model

Parameters	Values
Density $[Kg/m^3]$	1900
Young's Modulus E_o^{j+u} $[N/mm^2]$	3527
Tensile bond strength f_{tb} $[N/mm^2]$	0.5
Mode I fracture energy G_f^1 $[N/mm]$	0.035
Crack bandwidth h $[mm]$	68.68

the load displacement curve, see Figure 3-2. Also, dead load of the wall is added as gravity load in the Global negative Y direction. Refer Figure 3-57 for the model generated with the meshing and boundary conditions. The distributed load is applied on the front face in the Global negative Z direction and has not been shown for clarity of Boundary conditions and meshing.

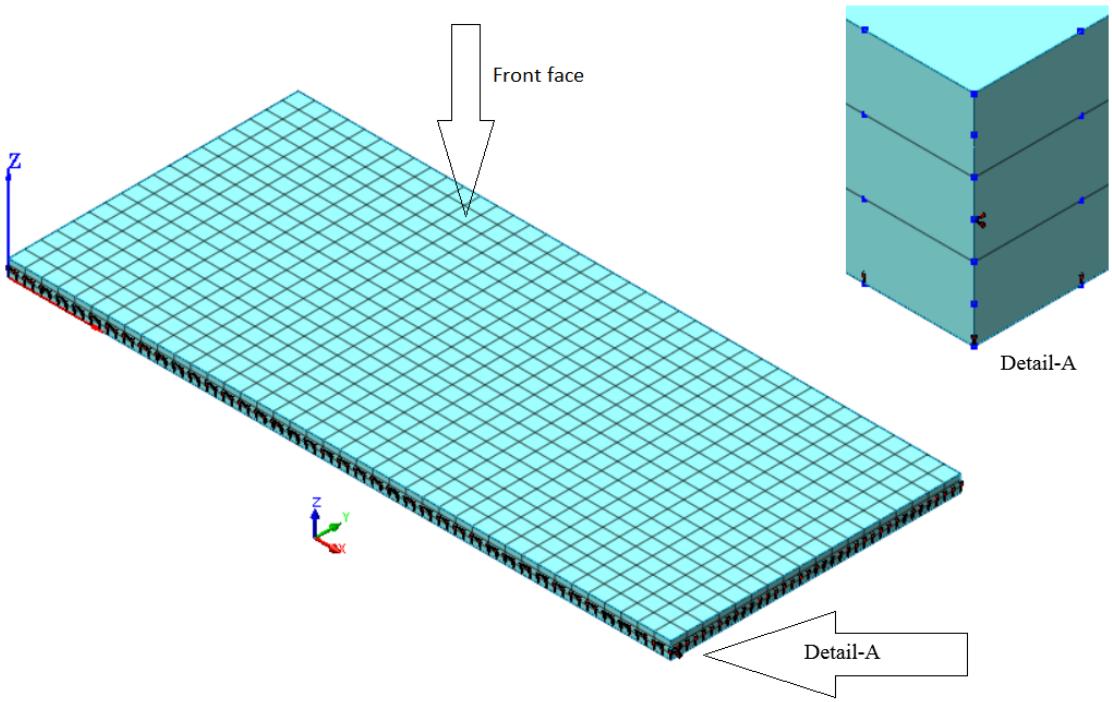

Figure 3-57: Finite element model with boundary conditions created using Midas FX+

Constitutive model The Modelling is done at a macro scale to save computational time and memory and hence the bricks, mortar and the interface are smeared into continuum. This concept of Total strain based smeared cracking model and the constitutive model are described in detail 3-3. The parameters used are listed in Table 3-7, the crack bandwidth is deduced as $h = \sqrt[3]{V}$ where V is the volume of the solid element.

3-5-1 Non linear Static Analysis

Arc length Control Procedure

Since the Force control procedure yields only the peak load and diverges post peak, and the post peak behaviour is looked into with more attention, the Arc length control procedure is used for obtaining post peak behaviour of the Masonry walls. A global arc length procedure enhanced with line search option for stabilizing the convergence behaviour and increasing the rate of convergence is used. The arc length control is carried out with the Newton raphson iterative process with a maximum of 50 iterations per load step for a fine mesh of solid elements shown in Figure 3-57 to avoid mesh objective results. The number of iterations is kept low in comparison to the shell element model for reasons pertaining to computational memory and time. However, a tolerance of 0.001 for the force and displacement norms is used instead of the default value of 0.01. The load is applied in uniform small steps which are $\frac{1}{200}th$ of the load applied - 5000 N/mm^2.

Post-processing and Results

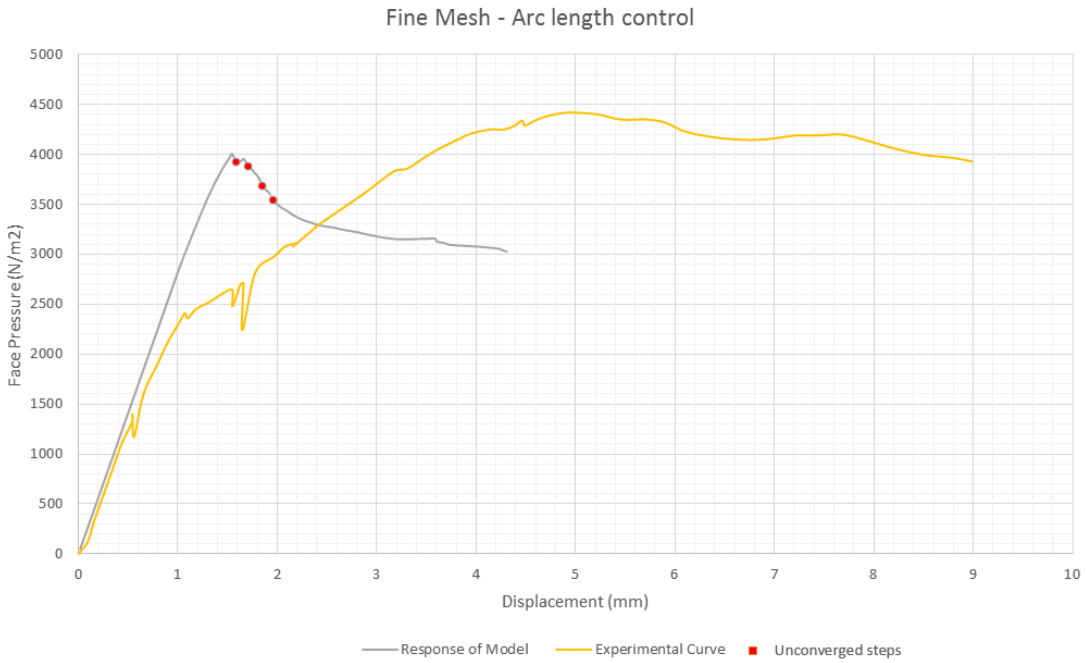

Figure 3-58: Arc length controlled non-linear static analysis of the Solid element model

The response of the solid element model to non-linear static analysis with the arc length control is shown in Figure 3-58. The peak load reached is not close to the experimental peak load and the post peak behaviour as well is quasi brittle unlike the experimental behaviour. The ductility observed in the experiment is attributed to the redistribution of moment capacity to the macro horizontal crack in the middle of the wall but this behaviour requires the wall to possess orthotropy. This could be a reason why a ductile behaviour is not obtained in the response of the model. Also, provision of localized zone to observe orthotropy in

this case would be tedious considering the meshing and the computational time and memory constraints. Hence, it's left out of the scope of this study.

The post peak response is also not globally convergent for a force and displacement norm of 0.001 and the 4 non converged steps shown in red colour on the plot haven't converged after 50 iterations and the rate of convergence is very low indicating the fact that the non-linear static analysis is highly unstable in finding the correct equilibrium path.

Effect of discretization along thickness It is a known fact that solid elements when used in bending type problems could give stiffer response than expected from analytical solutions due to the problem of locking. Hence a study is done by varying the number of elements along the thickness of the wall and the change in the response of the model is observed.

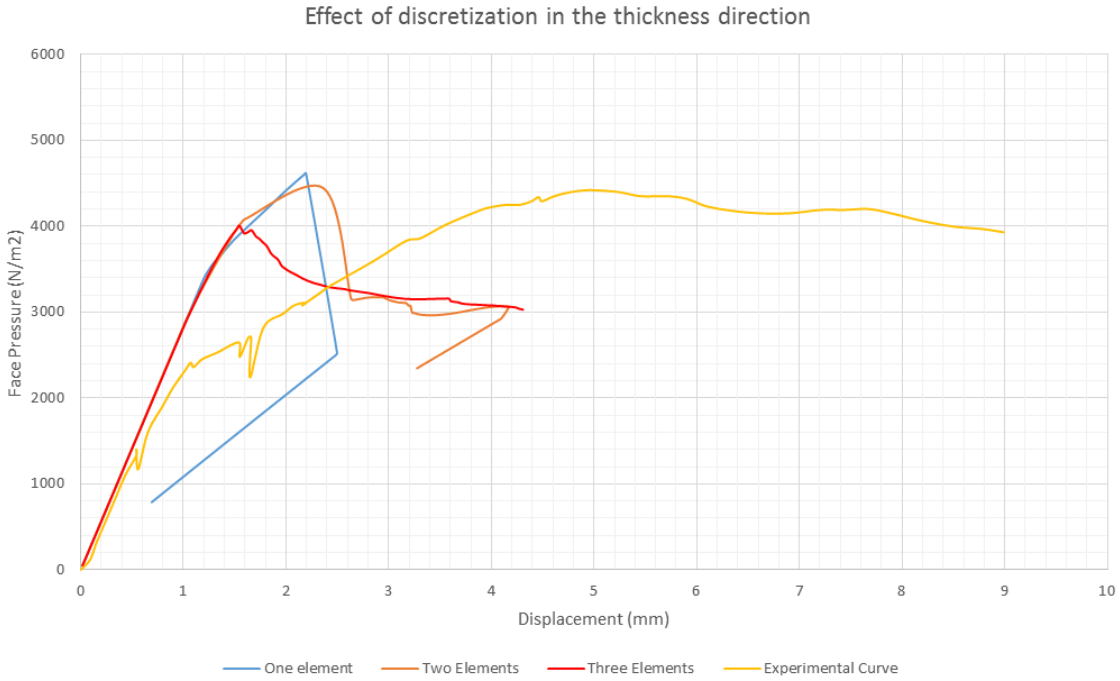

Figure 3-59: Effect of discretization along thickness of the Solid element model

Figure 3-59 shows the difference in the response of the model when the number of elements in the thickness direction is decreased from three to one. The peak load is over estimated when one or two elements are used as against the three elements case. This is due to the fact that with increase in the number of elements in the thickness direction, the number of integration points where the stresses are computed goes up from 3 in the case of one element to 9 in the case of three elements. It's also observed that use of less elements in the thickness direction gives highly unstable post peak behaviour in comparison to the three elements case. This also could be attributed to the fact that solid elements aren't as suited to bending type problems as shell elements due to the locking phenomenon.

Principal strain plots and Crack patterns Principal strain plots and crack patterns in the solid element model (with three elements in the thickness direction) are shown in this section.

The values of ultimate peak strain and ultimate crack strain are calculated as follows :

$$\varepsilon^{cr}_{ult.nn} = \frac{G^1_f}{h * f_{tb}}$$

$$\varepsilon^{cr}_{ult.nn} = \frac{0.035N/mm}{68.68 * 0.5} = 1.02 \times 10^{-03}$$

$$\varepsilon^{peak}_{nn} = \frac{f_{tb}}{E^{j+u}_o} = 1.417 \times 10^{-04}$$

The legend for the principal strain plots used is a norm. However the crack strains are not shown according to a generic legend in the crack patterns:

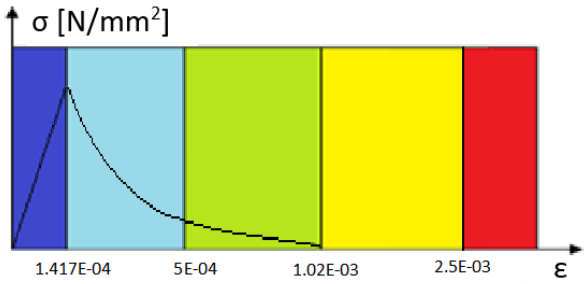

Figure 3-60: Legend for the principal strain plots - Solid element model

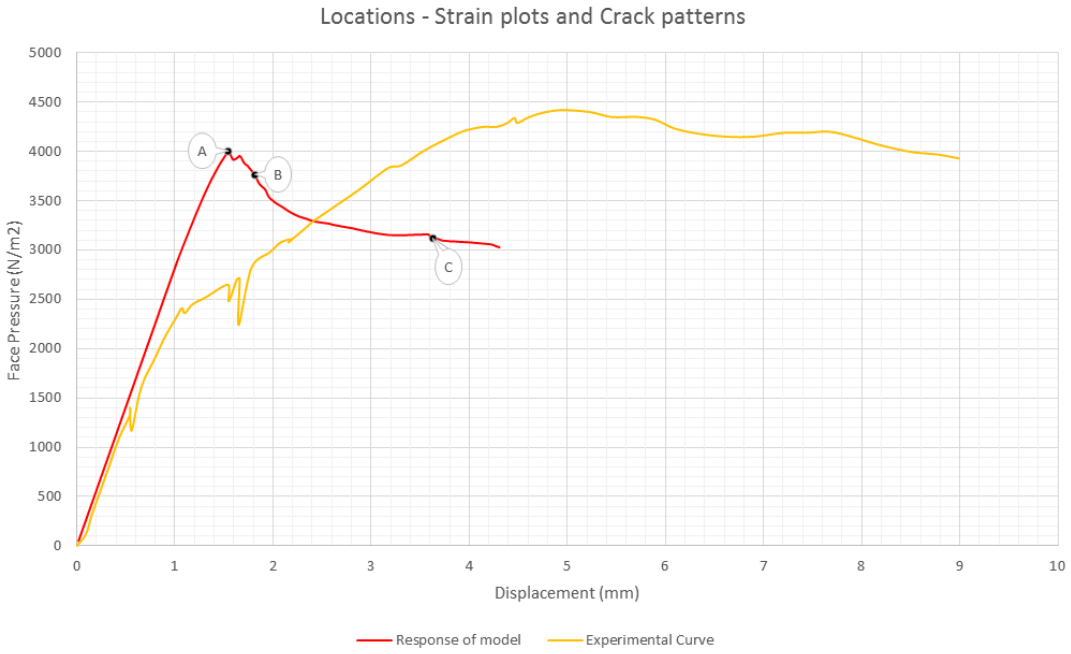

Figure 3-61: Locations for crack patterns and principal strain plots

Figure 3-61 shows locations A, B and C for which the principal strain plots and crack patterns are shown in Figure 3-62 and Figure 3-63 respectively. These are shown for the side of the wall which is not loaded i.e the the face of the wall in tension.

The principal strain plots are in accordance with Figure 3-60 and shows the progressive formation of the horizontal crack and the deformed elements along the crack. The principal strain plot A shows the middle of the wall having micro cracks. Plot B can be used to infer the commencing of the formation of the macro crack which is seen as the red line at the centre of the wall. The smearing out has spread to the region around the macro crack. Plot C shows the development of the macro crack into diagonal cracks. The corresponding crack pattern C shows that the crack has indeed opened up by reaching the loaded face of the wall. It is interesting to note that the elements close to the macro crack are highly deformed and contorted. But the panel is entirely cracked at a micro level. The green legend indicates latter stages of softening. The pattern cannot be clearly understood as a yield line pattern as this is not a discrete crack.

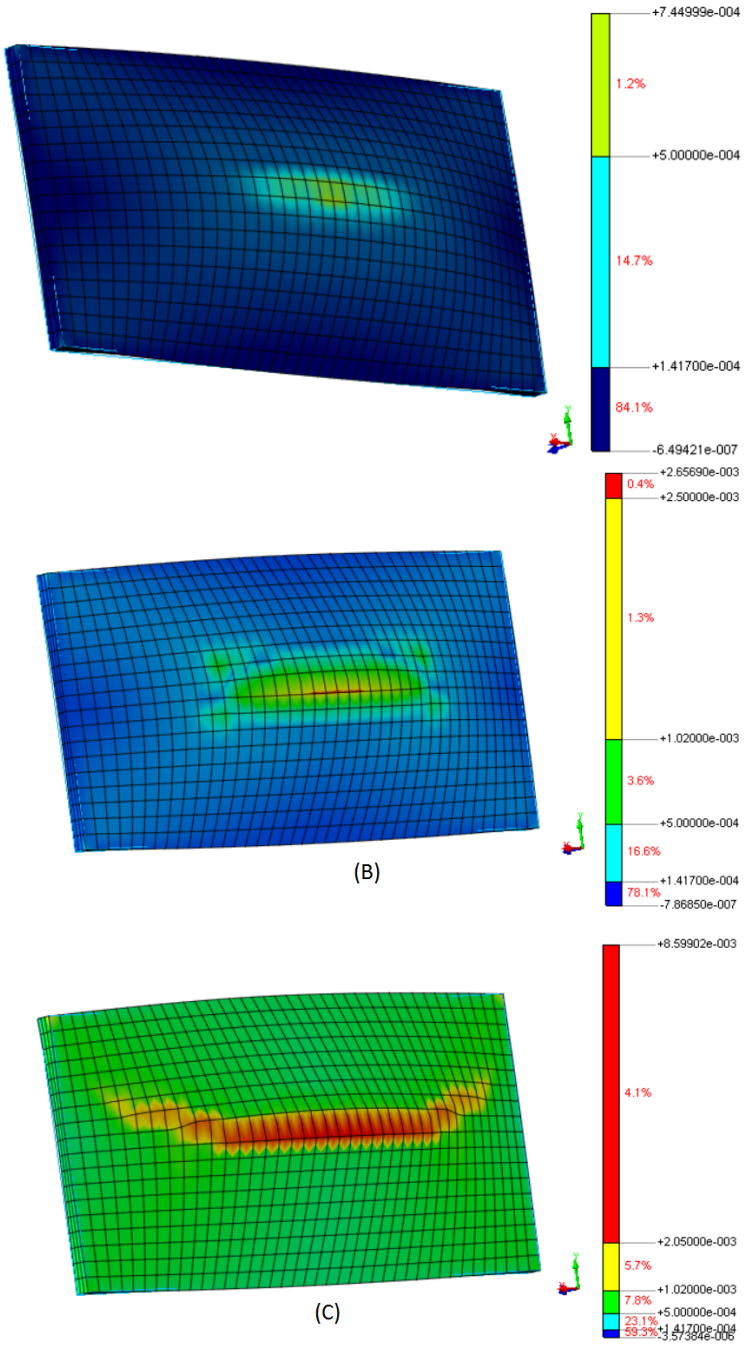

Figure 3-62: Principal strains at points A, B, and C of the load displacement curve

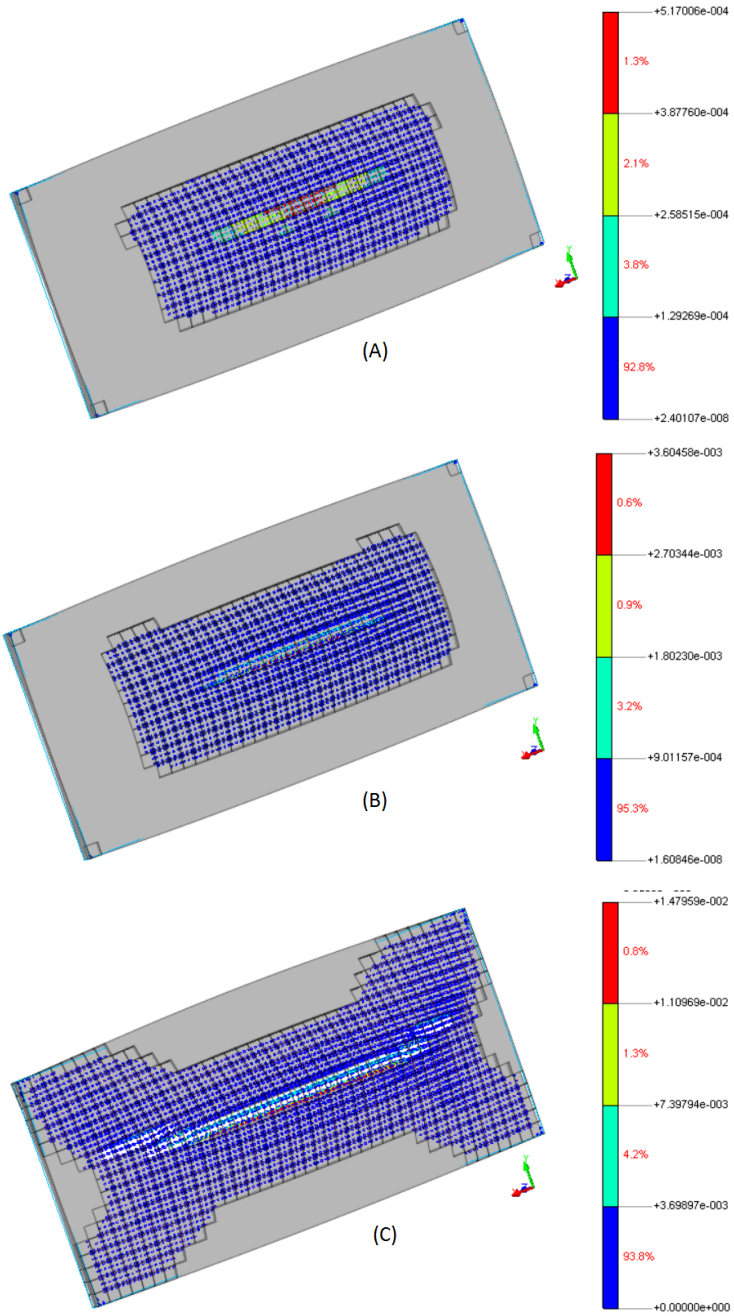

Figure 3-63: Crack pattern at points A, B, and C of the load displacement curve and the crack strain legend.

3-5-2 Quasi-dynamic Analysis

The quasi-dynamic approach described in detail in previous sections is adopted to study the response of the solid model. Since the approach has been described quite extensively, only the results are shown. The parameters used are given in Table 3-8

Table 3-8: Quasi-dynamic analysis parameters - Solid element VdP model

Parameters	Values
Rise Time T_d $[s]$	0.316
Mode 1 Time period T_1 $[s]$	0.0418
Damping ratio ζ	0.05
Rayleigh Stiffness damping coefficient b $[s]$	2.05E-04
Young's Modulus E_o^{j+u} $[N/mm^2]$	3527
Tensile bond strength f_{tb} $[N/mm^2]$	0.5
Mode I fracture energy G_f^1 $[N/mm]$	0.035
Crack bandwidth h $[mm]$	68.68

The response is as shown in Figure 3-64. The process shows a ductile post peak response and is quite appreciable as against the shell element model quasi-dynamic response considering the aspects of dynamic equilibrium. The dynamic effects post peak can be interpreted as a loss of static equilibrium between the applied load and the reaction forces (response of model) as seen beyond point A which is the peak load. This is shown in Figure 3-65. At the same time the acceleration gained by the system shoots up which substantiates the interpretation as shown in Figure 3-66. It is a globally converged procedure with tolerance of 0.001 for force and displacement norms unlike the shell element model.

The inertia effects due to the release of crack energy upon macro crack formation is interpreted using the following calculations:

Calculations Area X in Figure 3-65 is the amount of Force F with regards to loss of static equilibrium considered.

$$F = AreaX * Load * Areaofwall = (0.5 * 0.4 * 2) * 5000N/m^2 * 7m^2 = 14000N$$

Mass of the wall:

$$M = Volumeofwall * Density = 0.7m^3 * 1900Kg/m^3 = 1330Kg$$

As an approximation (neglecting the damping force and the restoring force from stiffness),

$$F = M * acceleration$$
$$acceleration = F/M = 10.5m/s^2$$

The acceleration values as seen in Figure 3-66 are at an average around 10 m/s^2 but there are few peaks, 4 to be precise, which are very high. These could be some numerical problem in the solution procedure.

Figure 3-64: Quasi-dynamic analysis for Solid element model, Global 'Z' reaction forces per unit area taken as the equivalent face pressure

Principal strain plots and Crack patterns Principal strain plots and crack patterns in the solid element model for the quasi dynamic analysis which shows post peak behaviour is of interest. These plots (with three elements in the thickness direction) are shown in this section. The values of ultimate peak strain and ultimate crack strain are calculated as follows :

$$\varepsilon^{cr}_{ult.nn} = \frac{G^1_f}{h * f_{tb}}$$

$$\varepsilon^{cr}_{ult.nn} = \frac{0.035N/mm}{68.68 * 0.5} = 1.02 \times 10^{-03}$$

$$\varepsilon^{peak}_{nn} = \frac{f_{tb}}{E^{j+u}_o} = 1.417 \times 10^{-04}$$

The legend for the principal strain plots used is a norm. However the crack strains are not shown according to a generic legend in the crack patterns:

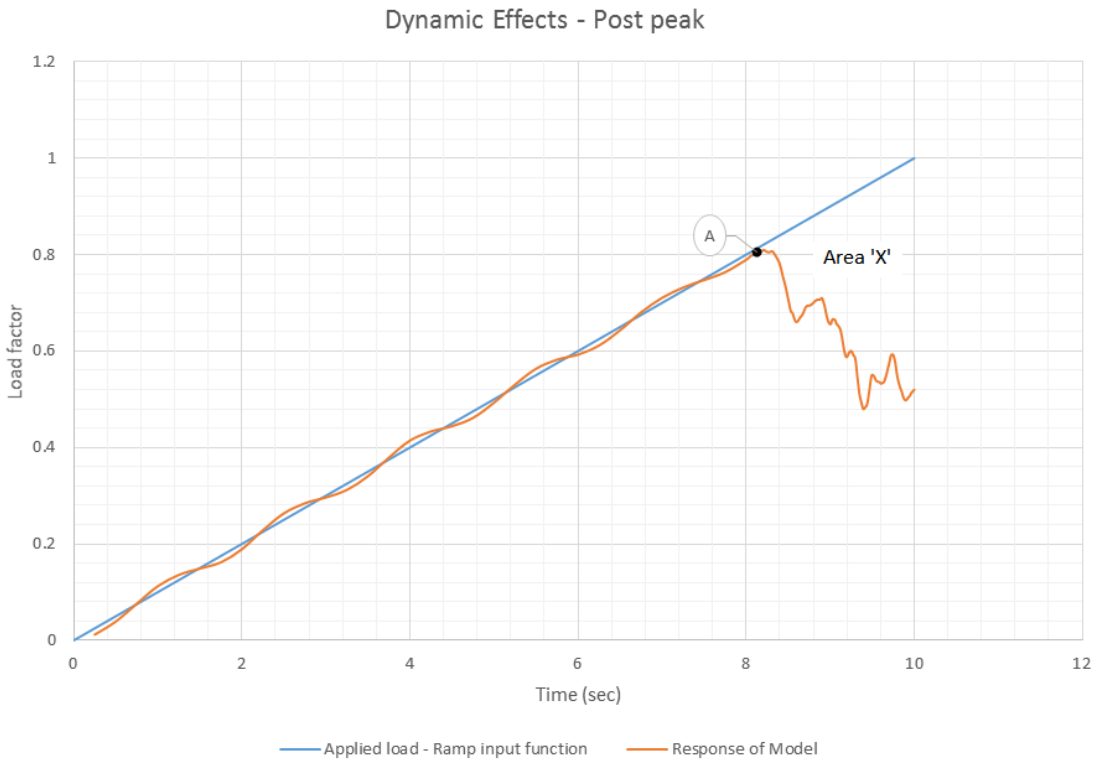

Figure 3-65: Post peak - Dynamic equilibrium,Applied load and the Global 'Z' reaction forces per unit area represented in relation to the maximum load applied 5000 N/m^2 as load factor

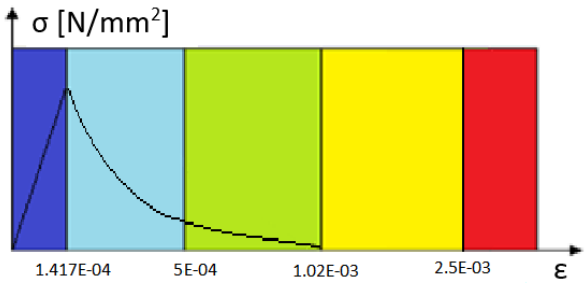

Figure 3-67: Legend for the principal strain plots - Solid element model

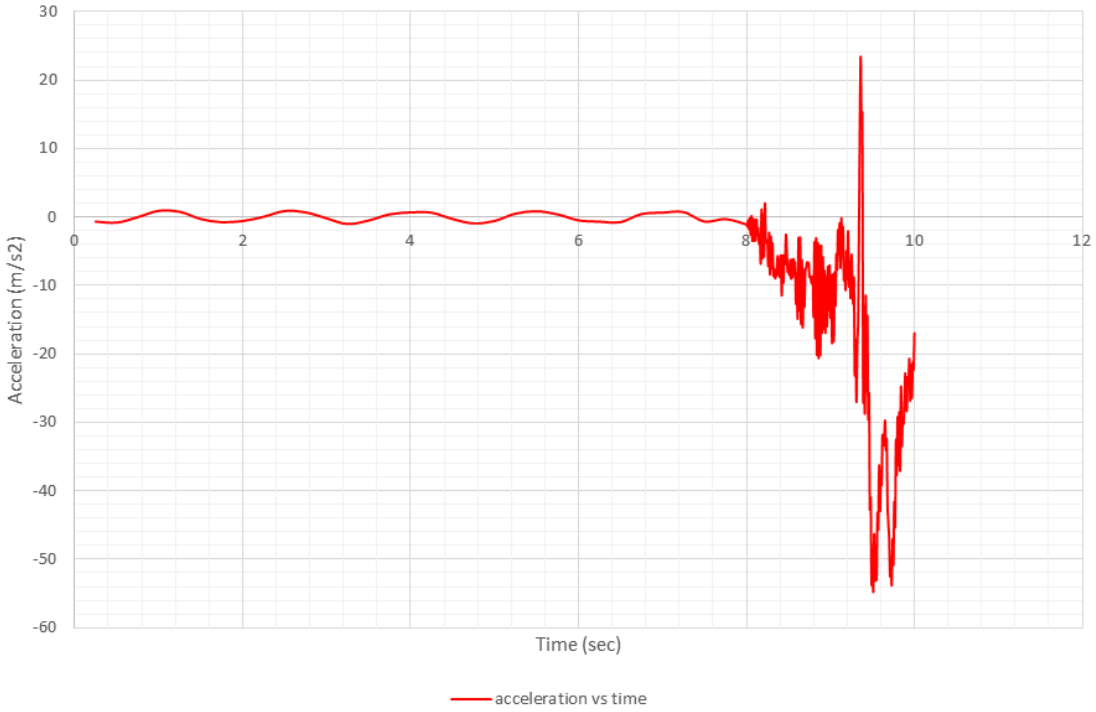

Figure 3-66: Inertia effects post peak

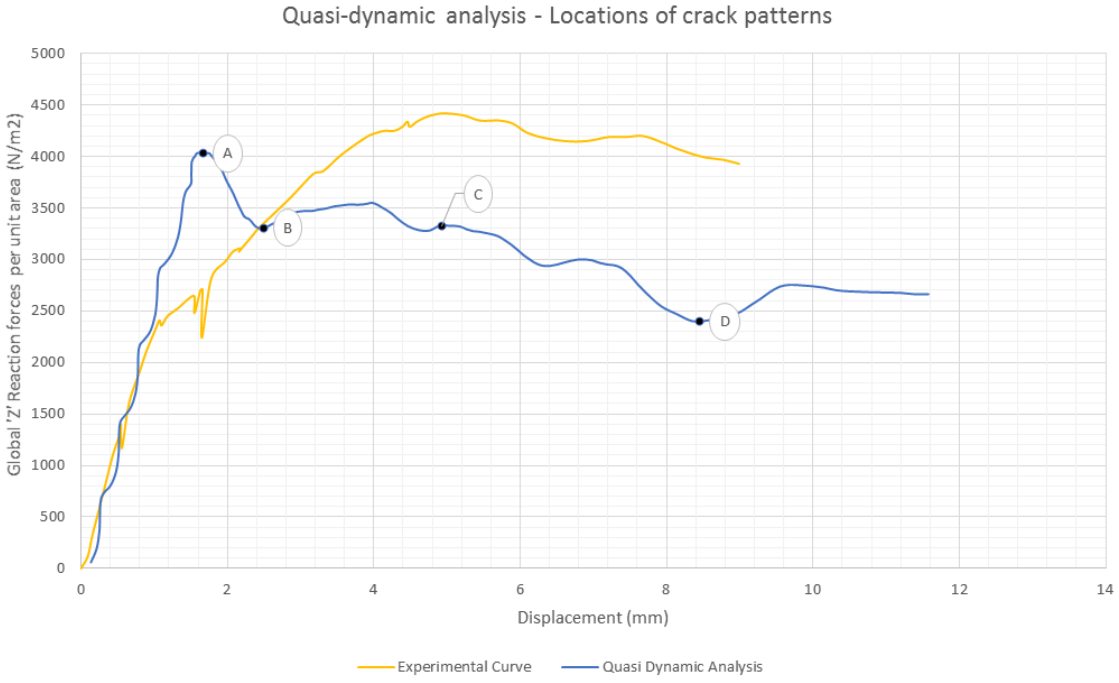

Figure 3-68: Locations for crack patterns and principal strain plots, Global 'Z' reaction forces per unit area taken as the equivalent face pressure

Figure 3-68 shows locations A, B, C and D for which the principal strain plots and crack patterns are shown in Figure 3-69, Figure 3-70 and Figure 3-71, Figure 3-72 respectively. These are shown for the side of the wall which is not loaded i.e, the face of the wall in tension.

The principal strain plots are in accordance with Figure 3-67 and shows the progressive formation of the horizontal crack and the deformed elements along the crack. The principal strain plot A shows the middle of the wall having micro cracks. Plot B shows the formation of macro crack and this is clearly seen in the cracking pattern where the horizontal crack has opened up. The smearing out has spread to the region around the macro crack and hence is represented by sky blue colour meaning the rest of the wall also has started to soften. Plot C shows the development of the macro crack completely. The corresponding crack pattern C shows that the crack has indeed opened up by reaching the loaded face of the wall. It is interesting to note that the elements close to the macro crack are highly deformed and contorted. But the panel is entirely cracked at a micro level. The green legend indicates latter stages of softening.

The pattern can be clearly understood as a yield line pattern in the case of the quasi-dynamic response as a ductile response is obtained courtesy the clear formation of the diagonal crack as is seen in the pattern D. The rest of the wall though has seriously cracked as well. This part of the response wasn't obtained in the Arc length controlled non-linear static analysis and hence the quasi-dynamic analysis helps understand the post peak behaviour in a better way.

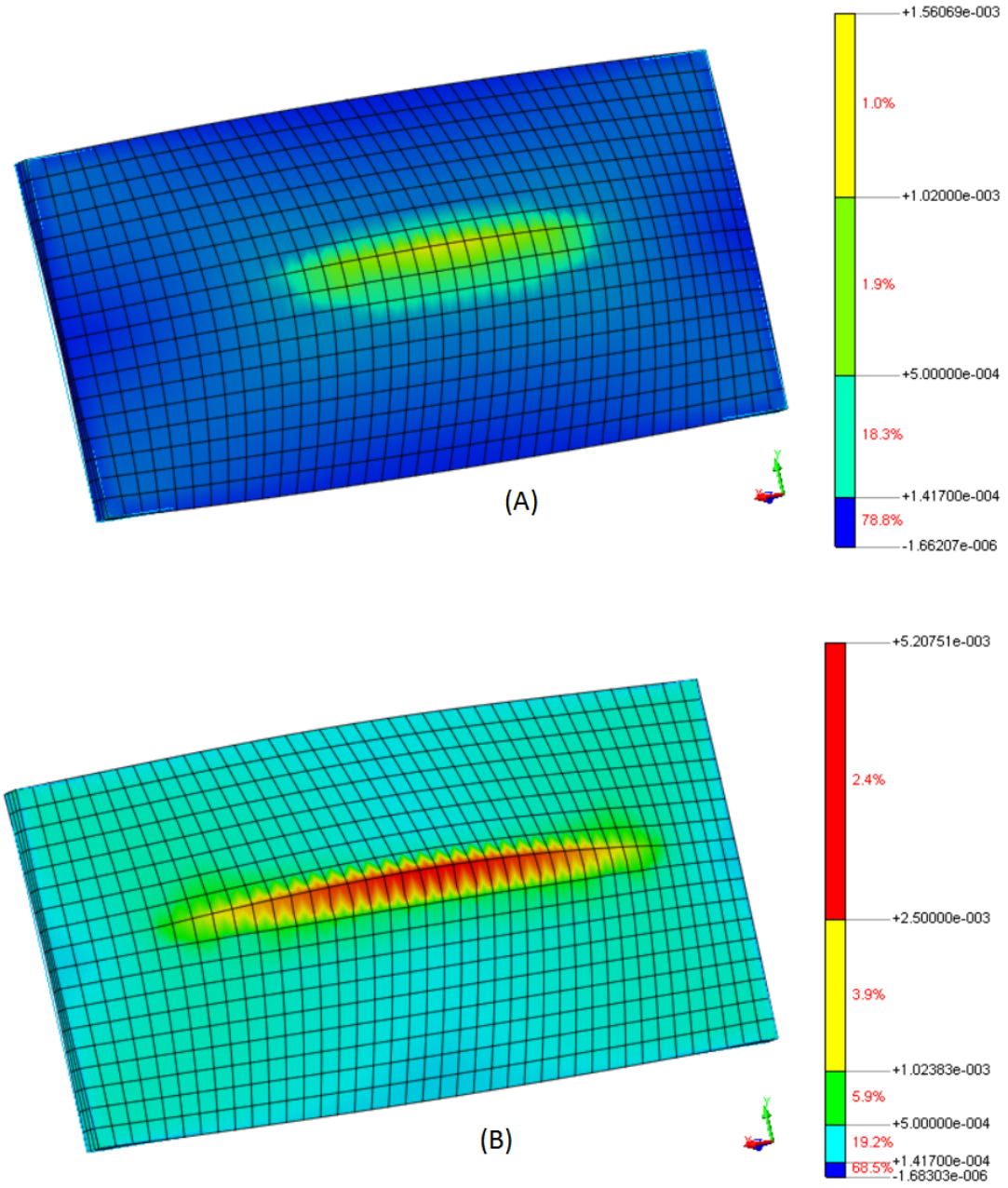

Figure 3-69: Principal strains at points A and B of the load displacement curve

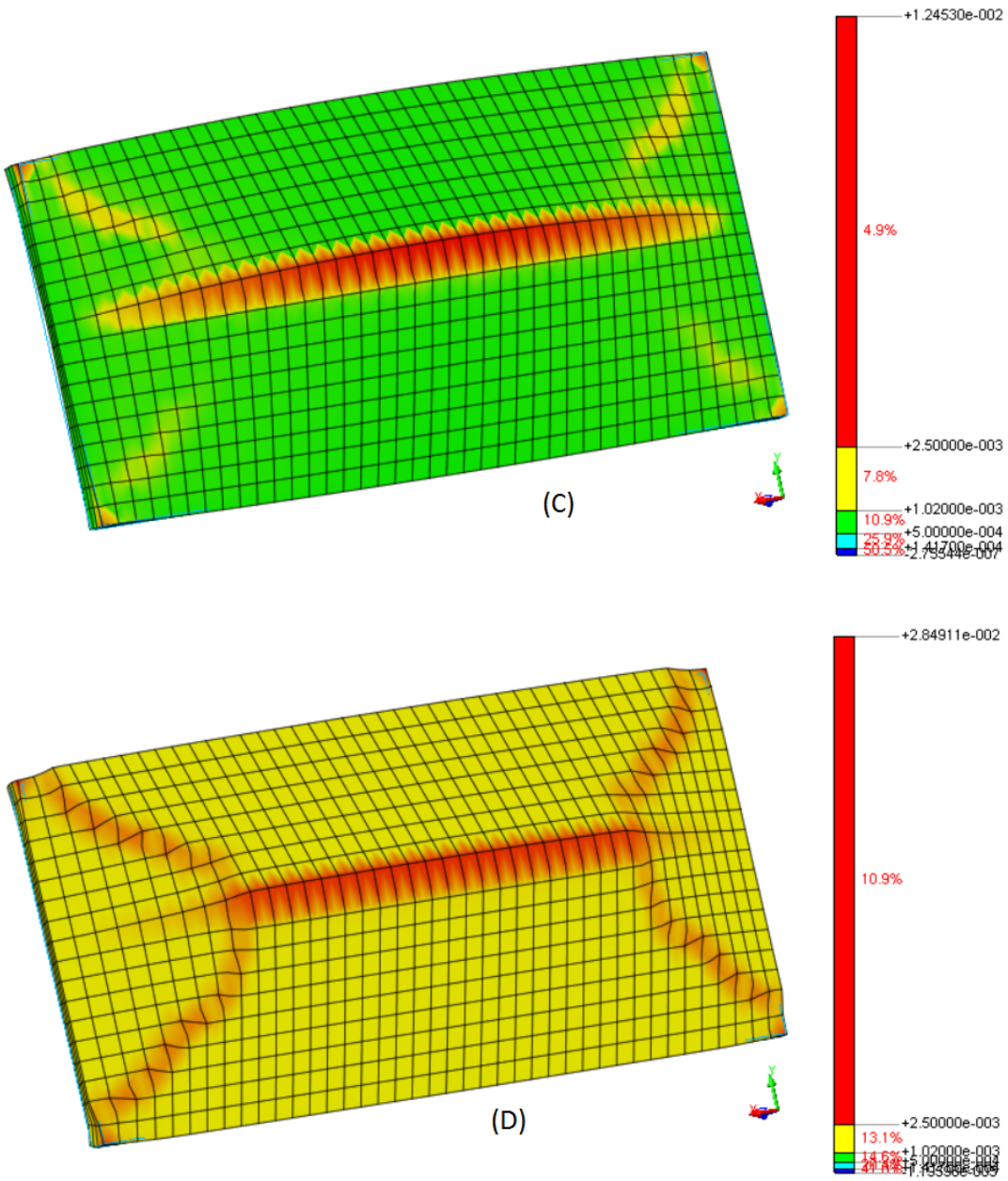

Figure 3-70: Principal strains at points C and D of the load displacement curve

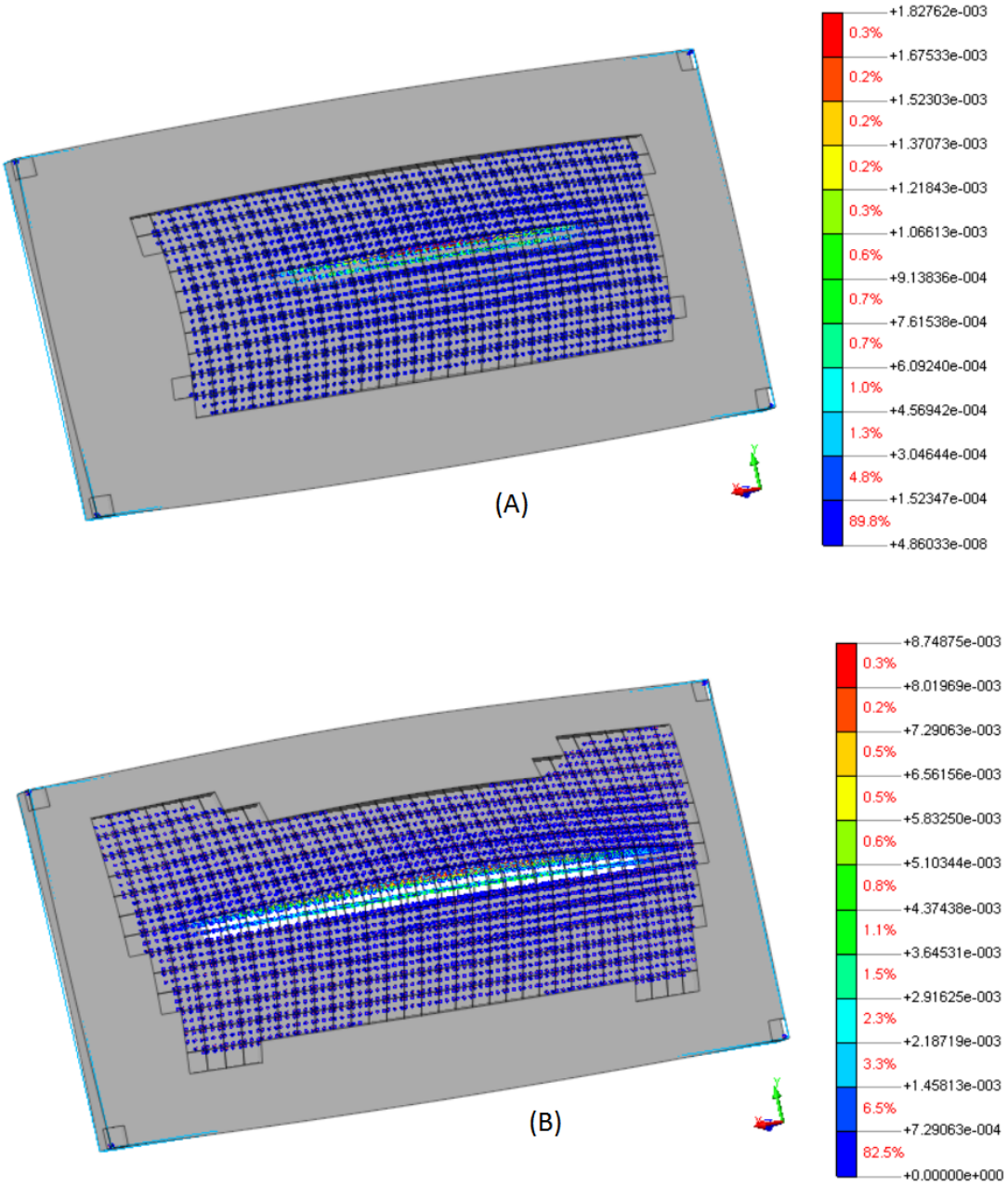

Figure 3-71: Crack pattern at points A and B of the load displacement curve and the crack strain legend.

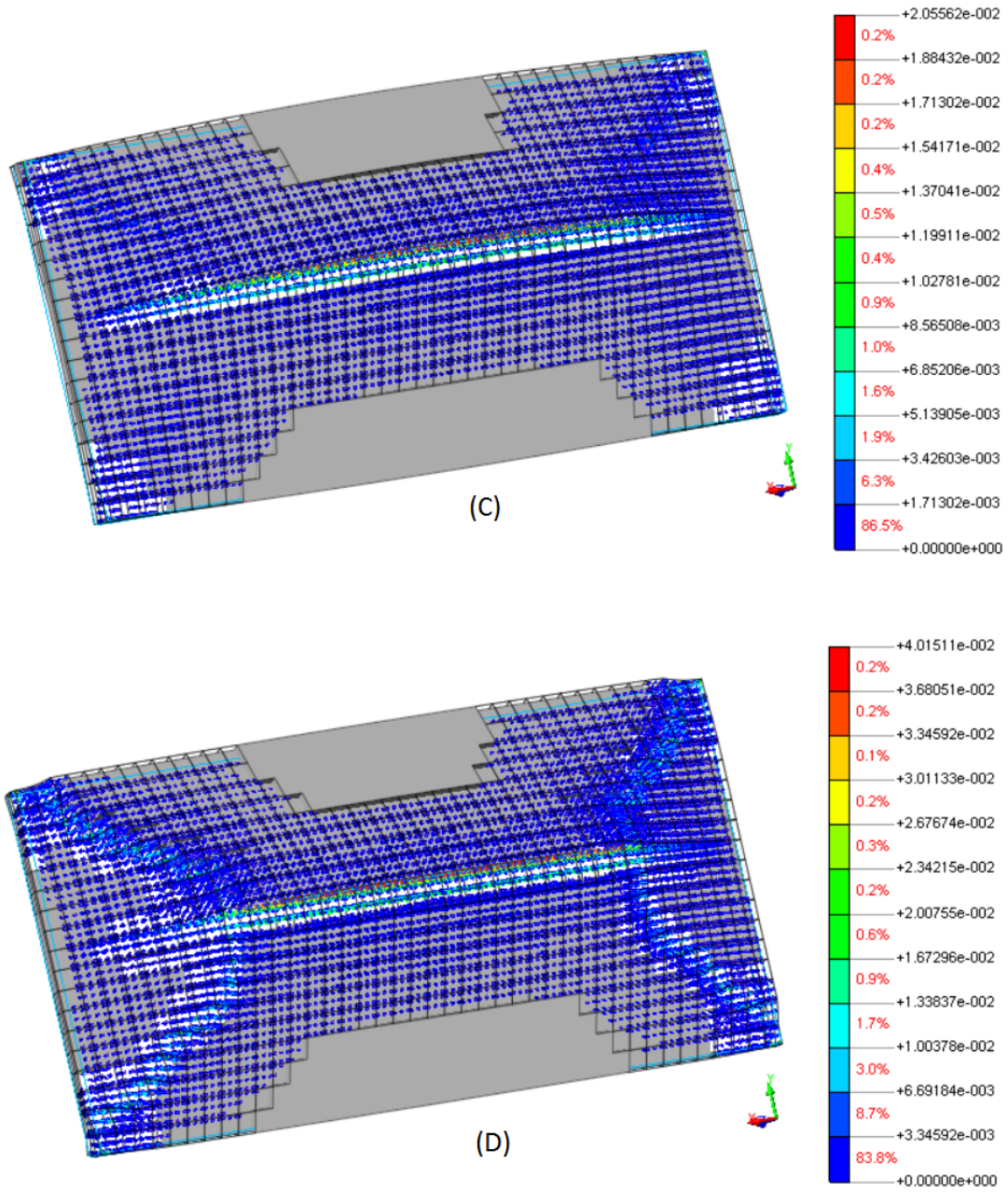

Figure 3-72: Crack pattern at points C and D of the load displacement curve and the crack strain legend.

3-6 Comparison and remarks

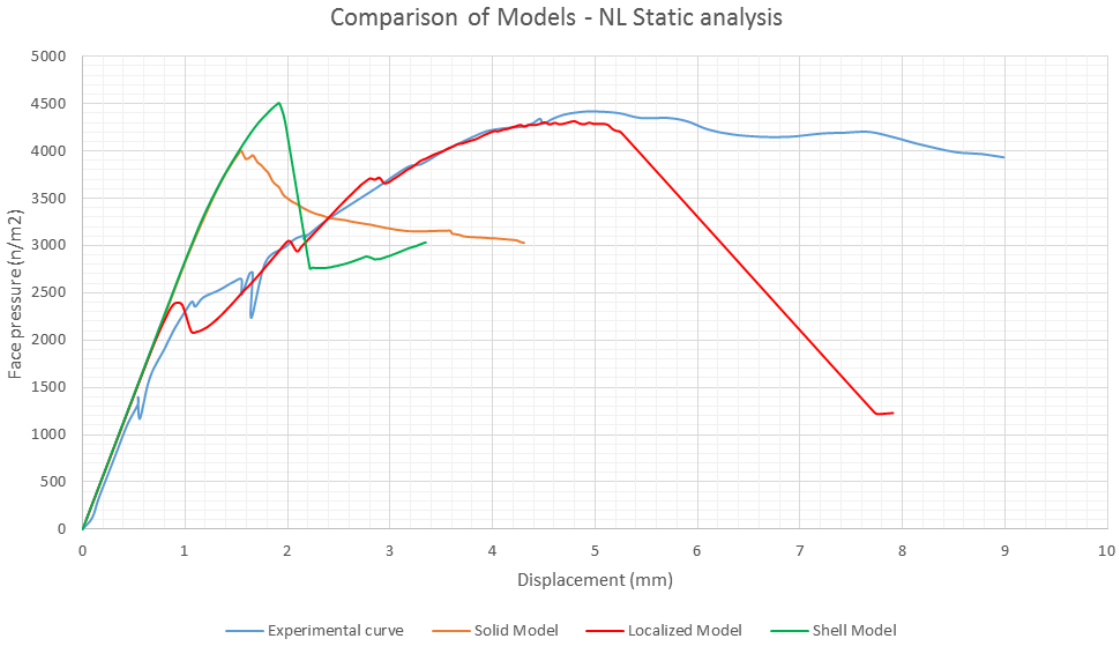

Figure 3-73: Comparison of the models for non-linear static analysis

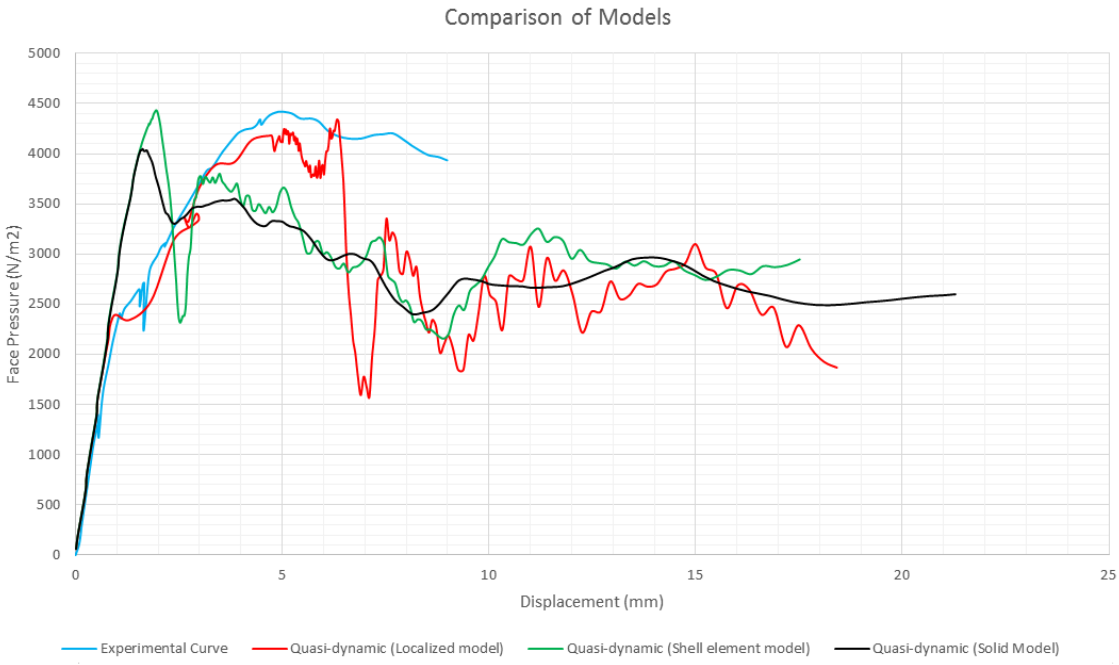

Figure 3-74: Comparison of the models for Quasi-dynamic analysis

Out of the solution procedures used for the simulation of post peak behaviour in two way out of plane bending of Masonry walls, Quasi-dynamic analysis is the only procedure able to simulate the post peak behaviour to some extent (as oscillations) but is not close to the experimental results. Several other attempts to use displacement control to achieve post peak behaviour weren't a realistic representation as the simulation of two way bending is possible only with the definition of the displacement profiles along both directions which is not possible in TNO DIANA.

Figure 3-73 is a comparison between the shell, localized and solid models' response to a non-linear static analysis where the load is incremented with the arc length control. Although the parameters used are different, this comparison curve can be qualitatively used to infer the need for orthotropy to simulate a reliable pre peak response in the first place. Figure 3-74 shows the same comparison for quasi-dynamic analysis and although it's a technique to obtain post peak response the procedure's results are not satisfactory due to highly dynamic response consisting of the interaction of modes of vibration.

Chapter 4

Model - Griffith Walls

4-1 Experiment by Griffith et al.

The second benchmark chosen for this study is work of Griffith et al. on the Cyclic testing on Unreinforced masonry walls 2006 which has been described in detail in this section. This is one of the rare experiments conducted in two way bending in Out of plane study of Masonry walls. Wall II from the set of walls tested is used for the modelling purpose.

In this report quasistatic cyclic tests on eight full scale masonry walls by the application of uniform distributed loads using a system of airbags are described. The tests were carried out in the laboratories of Civil & Environmental engineering faculty of the University of Adelaide. The panels were made with standard clay brick units of dimensions 230 x 110 x 76 mm and a general purpose mortar designed in the laboratory. The tension (inside face) and the compression sides (outside face) of the wall, the loading set up with air bags and the positions of displacement transducers and load cells are shown in Figure 4-1. The walls were simply supported on top and bottom edges and moment resiting connections along the vertical edges and loaded with air bags, simulating wind induced pressures assuming a quasi static response of the panels. Additional tensile bond and bond wrench tests were carried out, to obtain a complete data set that makes simulation of the tests possible without having to guess important parameters as the flexural tensile bond strength f_{tb} and compressive strength f_c.

Eight walls of different geometry with and without openings and overburden pressure have been tested and analysed for a comprehensive insight into the two way bending in the out of plane direction. The material properties of the masonry and the behaviour of the panels were recorded in a detailed manner, allowing for a full non-linear evaluation with the finite element method, the important results of which are listed in Table 4-1 which are values for Wall 2. Their dimensions and boundary conditions are pictorially presented along with the load displacement curves as shown in Figure 4-4. The crack patters are shown in Figure 4-3. The support details used to simulate the boundary conditions are shown in Figure 4-2.

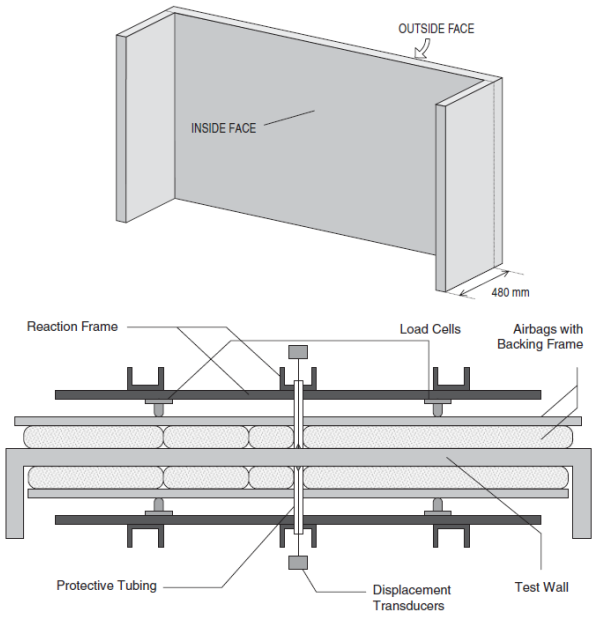

Figure 4-1: Compression (outside) and the Tension (inside) sides of the Panel-test arrangement (without loading arrangement) and Air bags setup used for loading

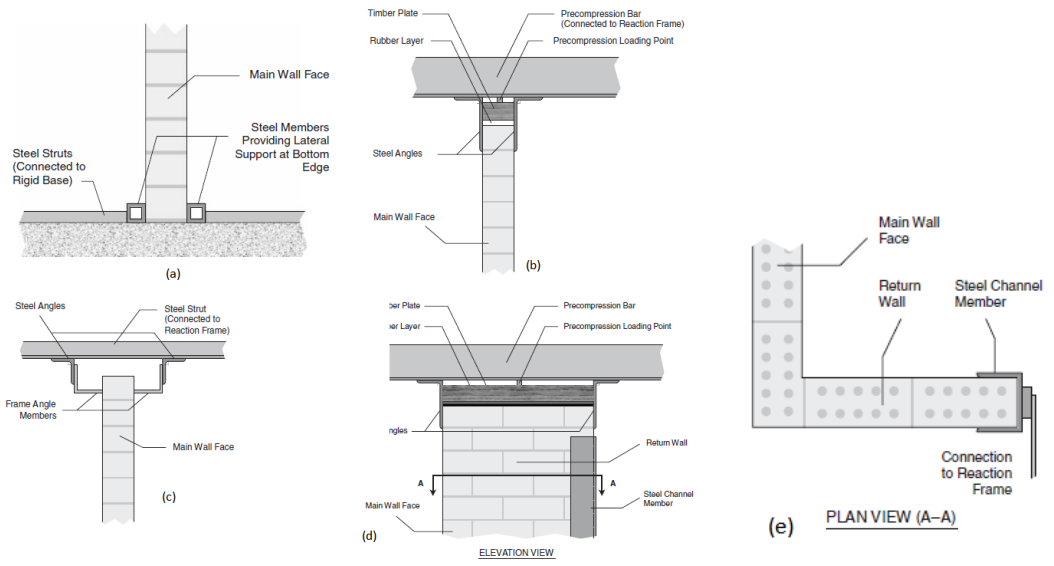

Figure 4-2: Support details at (a) bottom of the wall (b) top edge of the wall with precompression (c) topd edge of the wall without precompression (d) return walls' top edge connection and (e) return wall vertical edge support

Table 4-1: Masonry properties - Griffith Wall 2

Parameters	Values
Young's Modulus E_m $[N/mm^2]$	2240
Flexural tensile strength f_{mt} $[N/mm^2]$	0.52
Compressive strength f_{mc} $[N/mm^2]$	13.6

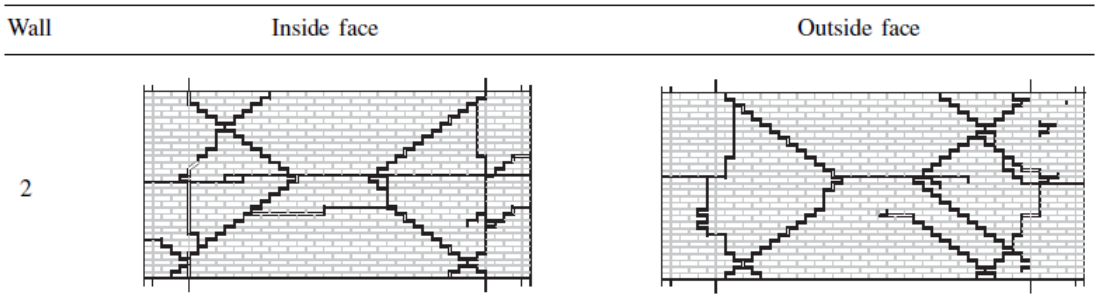

Figure 4-3: Post cyclic testing crack pattern in Wall 2

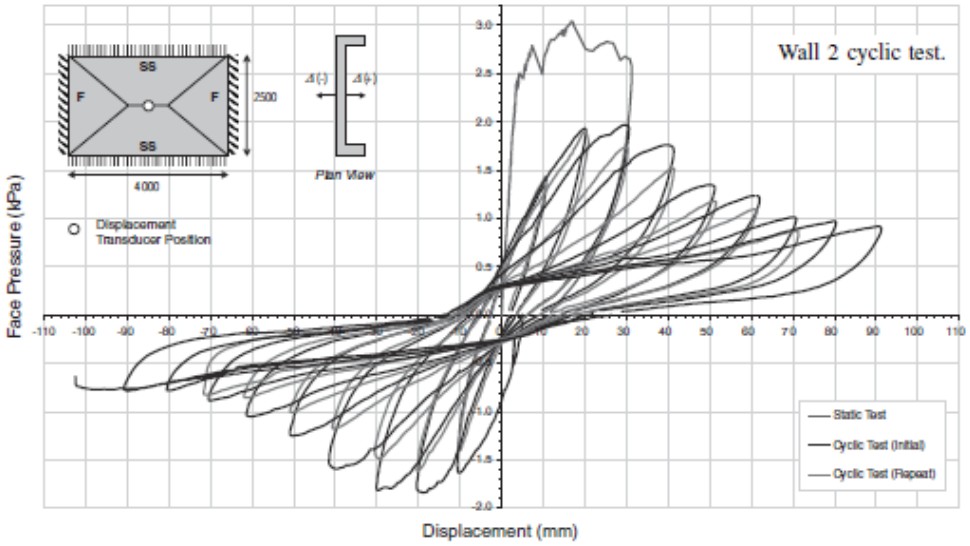

Figure 4-4: Load-deflection diagram of Wall 2

4-2 Numerical Modelling - An Overview

4-2-1 Finite Element Discretization

In this section, an overview of the finite element discretization / modelling approaches and the different solution procedures employed for the Griffith wall experiments, to obtain a stable post peak behaviour close to the experimental observation, is presented. Based on the results of Van der Pluijm panel model, the shell element and it's variation, the localized model, are considered for this section. But only the shell element model is presented. Due to the additional computational time and memory requirement as against shell element model, the solid element model is omitted from this section of the study.

Modelling approaches for Griffith wall tests:

- Shell element Model

4-2-2 Solution procedures

In order to analyse the Models created using the different approaches could be used. All procedures used for Van der pluijm model are used again.

- Non linear static analysis
  - Force controlled incremental procedure
  - Arc length controlled incremental procedure
- Quasi-dynamic Analysis - including the inertia and damping effects.

A consummate overview of the study is as follows:

Table 4-2: Numerical Modelling overview - Griffith Models

		Finite Element Discretization
		Shell Element Model
Solution Procedures	1) Non linear static analysis	
	• Force control	-
	• Arc length control	4-3-1
	2) Quasi-dynamic analysis	4-3-2

4-3 Shell Element Model

Preprocessing

Geometry The geometry of the wall II is created using the pre-processor Midas Fx+ version 3.3.0 with the dimensions of $4.0 * 2.5\ m^2$. The return wall length is $0.48\ m$. The thickness of the wall and the return wall, $0.11\ m$, is incorporated in the thickness of the curved shell elements used to create a 2.5D Model. The geometry of the wall along with the Meshing is shown in Figure 4-5.

Meshing and Elements The geometry of the Panel is then meshed using Isoparamteric quadrilateral curved shell elements shown in Figure 3-6 as the thickness of the wall is very small as compared to the two main dimensions of the wall. The CQ40S element described elaborately under Van der pluijm wall modelling is used here as well with 3x3 gaussian in plane integration and 11 point simpson integration in the thickness direction. The meshing is done to a fine level to avoid mesh objective results. 40 elements were provided in the longitudinal direction of the wall and 25 elements in the direction of height of the wall.

Boundary conditions and Loads The wall is simply supported along the top edges to restrain out plane displacements and hence is given restraints all the edges of the model in the global z direction. The bottom of the wall is supported in the Global Y direction for the gravity load. The horizontal edge of the return wall is restrained for axial displacements in the global X direction and the vertical edges are restrained for in global X and Z directions to simulate the supports provided as shown in Figure 4-2
The loading applied using the air matresses placed between the reaction frame and the panel to create an uniform distributed load is simulated using a distributed face load in Midas FX+ and a value of 5000 N/m^2 is given which is well above the failure load for wall 2 as seen in the load displacement curve, see Figure 4-4. Also, dead load of the wall is added as gravity load in the Global negative Y direction. Refer Figure 4-5 for the model generated with the meshing and boundary conditions. The distributed load is applied on the face in the Global negative Z direction and has not been shown for clarity of Boundary conditions and meshing.

Constitutive model Macro scale model is created and the Total strain based smeared cracking model, see Figure 4-6, is used with isotropic properties. The compression behaviour is idealized and the tension behaviour is treated as elastic followed by exponential softening with f_{tb} and Mode I Fracture energy G_f^1 as tensile bond strength and Mode-I fracture energy. The constitutive model effectively looks as shown in Figure 4-6. Parameters assumed are Poisson's ratio $v = 0.15$ and constant shear retention function for the shear behaviour with a factor of 0.01 for initial analyses. This analysis would help us determine the crack pattern which could be used as a precursor for the localized model.

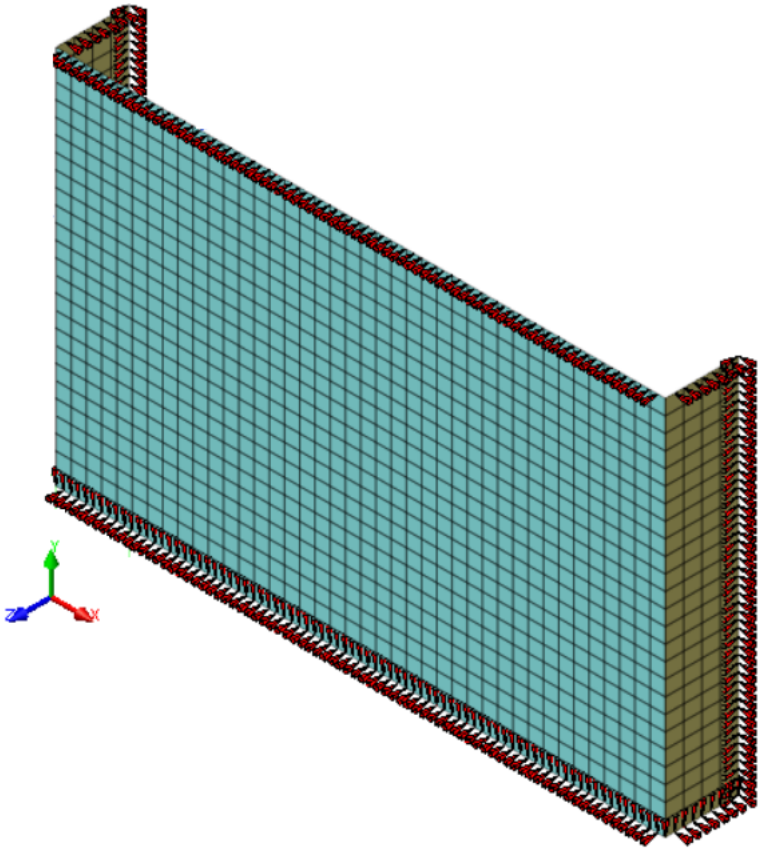

Figure 4-5: Finite element model with boundary conditions created using Midas FX+

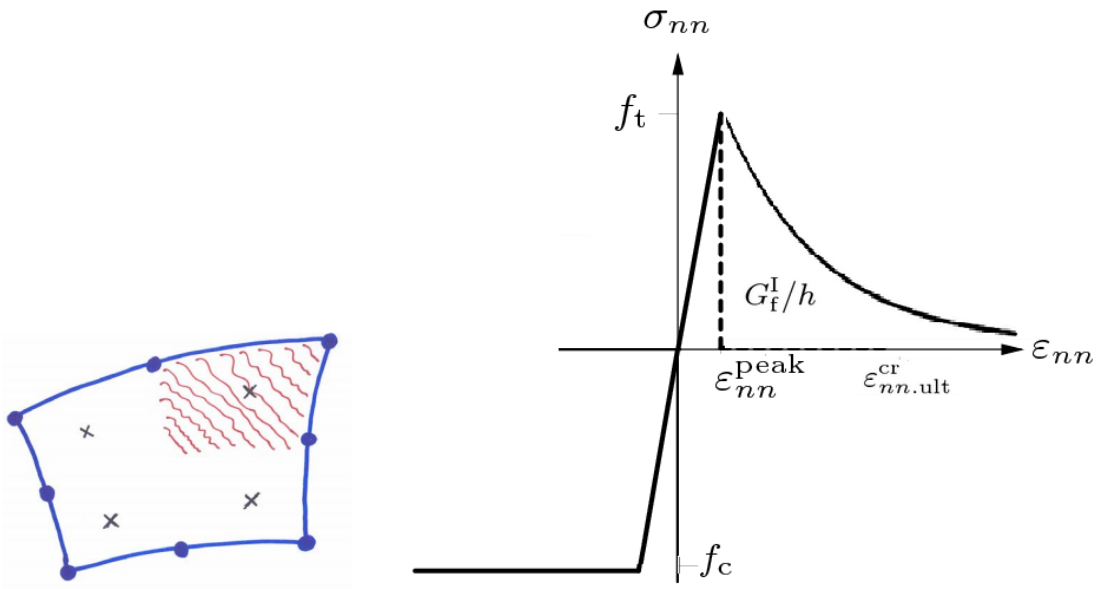

Figure 4-6: Smeared cracking, Course CIE5148 and Constitutive Model

4-3-1 Non linear Static Analysis

Arc length Control Procedure

Since the Force control procedure yields only the peak load and diverges post peak, the Arc length control procedure is used for obtaining post peak behaviour of the Masonry walls. A global arc length procedure enhanced with line search option for stabilizing the convergence behaviour and increasing the rate of convergence is used. The procedure is carried out with the Newton raphson iterative process with a maximum of 100 iterations per load step. The load is applied in uniform small steps which are $\frac{1}{200}th$ of the load applied - 5000 N/mm^2. The solution is not globally convergent and is highly unstable post peak with non converged steps. The convergence tolerance for the force and displacement norms is 0.001. The choice of Mode 1 Fracture energy value is based on a paramteric analysis conducted similar to Figure 3-12.

Table 4-3: Masonry parameters - Griffith wall 2 model

Parameters	Values
Density $[Kg/m^3]$	1900
Young's Modulus E_o^{j+u} $[N/mm^2]$	2240
Tensile bond strength f_{tb} $[N/mm^2]$	0.52
Mode I fracture energy G_f^1 $[N/mm]$	0.015
Crack bandwidth h $[mm]$	100

Post-processing and Results

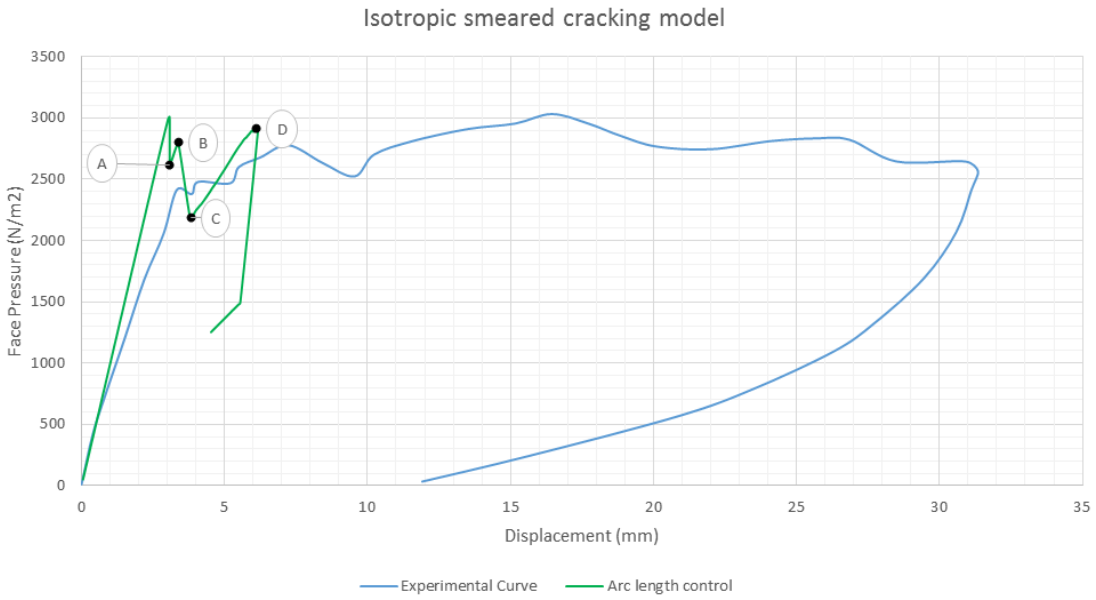

Figure 4-7: Mesh Objective results for Arc length control procedure

.The crack bandwidth is expressed as $h = \sqrt{A}$ where A is the planar area of the shell element.

$$\varepsilon^{cr}_{ult.nn} = \frac{G^1_f}{h * f_{tb}}$$

$$\varepsilon^{cr}_{ult.nn} = \frac{0.015N/mm}{100 * 0.52} = 2.88E-04$$

$$\varepsilon^{peak}_{nn} = \frac{f_{tb}}{E^{j+u}_o} = 2.32E-04$$

The legend for the principal strain plots used is a norm:

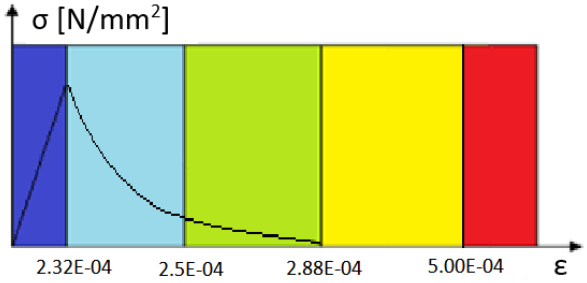

Figure 4-8: Legend for the principal strain plots

Figure 4-7 is the load displacement curve for the finest mesh created. It is oberved that the ascending branch of the curve has stiffness close to the experimental curve. However the stiffness doesn't reduce at a load of around 600 N/mm^2 as can be seen in the experimental curve. The response obtained doesn't reflect the true behavior owing to lack of orthotropy in the material model. Nevertheless the crack patterns are looked into for insight that would lead to the creation of localized model.

Point A shown in the capacity curve shown in Figure 4-7 is a point just below the peak load which is in good accordance with the experimental failure load of 3000 N/mm^2 but is the first non-converged step after 100 iterations. The Force and displacement variation seem to be increasing away from the convergence tolerance and would have led to divergence if the number of iterations is increased. But as the load steps were continued the behaviour is seen in the load displacement curve. There are three more non-converged steps post point A. The principal strain plots corresponding to points A, B, C and D are shown in Figure 4-9 and Figure 4-10. The principal strain plots are in accordance with Figure 4-8 and shows the complete formation of the horizontal crack and the deformed elements along the crack. The crack pattern shows the smeared out cracks starting at the centre of the wall and progressing horizontally. This then leads to serious cracking and opening of the crack and continuation to form the diagonal cracks. The pattern cannot be clearly understood as a yield line pattern as this is not a discrete crack but certainly the crack strains are greater along a yield line as compared to it's neighbouring elements.

The quasi-dynamic analysis approach similar to the Van der pluijm model is carried out to check for post peak behaviour using isotropic properties again.

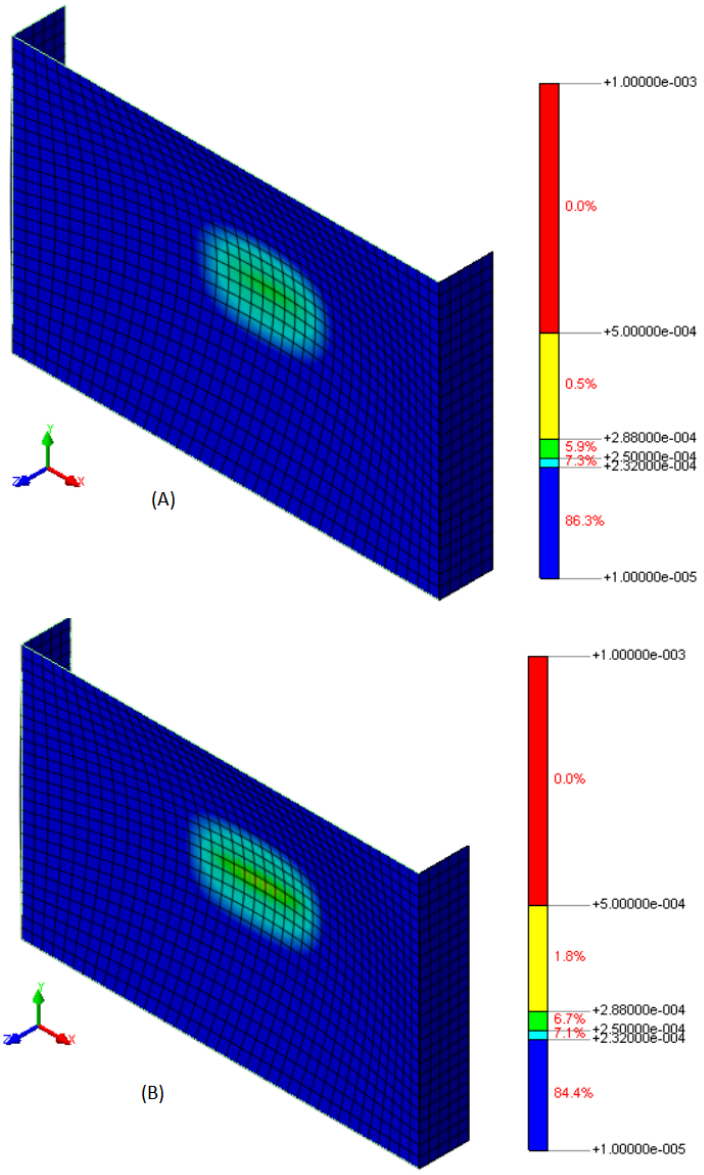

Figure 4-9: Principal strains at points A and B of the load displacement curve

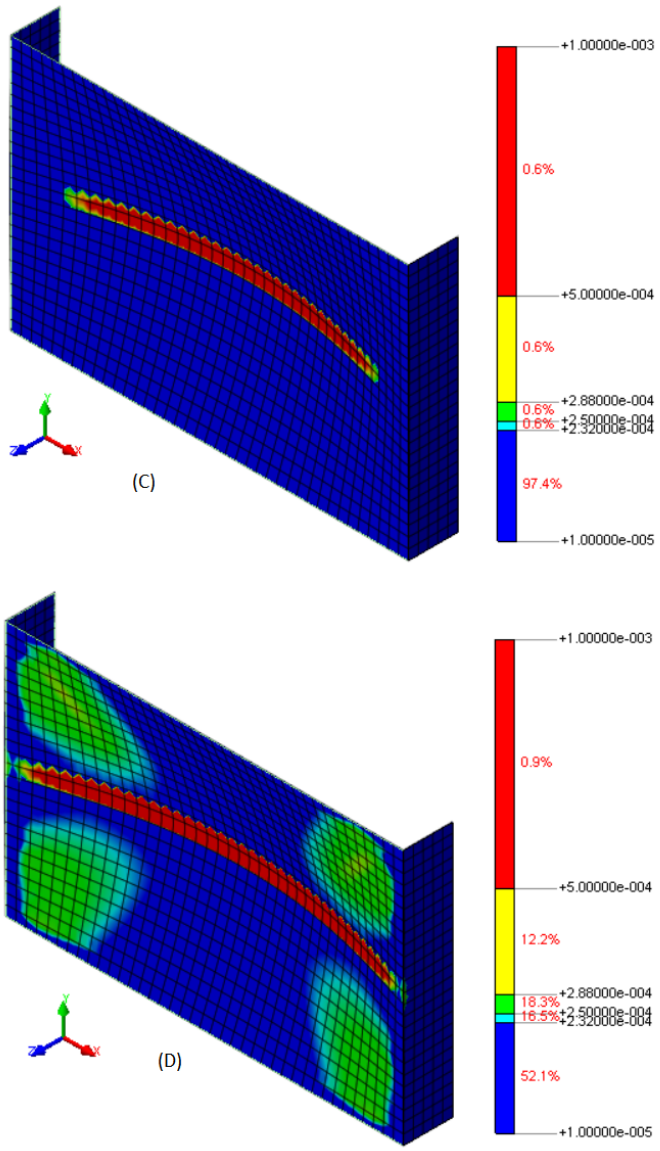

Figure 4-10: Principal strains at points C and D of the load displacement curve

4-3-2 Quasi-dynamic Analysis

The release of energy associated with crack opening was studied using the quasi-dynamic approach in the case of Van der pluijm model. Similar approach is used for Griffith wall 2.

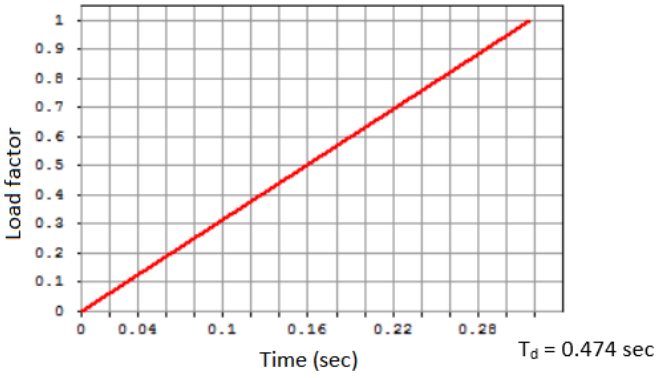

Figure 4-11: Load applied with respect to time

The load here is applied as a ramp function i.e load is applied as a function of time as shown in Figure 4-11. The maximum load (load factor of 1) is set to 5000 N/mm^2 which is the same as the non linear static analysis and is higher than the failure load of 3000 N/mm^2. The load is increased to its maximum over a period of time called the rise time T_d. The load is applied in time steps that are very small post peak as compared to the ones in the pre peak zone. Also, the use of tighter convergence tolerance for force and displacement norm is essential and hence a value of 0.001 is used instead of the default 0.01.

First an eigen value analysis is run and the rayleigh damping coefficients a and b are deduced taking into account the first mode and the fifth mode which cumulatively contribute to 56 % of the response in the direction of the load and a damping ratio $\zeta = 0.05$. Mode 1 and 5 shapes are shown in Figure 4-12 and Figure 4-13. The mass damping coefficent a is set to zero to avoid mass damping effects and only the stiffness damping is taken into account using a. Consistent mass and damping matrices are used. The Newmark integration scheme is used for time integration with integration constants $\gamma = 0.5$ $\beta = 0.25$ are used, as it is second order accurate. The rayleigh damping coefficients a and b corresponding to $\zeta = 0.05$ are found in the eigen value analysis.

The rise time is set to $T_d = 0.474s$ which is higher than the $T_1 = 0.074s$. The load steps are applied in 40 equal steps of 0.0079 s and 100 equal steps 1.58E-03 s for the stable post peak response. The parameters used for the Quasi-dynamic analysis are listed in Table 4-4.

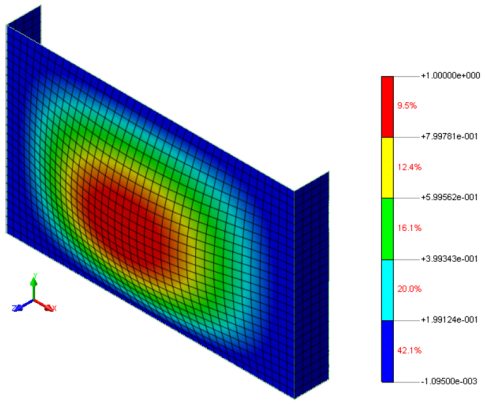

Figure 4-12: Mode 1 shape, Time period = 0.074 s

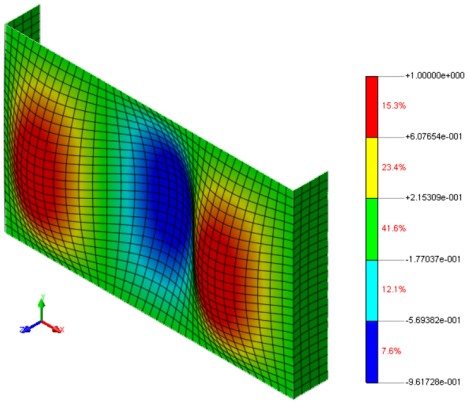

Figure 4-13: Mode 5 shape, Time period = 0.02 s

Table 4-4: Quasi-dynamic analysis paramters - Griffith Wall 2 model

Parameters	Values
Rise Time T_d $[s]$	0.474
Mode 1 Time period T_1 $[s]$	0.074
Damping ratio ζ	0.05
Rayleigh Stiffness damping coefficient b $[s]$	2.77E-04
Young's Modulus E_o^{j+u} $[N/mm^2]$	2240
Tensile bond strength f_{tb} $[N/mm^2]$	0.52
Mode I fracture energy G_f^1 $[N/mm]$	0.015
Crack bandwidth h $[mm]$	100

Post-processing and Results

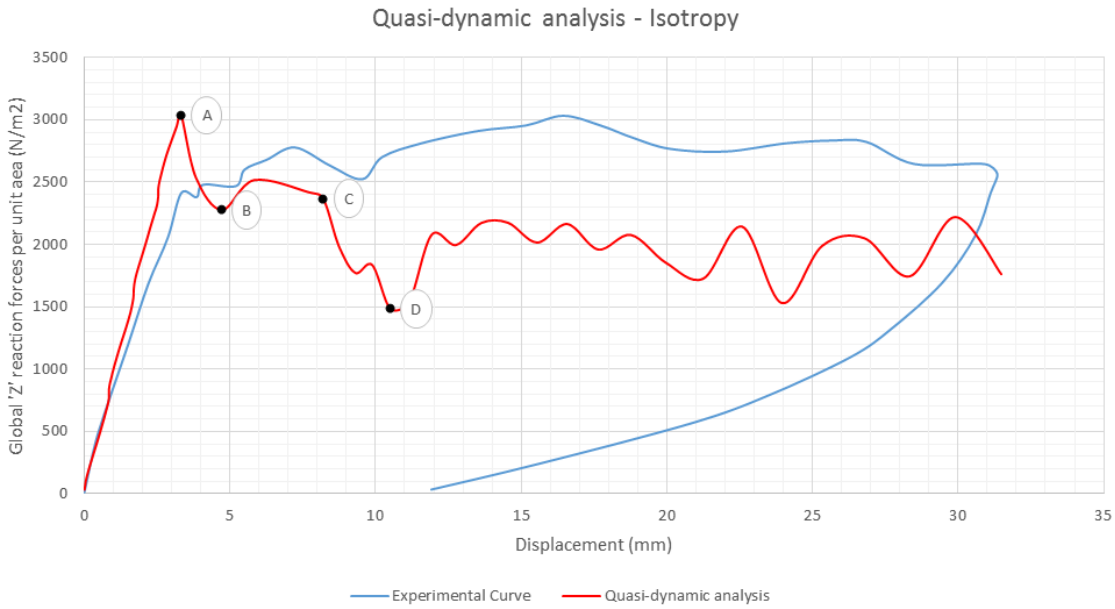

Figure 4-14: Load displacement curve obtained using Quasi-dynamic analysis, Global 'Z' reaction forces per unit area taken as the equivalent face pressure

The load displacement curve obtained for the Quasi-dynamic analysis is as shown in Figure 4-14. The applied load is increasing as is shown in the ramp input function, see Figure 4-11, to a valued of 5000 N/mm^2. However, the response of the model to the Quasi dynamic analysis shows the decrease of load beyond the peak where the macro crack propagation begins. This response has been obtained as a measure of the reaction forces from the supports for out of plane displacements against the out of plane displacement at the middle of the panel. The sum of reaction forces from the supports divided by the area is taken to be the distributed load on the panel for the loading to be presented in a capacity curve. It shows a post peak response unlike the non linear static analysis. The effect of inertia (dynamic effects) is seen post peak as was expected and is negligible in the ascending part of the curve.

Figure 4-15 illustrates the effect of inertia after the peak. The decrease of the reaction forces (represented as the uniform distributed face pressure) in relation to increase of the applied load shows the violation of static equilibrium and the onset of dynamic equilibrium. The acceleration vs time graph, Figure 4-16, also shows the acceleration experienced by the wall post peak. This dynamic effect could be attributed to the sudden release of energy due to the formation of the macro crack. The energy triggers the vibrations but it is damped out due to the viscous damping factor added in the model. The behaviour is not globally convergent but is appreciable as most of the non converged steps approach the tolerance of displacement norm.

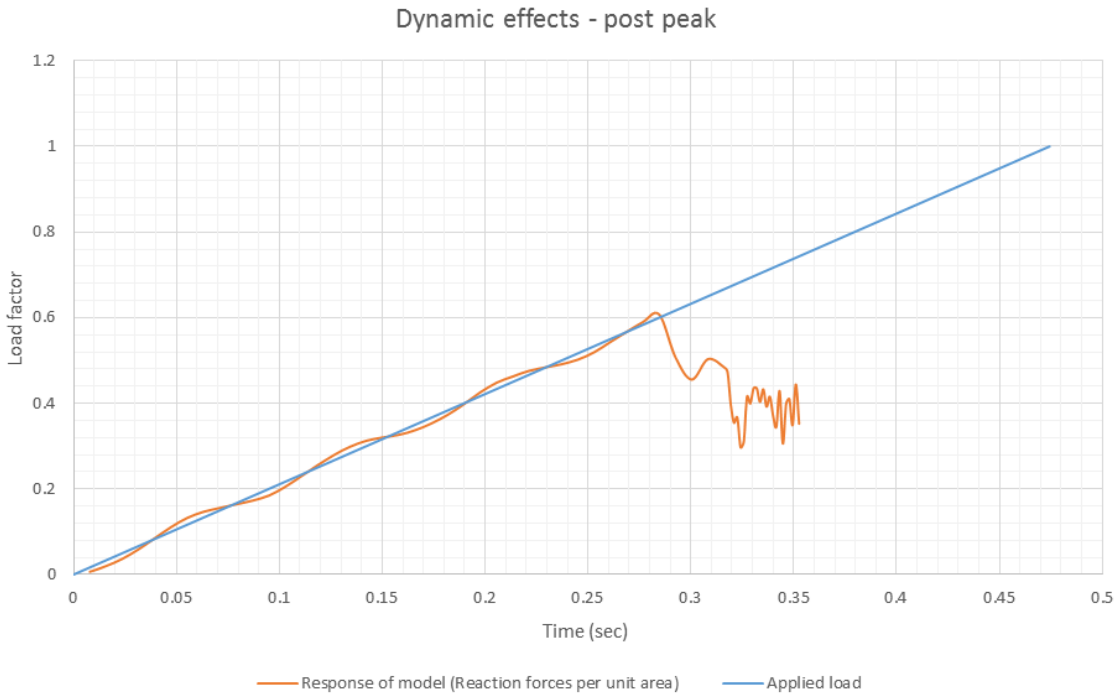

Figure 4-15: Dynamic equilibrium observed post peak, load factor is the ratio of the load/reactions forces per unit area, as the case may be, to 5000 N/m^2

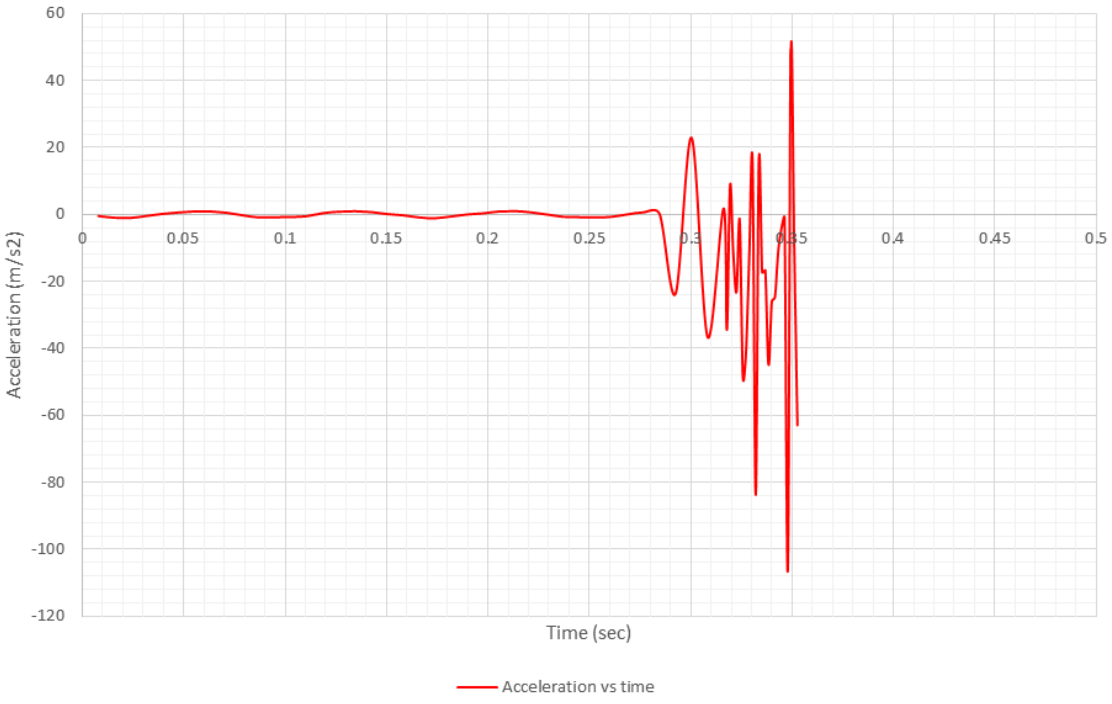

Figure 4-16: Inertia effects observed post peak

Principal strain plots The principal strain plots are presented according to Figure 4-8 and the formation of diagonal cracks is clearly seen in Figure 4-18 which couldn't be obtained using the non linear analysis. The points investigated are marked as A, B, C and D as shown in Figure 4-14.

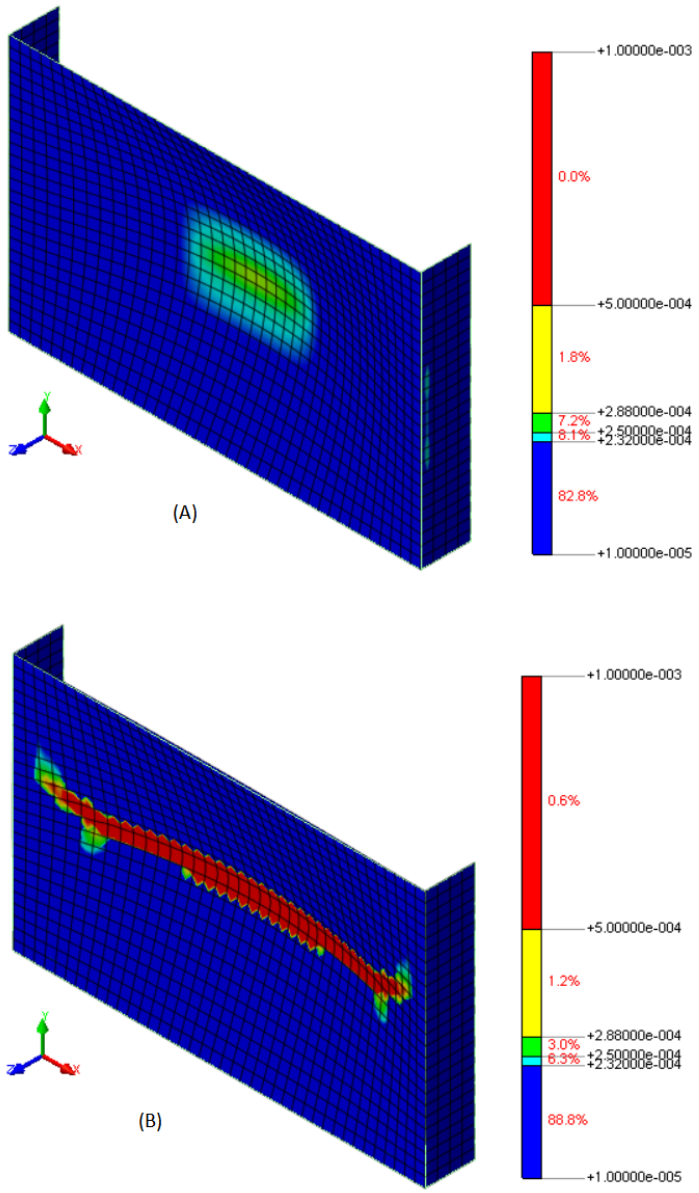

Figure 4-17: Principal strains at points A and B of the load displacement curve

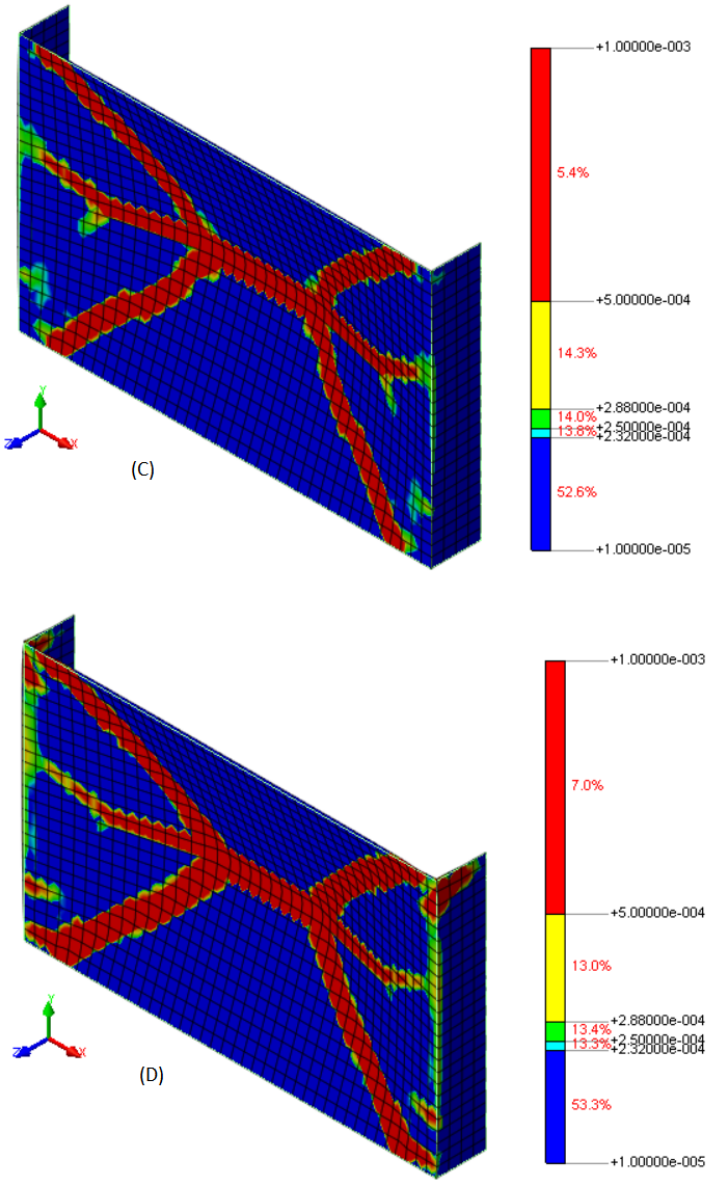

Figure 4-18: Principal strains at points C and D of the load displacement curve

Compression side crack pattern The assumption of ideal behaviour was made for compression regime. To be sure that the assumption was right and the crushing of the wall doesn't happen at the loaded face, the crack patterns at the last step of loading in the quasidynamic analysis is checked. The strain value of -6.07E-03 corresponds to the compressive strength of 13.6 N/mm^2 of the masonry. It can be clearly seen from the principal strain plots that the compression face of the wall experiences crushing only at the edges due to the moment resisting connection. Actually the tensile stresses are found on the loaded face as well and this has led to the crack pattern as shown in Figure 4-19.

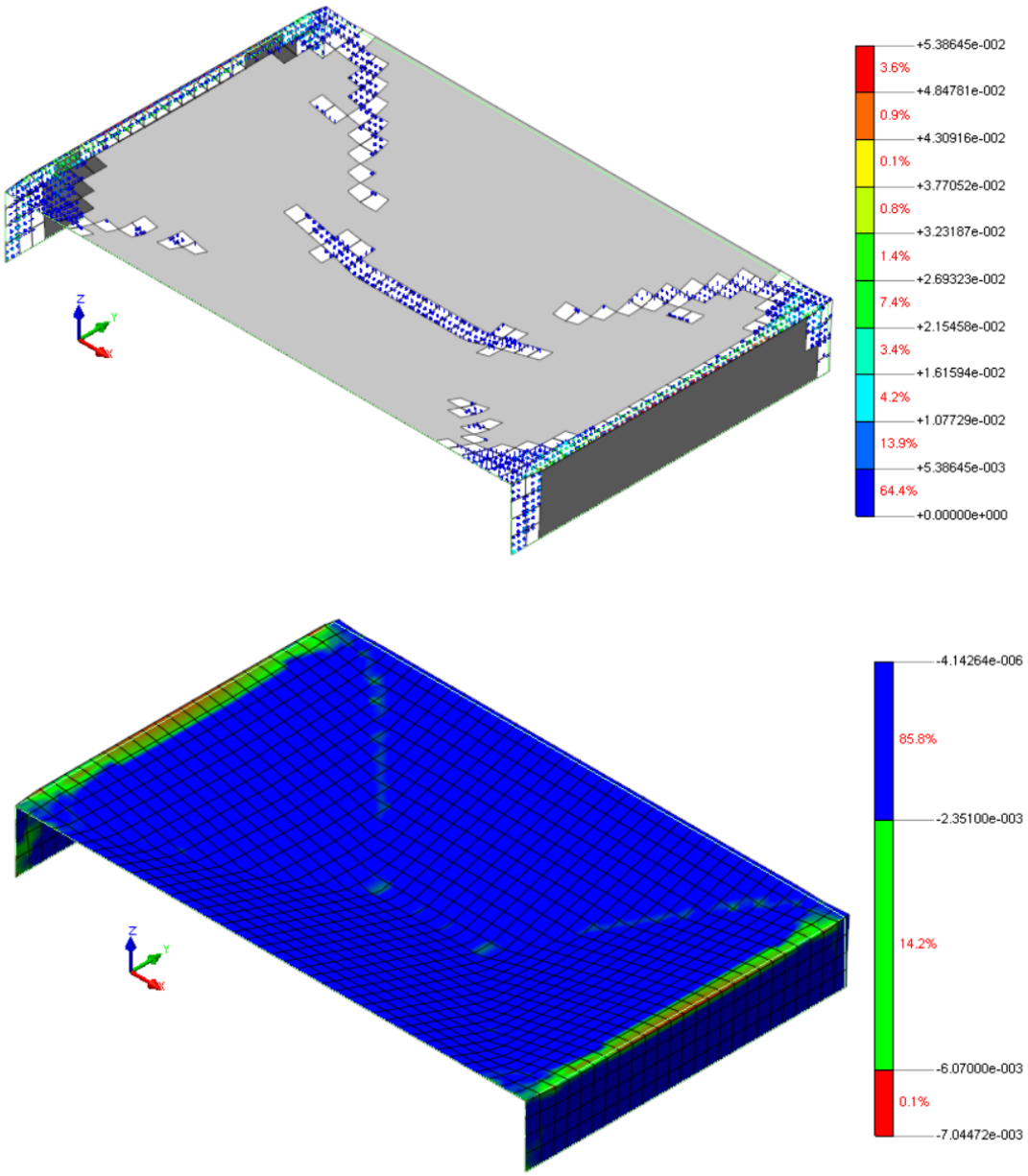

Figure 4-19: Crack pattern in the compressive side of the wall at the LAST step in the quasi-dynamic analysis and the corresponding principal strain plot

4-3-3 Conclusions

The shell element model in the case of Griffith walls gives a post peak response when subjected to the quasi-dynamic analysis as has been shown in the previous section. The crack patterns clearly demarcate the formation of the diagonal cracks and this is absent in the case of the highly unstable arc length controlled non linear static analysis. This can be seen in Figure 4-20. While quasi-dynamic analysis has a deviation from the actual response by about 20-25 % in the post peak zone.

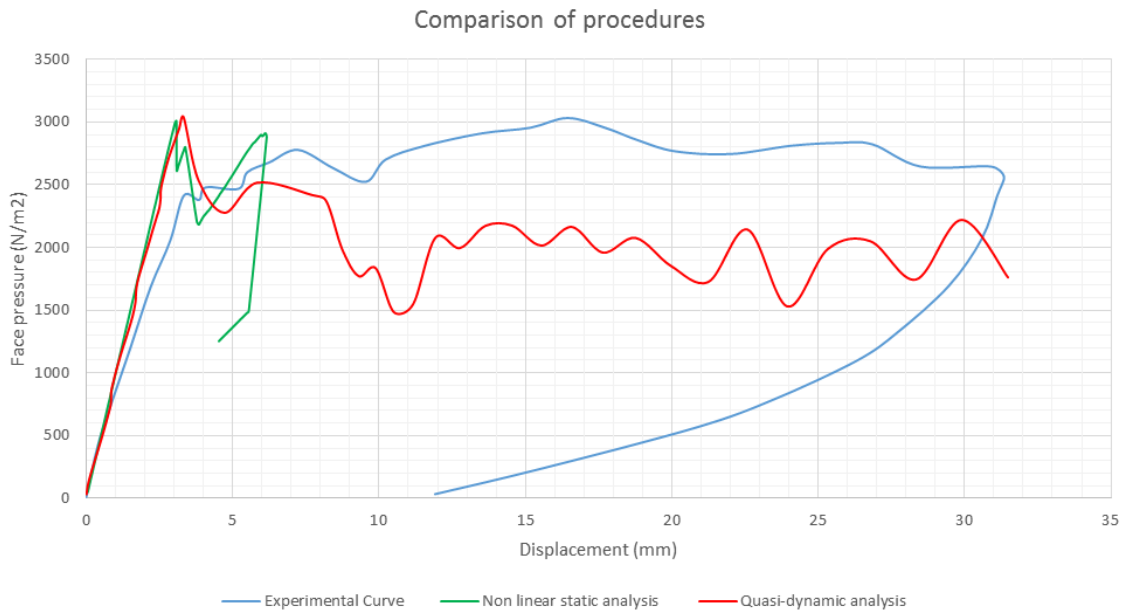

Figure 4-20: The non linear static and Quasi-dynamic analysis result comparison for Isotropic continuum Localized shell model of Griffith Wall-II

Chapter 5

Conclusions and Recommendations

5-1 Conclusions

The objective of the thesis was to validate the models created using the finite element software TNO Diana against the experimental benchmarks of Van der Pluijm and Griffith et al. The results obtained for both section lead to the following conclusions:

1. The response obtained is mesh objective for a fixed value of tensile strength and fracture energy parameters as the crack bandwidth (dependent on the size of the element) keeps changing with refinement. Therefore, the alternatives available (without having to change G_f^1 & f_{tb}) are to either have a constant value of crack bandwidth or use a finely refined mesh for further studies involving these finite elements.

2. The number of integration points along the thickness of the wall is key to predicting the capacity of the wall accurately and hence 11 integration points are to be used for analysis involving out of plane studies.

3. The effect of smaller time steps and tighter convergence tolerance on the response obtained using Quasi dynamic analysis are key.

4. The non-linear static analysis provides a post peak response which is highly unstable. The sudden drop in the load post peak could be attributed to the formation of the macro horizontal crack. Despite using very fine steps, the arc length control doesn't find any converged step between the peak and trough and hence the method is deemed unreliable to obtain post peak response of the out of plane bending of masonry.

5. The quasi dynamic analysis shows regain of strength as an effect of the triggering of the inertia effects and yields a post peak behaviour. This is quite reliable considering the tight convergence tolerance and smaller time steps used in the process but doesn't simulate the actual Van der Pluijm panel-II capacity curve. The experimental observation could be attributed to the fact that the post peak response is aided by the redistribution

of diagonal bending along the inclined cracks (seen in the experiment) to the horizontal bending along the vertical edges. This can also be explained by the idea that the diagonal cracks as compared to the horizontal cracks in the mechanism have a stepped pattern passing through head and bed joints having different strengths. Diagonal cracks thus have a higher tensile strength and fracture energy. This reflects the orthotropic nature of masonry.

6. It can be concluded that orthotropy is required to obtain a reliable pre-peak response in case of two way out of plane bending of the masonry walls as is confirmed in Figure 3-73 unlike the one way bending which can be simulated using thickness models shown in Figure 3-4 using isotropic continuum model.

7. The use of the Rankine hill type anisotropy which helps create the continnum masonry model with orthotropic effects needs strength, fracture energy parameters along the orthgonal directions and are not available in the test results. It's thus decided to create a variation of the shell element model simulating the effect of orthotropy indirectly and provide the extent to which the model is reliable. This approach has yielded a reliable pre peak response and the post peak has been unstable with the non linear static analysis. The quasi-dynamic approach gives insight about post peak in a better way.

8. Use of solid elements is associated with higher computational time and memory. Nevertheless, the results are stable post peak in the quasi dynamic approach and the idea of using predefined surface interfaces along the yield line failure could be investigated in the future.

9. The boundary conditions required to simulate the behaviour using solid elements are a little different as compared to the shell element model which could be the reason why the prediction of capacity (for the same isotropic masonry properties) is lesser in the case of the solid element model.

5-2 Recommendations

1. Experimental tests for the determination of Mode-I fracture energy and tensile strength parameters along orthogonal directions are required in conjunction with the main testing of the out of plane response of URM walls. This is very important to simulate the behaviour of the URM in out of plane bending which requires orthotropy as concluded in the thesis. Also, the importance of having fracture energy values for the same is important as the ease of simulations becomes greater by avoiding multiple parametric analysis. The choice of these values are crucial as the Mode-I fracture energy value not only affects the ultimate strain reached but also the peak load as observed in the parametric analysis done in Van der pluijm model study 3-3-1.

2. The Quasi-dynamic approach needs further refinement and investigation with regards to rise time of the applied load and the effect of time steps.

3. Other numerical approaches like the use of predefined failure pattern like using interface elements in analogy to the yield line pattern has to be investigated for comparison to the existing models.

4. The localized model needs parametric studies with regards to the thickness of the local zone determined to understand the effect of confining the non-linearity within a confined zone.

5. With regards to obtaining a post peak response of greater accuracy and reliability, robust solution procedures like the sequential linear analysis suited for softening behaviour of masonry is required for reliable and accurate results. The suitability of SLA needs to compared with the procedures used in this thesis for degree of reliability.

Bibliography

[1] P. Buis, "Dutch Houses Shiver Amid Gas-Field Quakes, The Wall street Journal," 2013.

[2] A. Hillerborg, M. Modeer, and P. Petersson, "Analysis of crack formation ad crack growth in concrete by means offracture mechanics and finite elements," 1976.

[3] R. Heeringa and D. Mclean, "Ultimate strength behaviour of reinforced concrete block masonry walls, Proceedings of 5th North American Masonry Conference, Urbana-Champaign, Illinois, USA," tech. rep., 1990.

[4] D. Bhende and D. Ovadia, "Out-of-Plane strengthening scheme for reinforced masonry walls," 1976.

[5] RILEM, "Technical recommendations for the testing and use of constructions materials," tech. rep., 1994.

[6] M. Tomazevic, M. Lutman, and L. Petkovic, "Seismic behaviour of masonry walls: experimental simulation, Journal of Structural Engineering," 1996.

[7] J. Vaculik, "Unreinforced masonry walls subjected to out of plane seismic actions, PhD Thesis," 2005.

[8] J. Rots, "Numerical Simulation of Cracking in Structural Masonry," 1991.

[9] Brinker, "Yield line theory and material properties of laterally loaded masonry walls," 1984.

[10] S. Lagomarsino, A. Penna, A. Galasco, and S. Cattari, "An equivalent frame model for the nonlinear seismic analysis of masonry buildings," 2013.

[11] S. Casolo, "Modelling the out-of-plane seismic behaviour of masonry walls by rigid elements," 2000.

[12] R. Van der Pluijm, "Tests on Laterally Loaded Clay Brick Panels," tech. rep., 2000.

[13] Griffith, Vaculik, Lam, and Nelson, "Cyclic testing of unreinforced masony walls in two way bending," 2007.

[14] T. van Eck, F. Goutbeek, H. Haak, and B. Dost, "Seismic hazard due to small-magnitude, shallow-source, induced earthquakes in The Netherlands," *Engineering Geology*, 2006.

[15] R. Van Der Pluijm, "Out-of-Plane Bending of Masonry Behaviour and Strength," 1999.

[16] G. Vasconceles, "Experimental investigations on the mechanics of stone masonry: Characterization of granites and behaviour of ancient masonry shear walls, PhD Thesis," 2005.

[17] A. Anthoine and G. Magonette, "Shear-compression testing and analysis of brick masonry walls, Proceedings of 10th European Conference on Earthquake Engineering, Balkema, Rotterdam," tech. rep., 1995.

[18] K. Kikuchi, G. Yoshimura, A. Tanaka, and K. Yoshida, "Effect of wall aspect ratio on seismic behaviour of reinforced fully grouted concrete masonry walls, Proceedings of 9th North American Masonry Conference, Clemson, South Carolina, USA," tech. rep., 2003.

[19] T. Paulay and M. Priestley, "Seismic design of reinforced concrete and masonry buildings," 1992.

[20] H. Derakhshan, M. C. Griffith, and J. M. Ingham, "Airbag testing of multi-leaf unreinforced masonry walls subjected to one-way bending," *Engineering Structures*, 2013.

[21] M. Gerardin and P. Negro, "The European Laboratory for Structural Assessment(ELSA) and its Role for the Validation of European Seismic Codes, Proceedings of EuroConference on Global Change and Catastrophe Risk Management: Earthquake Risks in Europe, Laxenburg, Austria," tech. rep., 2000.

[22] M. Paquette and J. Bruneau, "Pseudo-Dynamic testing of unreinforced masonry building with flexible diaphragm, Journal of Structural Engineering," 2003.

[23] R. Drysdale, A. Hamid, and L. Baker, "Masonry structures: behaviour and design, The Masonry Society, Boulder, Colorado, USA," tech. rep., 1994.

[24] K. Doherty, M. Griffith, N. Lam, and J. Wilson, "Displacement based seismic analysis for out of plane bending of unreinforced masonry walls," 2002.

[25] M. Griffith, N. Lam, J. Wilson, and K. Doherty, "Experimental investigation of unreinforced brick masonry walls in flexure," 2004.

[26] P. Lourenco, "Anisotropic sofening model for masonry plates and shells," 2000.

[27] S. Roca, C. Molins, A. Mari, and M. Asce, "Strength Capacity of Masonry Wall Structures by the Equivalent Frame Method," 2005.

[28] P. Lourenco and J. Rots, "Multisurface interface model for analysis of masonry structures," 1997.

[29] J. Rots, "An experimental/Numerical basis for practical design rules for Structural Masonry," tech. rep., 1994.

[30] P. Lourenco, "Computational strategies for masonry structures, PhD Thesis," 1996.